Single-Molecule Microscopy Studies of Amyloid-β Oligomer Binding on Live Cells

by

Robin D. Johnson

A dissertation submitted in partial fulfillment
of the requirements for the degree of
Doctor of Philosophy
(Biophysics)
in The University of Michigan
2012

Doctoral Committee:

Professor Duncan G. Steel, Co-Chair
Professor Ari Gafni, Co-Chair
Professor Ronald Holz
Associate Professor Kristen Verhey
Associate Professor Michal Zochowski

“ ‘The best thing for being sad,’ replied Merlyn… ‘is to learn something. That is the only thing that never fails.’ ”

— T.H. White, *The Once and Future King*

“Just keep swimming. Just keep swimming. Just keep swimming, swimming, swimming…” — Dory in *Finding Nemo*

DEDICATION

Dedicated to my parents, Leslie E. Johnson, M.D., and Kathleen M. Johnson, M.D.,
who taught a little girl from the heartland
that she could grow up to be
whatever she wanted.

ACKNOWLEDGMENTS

A number of great people have helped me get to this point in my graduate studies. First and foremost, I want to thank my research advisors, Professors Ari Gafni and Duncan Steel. They take science and mentorship seriously, meet life with humor and grace, and treat their laboratory members with dignity and respect. I have been deeply fortunate to have them as mentors and role models. I would also like to thank my thesis committee, Ronald Holz, Kristen Verhey, and Michal Zochowski, for their support and scientific counsel.

The Gafni/Steel laboratory has been a marvelously friendly and collegial workplace. Thanks to my coworkers Kathleen Wisser and Joe Schauerte, Ph.D., for great scientific discussions, advice on working with Aβ, and help with experimental design and execution over the years. Kathleen maintained SH-SY5Y cells for this project and continues work on the neuronal spine density assays. Joe's assistance with and instruction on fluorescence lifetime measurement and other techniques have been invaluable. Kathleen and Joe go above and beyond the call of duty when it comes to helping educate graduate students, and I am deeply grateful for their kindness and friendship. Thanks to my fellow graduate student, Chun-Chieh "Andrew" Chang, for helpful scientific discussions and for assistance with the single-particle tracking experiments and data analysis. It has been a privilege to work with Andrew and with all the past members of the Gafni/Steel laboratory: Hao Ding, Pamela Wong, Jamie Van Etten, Pavithra Aravamudhan, Edgar Lee, and Justin Klein. Special thanks to Hao Ding, who developed the single-molecule photobleach data analysis software used in this project.

Rotation students Becky Simon and Nicole Motl and REU student Taylor Allen worked diligently on calcium indicator studies in SH-SY5Y cells. Manoj Kowshik, a freshman Physics major at the University of Michigan, helped analyze single-molecule data in spring 2012 and was a joy to have around the laboratory.

Thanks to Dr. Michael Sutton, our collaborator on the primary hippocampal neuron project. Mike's ideas, experience, and insight helped guide the project from the beginning, and it would not have been possible without his assistance. Thanks also to Cindy Carruthers, Christian Althaus, Amber McCartney, and Trace Henry in the Sutton laboratory, who supplied me not only with protocols, reagents, and neurons, but also with great advice, warm smiles, and lots of encouragement. A big thanks to Liz Shtrahman in Michal Zochowski's laboratory for providing primary hippocampal neuron cultures for preliminary calcium indicator studies.

Confocal microscopy was performed in the Microscopy and Image-Analysis Laboratory (MIL) at the University of Michigan, Department of Cell & Developmental Biology. I want to thank Shelley Almburg and Chris Edwards of the MIL for training and technical advice. Thanks also to Sara Grosky, Ann Titus, and the rest of the Biophysics faculty and staff for their support and assistance.

My deepest thanks go to Dr. Ronald Koenig, University of Michigan MSTP director, to Ellen Elkin, Laurie Koivupalo, and Hilkka Ketola in the MSTP office for their continuing support, and to my MSTP classmates, who are like family to me. MD/PhD is a long road, and it has been amazing to have them as fellow travelers. Special thanks to Bryan Petersen, who assisted with the flow cytometry experiments.

Thanks to all my science teachers and my undergraduate research advisor, Dr. Laura Moore. I also want to acknowledge my high school and college swim coaches, Jim Bucher and Teresa Fish. Their impact on my character has extended far beyond my years as a competitive swimmer.

Thanks to Andrea Morris and Neha Kaul for scientific discussions, moral support, and friendship, and to all my other friends. To my companions in outdoor adventures, in particular: I wouldn't have made it through without the Sunday morning bike rides, the 7 A.M. pool dates, the ten mile runs out at Pinckney, and the random weekends spent backpacking in the New Mexico wilderness. Thanks for pushing me to do my best and for helping me remember that there's a great big world outside of science and medicine.

Logan Cook has been an island of stability, comfort, and humor in a tumultuous sea, this final year of graduate school.

Finally, my thanks and love to my family for their faith, encouragement, and inspiration: my grandparents, Harriett Johnson, Alta Myers, and Robert T. Myers, M.D.; my parents, Leslie and Kathleen Johnson; my brother Luke and his wonderful wife Kristina; and my sister, Anna Mae.

TABLE OF CONTENTS

LIST OF FIGURES

LIST OF TABLES

LIST OF ABBREVIATIONS

Aβ……..amyloid-β peptide
AD…….Alzheimer's Disease
ADDL……amyloid-derived diffusible ligand
APF……annular protofibril
APP……amyloid precursor protein
α7nAchR……..……α7 nicotinic acetylcholine receptor
hAPP……..human amyloid precursor protein
FAD……..familial Alzheimer's Disease
HFIP……hexafluoroisopropanol
HL488…….HiLyte Fluor 488
HL488Aβ40……....amyloid-β(1-40) labeled with HL488 at the N-terminus
HL647…….HiLyte Fluor 647
HL647Aβ……..HiLyte Fluor 647-labeled amyloid-β
HL647Aβ40……....amyloid-β(1-40) labeled with HL647 at the N-terminus
HL647Aβ40……amyloid-β(1-42) labeled with HL647 at the N-terminus
HL647cAβ40……..amyloid-β(1-40) labeled with HL647 by C2 maleimide linkage
HL647cAβ42……..amyloid-β(1-42) labeled with HL647 by C2 maleimide linkage
LTD. …….long-term depression
LTP……..long-term potentiation
MAP2……..microtubule-associated protein 2
mGluR5..……..metabotropic glutamate receptor 5
NMDA……N-methyl-D-Aspartate
NF…….neurofilament
PSD-95……post-synaptic density protein 95
ThT……...thioflavin T

TIRF……..total internal reflection fluorescence

ABSTRACT

Soluble oligomers of amyloid-β peptide have been implicated as the proximal neurotoxins in Alzheimer's disease. However, the precise stoichiometric identity of the neurotoxic aggregate(s) and the mechanisms by which these species induce neuronal dysfunction remain uncertain. Amyloid-β (Aβ) may damage cells by binding to and interfering with membrane integral protein receptors or by directly disrupting the neuronal cell membrane, allowing Ca^{2+} to leak into the cell. Physiologically relevant experimentation is hindered by the low endogenous concentrations of the peptide, the metastability of Aβ oligomers, and the wide range of observed interactions between Aβ and biological membranes. Single-molecule microscopy represents one avenue for overcoming these challenges. Using this technique, we find that monomeric amyloid-β oligomerizes at low nanomolar concentrations on exposure to physiological buffers and glass or poly-D-lysine coated surfaces. Amyloid-β(1-40) forms larger oligomers or clusters within minutes of binding to SH-SY5Y neuroblastoma cells but induces only minor Ca^{2+} leakage. Aβ binds to the neurites of primary rat hippocampal cells with higher affinity. While amyloid-β(1-40) (Aβ40) and amyloid-β(1-42) (Aβ42) form larger oligomers than those detected on slides immediately after binding, a 1:1 mix of the two peptides results in smaller neurite-bound oligomers than those detected on-slide or for either peptide alone. On-neurite oligomer growth over time requires the presence of solution peptide. With 1 nM peptide in solution, Aβ40 oligomers do not grow over the course of 48 hours, Aβ42 oligomers grow slightly, and oligomers of a 1:1 mix grow substantially. These results are significant in light of the increased Aβ42:Aβ40 ratios correlated with familial Alzheimer's disease mutations. While the majority of neurite-bound oligomers are immobile, a small population exhibits diffusive or directed motion. Neurite-bound oligomers do not preferentially associate with synapses and bind at only slightly higher density on dendrites than on axons. These results point to a mechanism by

which small Aβ oligomers bind to neurons and grow at rates dependent on local Aβ42:Aβ40 ratio and peptide concentrations, with neurotoxicity emerging at some later point in time.

Chapter 1

Introduction to Alzheimer's Disease and Amyloid-β

1.1 Alzheimer's Disease

Alzheimer's disease, the most common cause of adult dementia, is the seventh leading cause of death in the United States. Approximately 1 in 8 adults over 65 suffers from Alzheimer's (AD), and while deaths attributed to many other major illnesses have decreased, deaths due to Alzheimer's increased 46% between 2000 and 2006 (Figure 1.1.1).

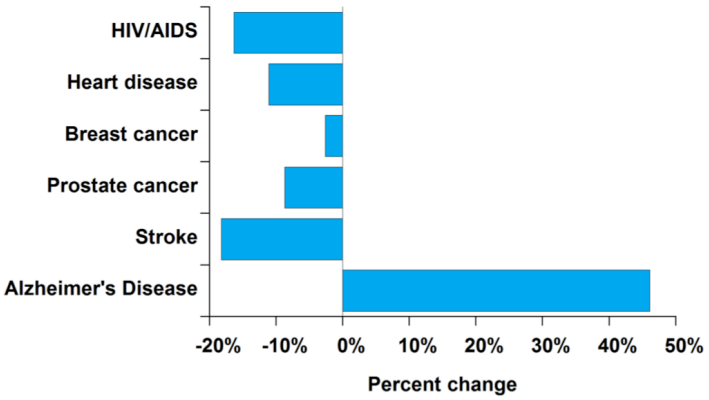

Figure 1.1.1 Changes in deaths due to various causes between 2000 and 2006. Figure adapted from [1].

While some of this increase is likely due to improvements in diagnosis, Alzheimer's is likely to become an increasing burden on public health as healthcare improvements continue to extend lifespan in the developed world. Understanding AD at a molecular level may prove crucial to the development of targeted neuroprotective therapies, and with an aging population, these therapies will be desperately needed.

The classic histological lesions of Alzheimer's disease were first formally described by Alois Alzheimer in the early 1900's. On examining the brain of a deceased

patient afflicted with dementia, Alzheimer noted " 'one or several fibrils…[with] characteristic thickness and peculiar impregnability. Numerous small military foci…are determined by the storage of a peculiar substance in the cerebral cortex.' "[2]. In short, he recognized neurofibrillary tangles, intracellular deposits composed of the microtubule-binding protein tau, and neuritic plaques, extracellular aggregates composed primarily of fibrils of the amyloid-β peptide. In the years since Alzheimer's discovery, tau and amyloid-β (Aβ) have both been extensively studied as possible sources of the symptoms of AD.

1.2 Amyloid-β Production and Aggregation

Amyloid-β is a 39-to-43 residue peptide produced by cleavage of an integral membrane protein, amyloid-precursor peptide (APP). In the canonical APP processing pathway, α-secretase cleaves APP in the central part of the Aβ domain, with γ-secretase then liberating the remaining small fragment of the Aβ sequence. Production of Aβ occurs when β-secretase performs the first cleavage step at the N-terminus of the Aβ domain, and the γ-secretase cleavage site moves downstream[3].

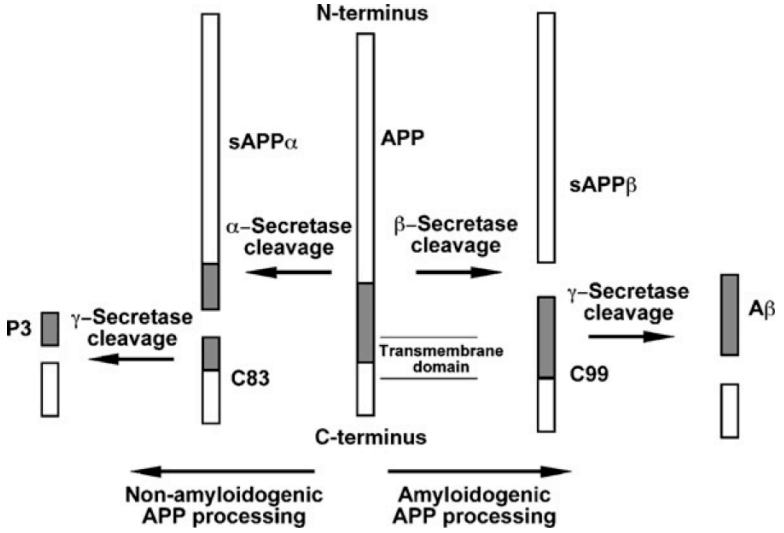

Figure 1.2.1 Schematic for Aβ production from amyloid precursor proten (APP). From [3].

Aβ is present in both normal and AD human brain tissue, albeit at low (picomolar to nanomolar) concentrations[4,5]. Aβ40 is the more abundant, less amyloidogenic form of

the protein, normally constituting about 90% of the soluble Aβ pool. The remaining 10% of the peptide is mostly Aβ42, a more amyloidogenic and more highly toxic form with two additional hydrophobic residues at the C-terminus (Figure 1.2.2).

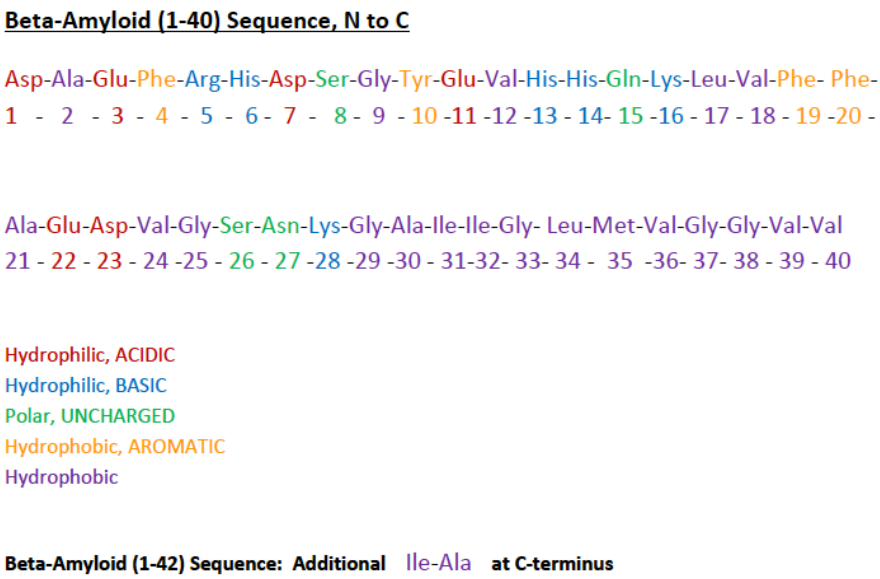

Figure 1.2.2 Aβ peptide amino acid sequence from N to C terminus.
Sequence taken from [6].

Monomeric Aβ is thought to be predominantly unstructured in solution; the middle segment of the peptide in particular likely samples a wide ensemble of conformations, depending on conditions[6,7]. At the low concentrations present *in vivo*, the oligomeric state of the peptide is also likely to be in a constant state of flux, with small aggregates (monomers to hexamers) interconverting in a dynamic equilibrium[8–10]. Above a certain critical concentration, oligomeric "seeds" rapidly add subunits to form fibrils, and aggregation proceeds via nucleation-dependent fibrillization. Monitoring this processs by fluorescence of Thioflavin T, a fluorophore activated by binding to β-sheet structure, reveals a sigmoidal aggregation curve (Figure 1.2.3). Aggregation is characterized by an initial lag phase, during which aggregation proceeds slowly, followed by rapid fibril formation, until fluorescence plateaus as the mixture of fibrils and small oligomers reach a stable equilibrium.

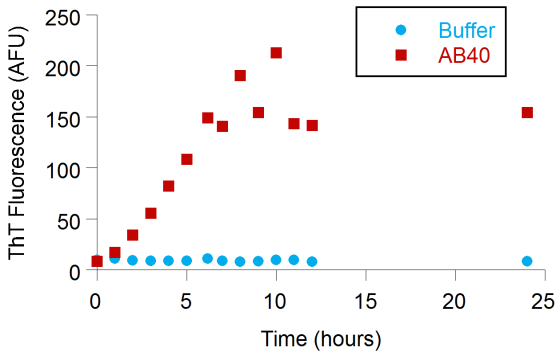

Figure 1.2.3 Aβ40 fibril formation as monitored by Thioflavin T (ThT) fluorescence.
A 46 μm aliquot of Aβ40 in 10 mM sodium phosphate buffer, pH 7.4, was incubated at 37°C with 60 rpm stirring. ThT fluorescence was monitored on a Jasco fluorimeter, ex. 440 nm, em. 485 nm, following addition of 15 μL of Aβ40 sample to 235 μL of 10 μM ThT.

Composed of peptide chains stacked in a cross-β sheet structure, Aβ fibrils are generally nanometers in diameter but may be micrometers in length. Large deposits of these structures are the primary component of the plaques originally identified by Alois Alzheimer in AD patients' brains. While these aggregates are polymorphic, most published structures contain monomeric peptide with a bend or turn occurring between residues 23-29, with the 10-13 residues immediately before and after this turn forming β-strands stacked into β-sheets[11,12].

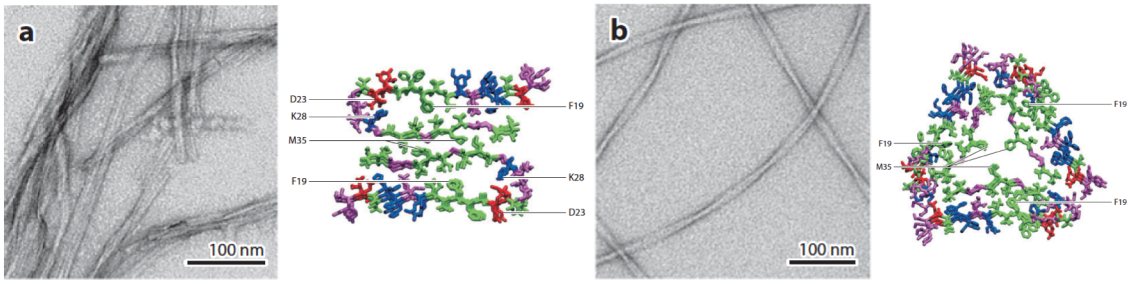

Figure 1.2.4 Two proposed fibril structures for Aβ40.
(a) The "striated-ribbon" model contains two protofilament strands per fibril. (b) The "twisted-pair" model contains three protofilament strands per fibril. Both structures contain a β-turn or bend at residues 23-29, with β-sheet structure before and after. Images from [12].

The physiological functions of both APP and Aβ are poorly understood. Both proteins may play a role in promotion of synaptic plasticity or synapse formation[13,14], and Aβ may transition from a physiological role to a neurotoxic one depending on its

concentration[15] and the ratio of different forms present in the brain. The roughly 10% of Alzheimer's disease cases that are genetic in nature (familial Alzheimer's disease, or FAD) are by and large correlated with mutations in presenilins, the catalytic subunit of γ-secretase, or in APP. Most of these mutations increase the ratio of Aβ42 to Aβ40, which may contribute strongly to AD development in these patients[3,16]. The APOE4 apolipoprotein E isoform, possession of which is a major risk factor for so-called "sporadic" late-onset Alzheimer's disease, has been shown to both stabilize oligomers[17] and reduce Aβ clearance[18].

1.3 Amyloid-β Oligomer Toxicity and Structure

The past 20 years have brought about a major shift in the AD experimental paradigm. Since Alzheimer's initial discovery of amyloid plaques, research had focused on amyloid fibrils as a likely causative factor for the clinical symptoms of AD, an idea referred to in the literature as "the amyloid hypothesis." More recently emerging evidence indicates, however, that small soluble oligomers of Aβ may be the critical neurotoxic species of the peptide, prompting a transition to an "amyloid oligomer hypothesis"[19–21]. Plaque load and insoluble Aβ aggregates correlate poorly with Alzheimer's disease symptoms as compared to soluble Aβ levels and synapse loss[22–24], and oligomers have largely been found to induce greater toxicity to cultured cells than similar quantities of fibrils[25–27].

The progress of research on these species has been inhibited by the multiplicity of different Aβ oligomers described, variations in the abilities of these oligomers to form fibrils (pre-fibrillar versus off-pathway), and the problem of linking oligomers prepared *in vitro* or detected in human-APP expressing mice to structures that are actually present in human AD brain. A vast array of distinct sub-fibrillar Aβ aggregates has been characterized and may contribute to AD neurotoxicity; some of these are depicted in Figure 1.3.1.

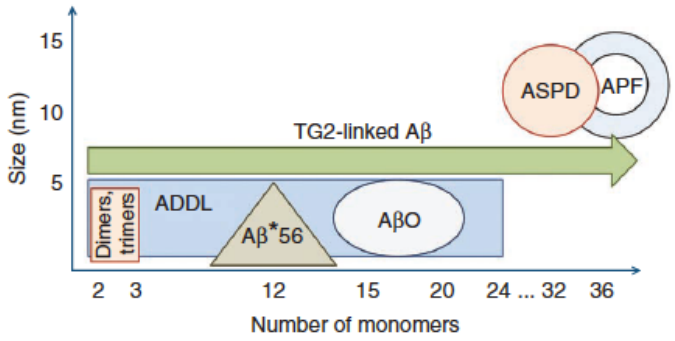

Figure 1.3.1 Aβ oligomers prepared in vitro or detected in brain-derived samples. These include low-n-oligomers such as SDS-stable dimers, trimers, and tetramers, ADDL's (amyloid-derived diffusible ligands), the Aβ*56 dodecameric oligomer, AβO's, ASPD's (SDS-stable amylospheroids), and APF's (annular protofibrils). Figure from [21].

Two specific exchanges in the literature provide examples for the level of confusion that wildly differing preparation protocols and inadequate characterization of oligomers can cause. Several widely used *in vitro* oligomer preparation protocols include treatment with hexafluoroisopropanol (HFIP) for initial monomerization of the peptide. In 2005, Demuro et al. showed that oligomers formed from HFIP-treated Aβ induced immediate, drastic calcium leakage in SH-SY5Y cells, while monomers and fibrils did not[26]. Later experiments with model membranes attributed these changes to a membrane-thinning mechanism, by which Aβ oligomers carpet the membrane and gradually destroy its integrity[28]. Capone et al. later presented evidence that HFIP itself was sufficient to induce such changes and that the observed "membrane thinning effect" was likely due to trace quantities of HFIP still present in the samples[29]. Similar issues arose when Shankar, at al. reported the potent inhibition of long-term potentiation (LTP) by a cross-linked dimer version of Aβ(1-40), mutant S26C, citing this as evidence that dimers were sufficient to induce synaptotoxicity[30]. A later report by O'Nuallain and colleagues indicated that only when these dimers were allowed to aggregate to a much larger protofibrillar stage did they affect LTP. A freeze-thaw cycle like that used by Shankar and colleagues on the dimerized S26C peptide was sufficient to induce this aggregation[31]. These two cases illustrate not only the inherent difficulty of working with Aβ but also the need for a deeper understanding of the mechanisms by which the monomeric peptide forms neurotoxic aggregates under physiological conditions.

A brief discussion of a subset of these aggregates will help motivate the work discussed in this thesis. Low-molecular weight oligomers alone may be sufficient to cause significant damage to neurons. Dimers and trimers purified from human AD post-mortem brain tissue and from the medium of cells expressing human APP have recently been shown to induce deficits in long-term potentiation and increases in long-term depression[30,32]. The ratio of Aβ40 to Aβ42 in these oligomers was not characterized, and it has not been established whether these purified dimers aggregate quickly when frozen down, like the previously discussed S26C cross-linked dimers used in the same study[31]. Another recent study indicated that Aβ40 dimers, trimers, and tetramers exhibited nonlinear increases in cellular toxicity with molecular weight[25]. Amyloid-derived diffusible ligands, or ADDL's, generally prepared from synthetic Aβ42 by a method pioneered by William Klein's laboratory in the late 1990's, generally contain oligomers from 10 kDa to 100 kDa in molecular weight, or roughly trimers to 24-mers[33], as depicted in Figure 1.3.1. These small globular aggregates have been shown to bind specifically to synapses, reduce dendritic spine density, and alter normal tau sorting and localization[34–36]. In 2006, Lesne et al. detected an Aβ42 dodecamer in the brains of hAPP-expressing transgenic mice (Tg2576) that appeared to correlate well with memory deficits[37]. Once purified and injected into the brains of young mice, this aggregate (termed Aβ*56) caused long-term memory deficits, as measured by the Morris water maze. However, this species was not detected in Aβ purified from human AD brain[30,38].

Finally, several reports in the 1990's indicated that freshly solubilized Aβ was capable of forming cation-selective ion channels with stepwise conductances in biological membranes[39,40]. Pore-like protofibrillar structures formed from Aβ and other amyloids were later detected by electron microscopy and atomic force microscopy[41–43]. The imaged "annular protofibrils" or APF's were generally in the range of 10 to 20 nm in diameter, with 1 nm to 2 nm central pores, and appeared to contain between 4 and 6 distinct subunits, each likely containing multiple peptide monomers. These data were interpreted as evidence that Aβ and other amyloids might disrupt membranes in the same fashion bacterial pore-forming peptides[42]. Most discussions of these annular structures place their probable size between 12 and 60 monomeric peptides. One recent crystal structure for an amyloid-forming protein β-barrel (designated a "cylindrin") contains only

six subunits[44]. However, the central pore in such a structure is not likely to be hydrated, reducing the probability of cation conductance. Interestingly, an APF-specific antibody has recently been developed and used to further characterize these structures[45]. Kayed and colleagues found that APF's formed when pre-fibrillar oligomers were exposed to a hydrophilic/hydrophobic interface. Following purification and separation from the membrane, these structures retained their pore-like morphology, but not their ability to permeabilize membranes. Membrane disruption was necessarily preceded by APF formation within the same membrane[45].

The role of membrane interactions in the formation of toxic Aβ oligomers is a subject of particularly strong debate. A number of groups have found that pre-aggregated Aβ induces greater toxicity than monomeric or fibrillar Aβ, implying that oligomers formed in solution without contact with biological membranes must be capable of interacting with cell membrane moieties[26,46]. At least superficially, these reports contradict previously mentioned reports that treatment of biological membranes with un-aggregated Aβ leads to formation of cation-selective, stepwise conductance changes[39,40]. Zhang and associates recently used surface pressure measurements to determine the relative abilities of monomeric Aβ, ADDL's, and protofibrillar Aβ to insert into planar membranes[47]. Monomers of the peptide inserted into the membrane more rapidly than oligomers of either type and oligomerized following binding, in a distinct process from oligomerization in solution. Zhang et al. propose that intra-membrane and extra-membrane oligomerization may produce two separate pools of Aβ whose toxicities are mediated by completely distinct mechanisms[47]. Oligomers formed in the membrane may directly disrupt membrane integrity by transient pore formation, allowing toxic calcium leakage. At the same time, oligomers formed in solution may interact with specific cellular receptors, altering their function and resulting in toxicity. All in all, multiple mechanisms may be at work in this system, and multiple structures may be implicated in mediating the effects. A complete understanding of Aβ's toxicity will require identifying the specific molecular interactions involved.

1.4 Possible Mechanisms for Amyloid-β Oligomer Toxicity

As previously discussed, Aβ has been shown to induce toxicity in numerous respects. In addition to the changes in synaptic plasticity, dendritic spine loss and damage, altered tau physiology, and membrane disruption alluded to above, Aβ oligomers can induce oxidative stress, mitochondrial disruption, and impaired axonal transport[3]. For the purpose of introducing the current work, a review of the molecular mechanisms by which extracellular Aβ interacts with cells will suffice. A number of hypotheses have been put forth to explain the toxicity of extracellular amyloid-β oligomers. These can in general be grouped into mechanisms involving direct interaction with the cell membrane and mechanisms involving binding to or interaction with membrane integral protein receptors, summarized in Figure 1.4.1.

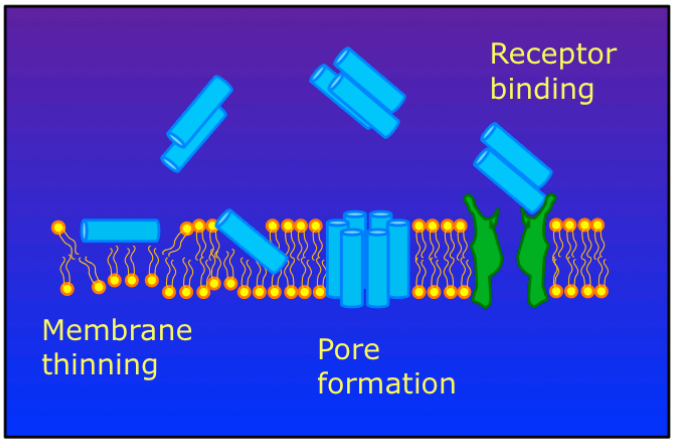

Figure 1.4.1 Possible mechanisms for amyloid-β oligomer-induced toxicity.
These include membrane thinning (the "carpet" mechanism), pore or channel formation, and binding to endogenous cellular receptors, particularly those present at the synapse.

As mentioned above, application of Aβ to both cellular and model membranes has been shown to cause conductance changes. The dominant hypothesis explaining these changes involves the formation of transiently opening membrane integral Aβ "pores" or "ion channels" as reviewed in the previous section. These structures are generally thought to be cation-selective, inducing toxicity by allowing catastrophic calcium leakage into the cell[42,48,49]. The majority of these studies were performed using un-aggregated or freshly solubilized Aβ at higher than physiological (micromolar) concentrations. While these preparations do not contain membrane-damaging solvents, the exact composition of the

initial sample in terms of oligomer size is not generally characterized. These pores can often be blocked by Zn^{2+} or by short peptides composed of residues 8-14 of the Aβ peptide[40,49–51]. A competing explanation for membrane conductance changes, termed the "carpet" mechanism, posits that Aβ oligomers uniformly coat membranes, forcing lipid head groups apart and resulting in general thinning of the membrane. This in theory removes the energetic barriers for ion transfer, allowing calcium and other cations to leak across the membrane. This mechanism was proposed to account for the immediate calcium leakage observed in SH-SY5Y cells by Charles Glabe's group in 2005[26] as well as for more gradual Aβ-induced changes in conductance later observed on model membranes[28]. Interestingly, most of the evidence for the "carpet mechanism" lies in studies performed with peptide pre-treated with HFIP, mentioned above as a membrane-toxic solvent[29]. More recently, oligomers formed from HFIP-pre-treated peptide have been shown to induce stepwise conductance changes as single, optically detectable channels[52], lending increased credence to the pore hypothesis. While such structures might induce only transient, local changes in calcium concentration, low-level leakage over extended time periods would have a decided impact on neuronal function. It should be noted that neuronal calcium levels play a pivotal role in intercellular signal transmission, intracellular signaling, synaptic plasticity, gene expression, and a variety of other processes. Even slight changes to calcium homeostasis can drastically impact neuronal physiology[53]. The requirement of long-term exposure for observable functional deficits might explain the age dependence of clinical Alzheimer's disease.

A number of specific components of the lipid bilayer have been implicated as possible binding sites where Aβ binding or on-membrane aggregation might begin. These sites include externalized phosphatidylserines[54,55], GM1 ganglioside-containing micro- or nano-domains[56,57], or regions with increased cholesterol content[58]. However, substantial evidence has also been put forth for protein receptors as probable Aβ binding sites. One recent study found that while blocking phosphatidylserine and GM1-gangliosides had little affect on Aβ binding, pre-treating SH-SY5Y cells with trypsin (and then neutralizing the trypsin) reduced Aβ binding by over 60%[59].

Most postulated membrane-integral protein "receptors" for Aβ have been proposed in an effort to explain the peptide's well-documented effects on synaptic

plasticity. Aβ promotes NMDA receptor endocytosis[60] but has not been found to bind directly to NMDA receptors[61]. Snyder and colleagues suggest that the endocytosis may be mediated by previously demonstrated high-affinity binding of Aβ to α-7 nicotinic acetylcholine receptors (α7nAchR's)[62]. Knockout of α7nAchR in hAPP-expressing model mice accelerates of AD-like pathophysiology but appears to be protective at late stages of cognitive decline[63,64]. Lauren et al. demonstrated that Aβ also binds with high affinity to cellular prion protein (PrP^C), and PrP^C knockout and treatment with anti-PrP^C antibodies eliminate Aβ-induced LTP deficits[65]. However, others failed to reproduce these results, calling the conclusions into question[66]. More recently, Aβ oligomers were found to bind to the membrane and subsequently to metabotrobic glutamate receptor 5 (mGluR5), promoting clustering of the receptor and reducing its diffusion[67]. This resulted in decreases in synaptically localized NMDA receptors. Finally, EphB2 receptors have been shown to play a part in up-regulating surface NMDA receptor levels, and Cisse and colleagues recently demonstrated that Aβ oligomers bind to the fibronectin III domain of this receptor and increase its destruction by the proteome[68]. Cisse et al. also showed that hAPP mouse cognitive and LTP deficits in the dentate gyrus can be rescued by EphB2 overexpression. In other words, Aβ oligomer binding to α7nAchR, PrP^C, mGluR5, and EphB2 have all been implicated as mechanisms by which surface levels of NMDA receptors might be reduced in Alzheimer's. A parallel hypothesis for deficits in long-term potentiation and increases in long-term depression is that Aβ blockage of glutamate transporters increases extrasynaptic glutamate levels, activating extrasynaptic NMDA receptors[32,69]. However, Li et al. present no direct evidence that Aβ binds to these transporters. Overall, proposed specific molecular targets for Aβ binding are numerous, and further research will be required to determine which if any of these sites are the key mediators of toxicity induced by soluble Aβ oligomers in Alzheimer's disease.

1.5 Microscopy of Aβ Binding on Live Cell Membranes

Previously, our group has utilized single molecule TIRF microscopy to study the size distribution of Aβ40 oligomers formed in solution at physiological concentrations[10]. We also recently used single molecule intensity measurements to examine which Aβ40

oligomers correlate with conductance changes on a model membrane[70]. These studies provide valuable insights into the mechanisms by which amyloid-β oligomers form, evolve, and interact with biological membranes. However, as many of the previously discussed possible mechanisms of toxicity can only be studied on the membranes of living cells, live cell imaging could serve as a highly useful complementary method to model membrane work. While live cell single molecule studies are limited by greater restrictions on imaging conditions (pH, temperature, and ionic strength must all lie within strict limits to maintain homeostasis), and by increased autofluorescence, they do provide us with an enhanced ability to answer certain physiologically critical questions. These include: to which particular sites on a neuron do oligomers bind? Are cell-bound oligomers mobile, or restricted by interactions with the cytoskeleton and other membrane-associated biomolecules? How is oligomer growth and aggregation at physiological concentrations affected by the increased complexity of the cell membrane, in comparison to model membranes? Immortalized neuronal model cell lines such as PC-12 and SH-SY5Y cells are easily maintained and can be used as a starting point for investigation of some of these unknowns. Cultured primary hippocampal neurons, however, more closely approach the cell types likely to be affected by Aβ *in vivo*, presenting a better opportunity to determine neuron-bound oligomer sizes, binding sites, and effects on neurophysiology.

A number of groups have begun to study Aβ membrane binding and mobility on live cells using fluorescence-based techniques. Using confocal microscopy, Bateman, et al. monitored the formation of fluorescently-labeled Aβ42 aggregates on living PC12 cells[71]. At low micromolar concentrations, they observed formation of two distinct types of large membrane-bound aggregates. More recently, Nag and colleagues have studied FITC-labeled Aβ40 bound to PC12 cell membranes after several minutes' exposure to near-physiological Aβ concentrations[72]. Fluorescence correlation spectroscopy and fluorescence lifetime measurements were used to characterize the mobility and membrane insertion of the peptide, but no specific cell-bound oligomers were identified. As previously discussed, Aβ aggregation is exquisitely sensitive to changes in concentration, and the physiological effects of the peptide may also be deeply impacted

by the amount of peptide in solution[15]. These studies were both performed at Aβ levels of at least 150 nM, significantly higher than *in vivo* levels.

Single-particle tracking experiments have provided insight into the motion of Aβ oligomers on cell membranes at low solution concentrations but have offered little insight into oligomer growth and binding on the cell. In one report, oligomers labeled with a fibril-specific quantum-dot tagged antibody were found to be more confined than those detected by a pre-fibril-specific tagged antibody, in one report[73], but no detail beyond "fibrillar" and "prefibrillar" was provided regarding the stoichiometric identities of the particles involved. Another single-particle tracking study used biotinylated Aβ oligomers coupled to streptavidin-linked quantum dots to measure diffusion coefficients of cell-bound oligomers[67]. Increased clustering of the oligomers at synapses was observed over time, but no information was gleaned regarding how membrane binding affected oligomer size or how oligomers themselves changed conformationally over time. In fact, both studies employed *in vitro* oligomer preparation protocols drawn from previously published work[33,46]. While these procedures are widely used to produce neurotoxic Aβ oligomers, as previously discussed, their utilization obscures mechanistic details about how Aβ oligomers may form from monomers in the brain. Their relationship to oligomers isolated from AD human brain[30], for instance, is poorly understood.

To truly gain an understanding of how physiological concentrations of Aβ oligomers bind to and develop on neuronal cell membranes over time, we adapted single molecule microscopy techniques to investigate the binding of freshly prepared Aβ peptide bound to live cells. Single-molecule microscopy provides several advantages for the study of this system. Experiments can be performed at low concentrations, so as to more closely simulate peptide concentrations in the brain. Dynamics of rapidly shifting oligomer populations and the motion of individual particles can be easily monitored over time. Single oligomers that might be lost in an ensemble measurement can be resolved and potentially associated with toxic effects. These properties combine to make single-molecule techniques uniquely well-suited for studies of Aβ-membrane interactions. The necessary modifications to our previous techniques will be described and novel insights into Aβ oligomer growth upon membrane binding, membrane-bound Aβ oligomer

evolution over time, oligomer motion, and oligomer binding sites will be presented in the following thesis.

1.6 Thesis Summary

In the current work, we present single molecule data showing that small Aβ oligomers form in solution and bind directly to living cells at physiological concentrations. In Chapter 2, we describe in detail the methods used to conduct these studies: single molecule TIRF microscopy, lifetime-adjusted single-molecule confocal microscopy, and a number of adjunct methodologies. Chapter 3 focuses on single molecule work characterizing the size distributions of Aβ40 oligomers bound to SH-SY5Y neuroblastoma cells at near physiological concentrations (50 nM). These oligomers, ranging in size from dimers to hexamers and larger, are relatively immobile and widely distributed on the cell body. Using slide-localized oligomers as a cross section of the species present in solution, we compare the sizes of cell-bound aggregates to the distribution observed for Aβ40 in solution. We find that cell-bound oligomers include a small proportion of distinctly larger (hexameric and greater) oligomers, demonstrating that oligomers may grow or colocalize following binding to the cell membrane. In the work discussed in Chapter 4, we extend single-molecule microscopy of Aβ oligomers to neurons in culture, examining the size distributions of oligomers of Aβ40, Aβ42, and a 1:1 mix of the two peptides on the neurites of primary rat hippocampal neurons. We study the evolution of these oligomers in the absence and presence of 1 nM peptide over up to 48 hours, demonstrating that while a 1:1 mix of the peptides initially produces smaller cell-bound oligomers, these oligomers grow more substantially over time than aggregates composed of either peptide alone. We also show that while the majority of cell bound oligomers do not exhibit motion, a small portion exhibit diffusive or directed motion on the neurite, and that cell-bound oligomers do not initially bind preferentially to synapses. Finally, in Chapter 5, we conclude with a discussion of the meaning of this work in the broader context of the amyloid-β field and present possible future directions.

Chapter 2

Methods: Single-Molecule Microscopy

2.1 Rationale for Single Molecule Studies of Amyloid-β

Single molecule techniques offer some advantages over ensemble methods simply in the level of detail of the data obtained. Ensemble methods produce averaged data; for example, one might perform an ensemble FRET experiment to get averaged information about a structural transition or run a FRAP experiment to measure an average diffusion constant. If behavior of a small population in a sample is responsible for a large downstream effect, the dominating effect of the majority can obscure the connection[74]. Populations that make comparatively small contributions to the overall signal are ignored. With single molecule techniques, the behavior of individuals is monitored and classified, greatly reducing the chances that such important relationships in the data will be overlooked[75].

Beyond this general rationale, studying amyloid-β oligomerization and membrane binding at physiological peptide concentrations presents a number of challenges which single molecule fluorescence microscopy is uniquely suited to overcome. Soluble Aβ is only detected at nanomolar to picomolar levels in the human brain[4,5]. While this can be an obstacle for many traditional ensemble biochemical methods, very low probe concentrations are actually required to reach low enough fluorophore density to resolve single molecules. Efforts to pinpoint the neurotoxic aggregates have also been complicated by the finding that at physiological concentrations, Aβ exists as a mixture of metastable species[8–10]. Single molecule microscopy experiments can be conducted with milliseconds-to-minutes temporal resolution, offering a window into changes occurring on this time scale. The data are literally snapshots of the distribution of Aβ species that exists at a certain moment in time, and when aggregates exhibit structural transitions, these changes can be visualized. Finally, Aβ-membrane interactions are complex and

variable, as previously discussed. Binding sites may include a number of membrane integral receptors and specific lipid moieties (see Section 1.4). Binding affinity and membrane permeabilization may be strongly affected by factors such as membrane curvature and charge [76]. The membranes of neuronal cell somas, neurites, dendritic spines, and postsynaptic densities are distinctive, chemically and morphologically[77–79] It follows that Aβ may have widely varying binding behavior and membrane effects in different cellular membrane compartments. Single molecule microscopy allows precise visualization of individual oligomers and their on-cell locations. Additionally, with the wide variety of fluorescent probes available, it can easily be used to determine whether particular membrane molecules may be acting as Aβ binding sites.

2.2 Confocal Photobleaching for Oligomer Size Measurement

High signal-to-background ratio is a requirement for single fluorophore detection, and confocal scanning microscopy can be used to achieve this. The advantage of confocal microscopy over traditional epifluorescence lies in its reduced out-of-plane fluorescence. In epifluorescence, a beam focused at the back focal plane of the objective is collimated by the objective lens for sample illumination. The laser beam illuminates all fluorophores in its cylindrical path in the axial direction; the detected fluorescence signal includes emission from all fluorophores in this volume. In confocal mode, the laser beam is focused at the plane to be imaged and scanned across the sample, providing the most intense illumination to a specific slice of the sample[74]. Out-of-focus fluorescence is greatly reduced by placing a small aperture between the sample and detector (Figure 2.2.1).

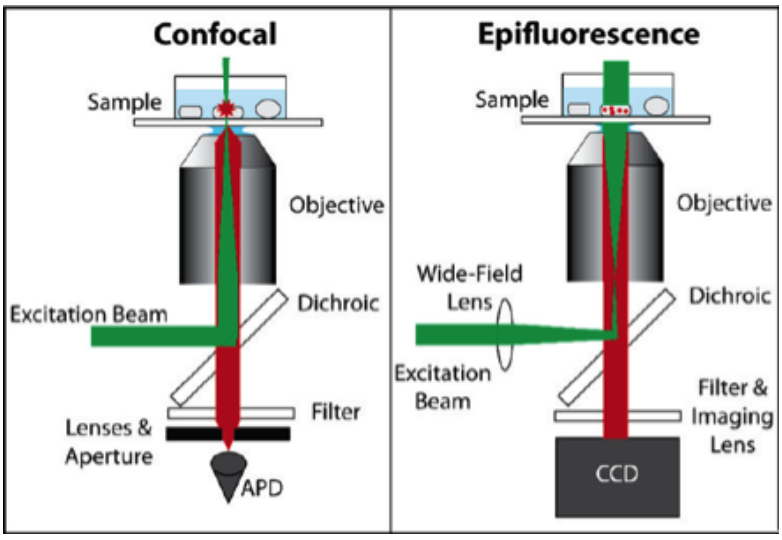

Figure 2.2.1 Optical pathways for fluorescence microscopy.
A pathway for confocal laser scanning microscopy is shown at left and one for epifluorescence microscopy is shown at right. Figure from [74].

Our laboratory and others have recently developed and validated confocal mode single-molecule photobleach step counting for measurement of small Aβ oligomer size at physiological concentrations. Dukes et al. tethered FAM (carboxyfluorescein) - labeled Aβ-biotin to a PEG-coated glass surface using a streptavidin-biotin linker; samples were prepared with 30 pM peptide. These samples were imaged in confocal scanning mode to obtain fluorescence photobleaching trajectories on single oligomers[80]. Dukes et al. showed that known accelerators of oligomerization (zinc, acidic conditions) did indeed promote formation of larger oligomers from the mostly monomeric starting mixture. Similarly, Ding immobilized single HiLyte Fluor 488-labeled oligomers on coverslips at 0.1 to 1 nM concentrations by spin-coating and obtained photobleaching trajectories in confocal scanning mode[10]. When specific oligomer populations were purified by gel filtration chromatography and applied to slides, the distribution of oligomers observed by single molecule photobleaching did indeed exhibit an increase in oligomers of that size and commensurate decreases in flanking oligomers. Both studies drew the conclusion that for Aβ labeled with a single fluorophore, photobleaching step count correlated well with the number of monomers present per oligomer.

Obtaining such trajectories in confocal mode does have a disadvantage in that large amounts of time are required for scanning samples and obtaining photobleach trajectories. As a result, acquiring data in a system that exhibits substantial changes over

time can be difficult. For studies in which interesting dynamics may be observed—for instance, diffusion of peptide on a membrane—other imaging modalities offer greater potential.

2.3 Total Internal Reflection Fluorescence (TIRF)

Total Internal Reflection Fluorescence (TIRF) microscopy has gained favor over the last 20 years as a method for achieving single molecule detection in samples with high background fluorescence. Like the confocal scanning microscopy method discussed above, TIRF mode imaging greatly reduces of out-of-plane fluorescence, but it also offers the advantage of obtaining wide field, real time images, so that both photobleaching trajectories (generally of static particles) and motion of diffusing or trafficked particles can be captured in the same data set.

2.3.1 Theory of TIRF Microscopy

Briefly, in TIRF, an illumination beam is directed toward the sample surface at just beyond the critical angle to normal. Due to the discrepancy between the index of refraction of a microscope coverslip (usually n_2 = 1.51-1.52) and that of the sample solution (n_1 = 1.3-1.4) or the air above a dry sample (n_1 = 1), the laser beam is completely reflected back into the coverslip, incidentally creating an evanescent fluorescent excitation field that penetrates, at most, a few hundred nanometers into the sample. The decay of the evanescent field intensity, moving upwards from the sample in the z-direction) is described by the following equation[81]:

$$I(z) = I(0)e^{-z/d} \qquad \text{Eq. 1}$$

The exponential decay distance, d, is determined by the angle of incidence θ, the wavelength of the incident light λ, and the respective indices of refraction in the coverglass n_2 and sample n_1, as follows[81]:

$$d = \frac{\lambda}{2\pi}(n_2^2 sin^2\theta - n_1^2)^{-1/2} \qquad \text{Eq. 2}$$

By modifying the angle of incidence, one can modulate the depth of penetration of the excitation field into the sample, thereby restricting excitation to those fluorophores near

the surface. This produces a vast reduction in background fluorescence as compared to epifluorescence mode imaging, a particular advantage for imaging single fluorophores in living cells.

TIRF geometry can be achieved by one of two generally used setups, a prism-based method or an objective-based method (Figure 2.3.1). We chose to use through-the-objective TIRF; although one major caveat of this method is the requirement of a high magnification, high numerical aperture (NA>1.45) objective lens, through-the-objective TIRF offers advantages in terms of the ease of switching between TIRF and epifluorescence and accessing one's sample.

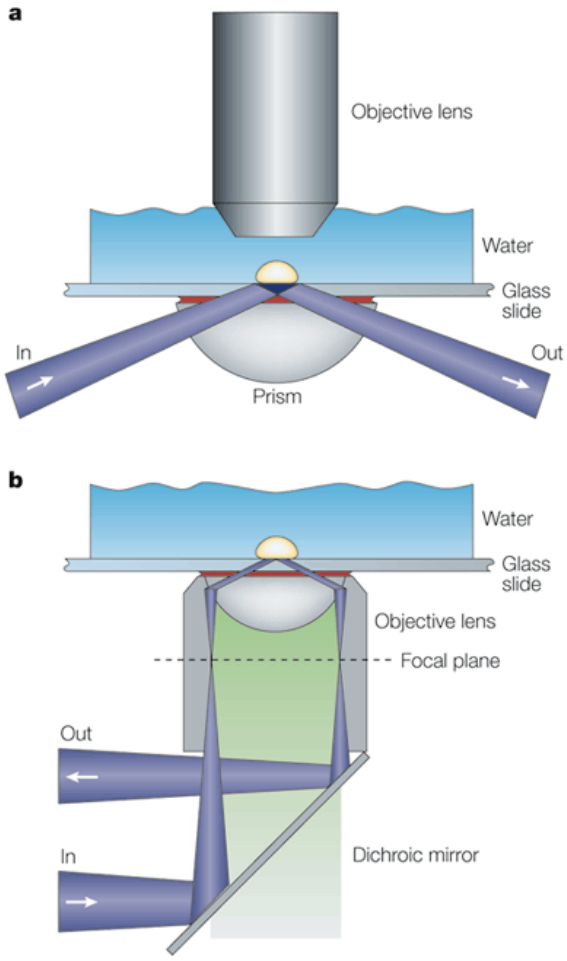

Figure 2.3.1 Two geometries for achieving Total Internal Reflection.
Shown are the prism-based (a) and through-the-objective based (b) configurations. Figure from [82].

In recent years, a number of groups have combined the single molecule photobleach method (Section 2.2) with TIRF microscopy in order to determine the number of subunits in cell membrane-localized proteins. Notable among these studies is Ulbrich and Isacoff's use of single molecule photobleaching to show that NMDA receptors composed of NR1 and NR3B subunits have a 2:2 stoichiometry, like the NR1:NR2B-containing receptor. Importantly, these studies were conducted on GFP-labeled proteins expressed and localized to the membranes of living *Xenopus laevis* oocytes[83]. Leake et al. used TIRF-mode single molecule photobleaching step intensity to estimate the number of GFP-MotB units per flagellar motor in living *E. coli* cells[84]. In both studies, photobleach steps were shown to be roughly equivalent in size. To achieve this result, TIRF penetration distance, laser power, and distance of each aggregate from the fluorophore must be equal across experiments. Given these conditions, however, such a result implies that only photobleaching step count but also initial particle fluorescence intensity can be used to measure oligomer size, at least for small aggregates.

As previously discussed, single molecule microscopy and the photobleaching step count method provide an opportunity to gain unique insight into amyloid-β oligomer size at physiological concentrations. Single molecule TIRF microscopy enables researchers to study the structure and dynamics of single protein aggregates on live cell membranes. The current work began with an effort to utilize these methods to determine the particular size distribution of Aβ oligomers that binds to living cells.

2.3.2 TIRF Microscopy: Data Acquisition and Analysis

Initial studies of single Aβ oligomers on live cell membranes were performed on a custom-built TIRF microscope, using an Argon positive laser (Coherent) for 488 nm illumination. After preliminary data revealed that autofluorescence prohibited single molecule detection at this wavelength (see Section 3.2 for discussion), further single molecule TIRF microscopy was performed on an Olympus IX-71 inverted microscope with 633 nm or 643 nm illumination. A HeNe red laser (633 nm, Uniphase) or a single-mode diode laser (643 nm, Power Technology, Inc.) was focused onto the back focal plane of a 60x, 1.45 NA Olympus PlanAPO TIRFM objective; laser power at the plane of

the coverslip was measured at 300 μW. Through-the-objective TIRF was performed by translation of a mirror just upstream of the objective lens. A multi-band pass SEMRock dichroic mirror was used to separate excitation from emission signal; a 620/60 excitation band pass filter (Chroma Technology Corporation) and 700/75 emission filter (Chroma Technology Corporation) were included in the setup. Images were acquired on a back-illuminated Ixon EMCCD camera, model DV887ACS-BV (Andor) and analyzed in ImageJ (for trajectories in solution) or in custom-written LabView photobleach trajectory software, as described (for spin-coated samples)[10].

2.4 Intensity-based Single Molecule Confocal Microscopy

As mentioned previously, both Ulbrich and Isacoff and Leake et al. offer evidence that fluorescence intensity as well as photobleach step count can be used to measure the stoichiometry of labeled protein aggregates in living cell membranes. We recently used confocal mode fluorescence intensity to measure oligomer size on black lipid membranes[70]. To measure oligomer size on living cells, we developed a protocol to correlate particles' confocal mode fluorescence intensity values with the number of Aβ monomers they contain. When laser power is below saturation, the fluorophore emission varies linearly with excitation power. Under these conditions, the slope of total intensity from a given volume versus the number of molecules present in the volume yields intensity-per-molecule. The fluorescence intensity of an oligomer can be divided by this value to yield the number of Aβ monomers present in the oligomer (assuming the quantum yields of the free dye and peptide-bound dye are the same, as discussed below).

2.4.1 Confocal Fluorescence Intensity Calibration

To determine the intensity of a single HL647 dye molecule in solution, a series of confocal scans were performed on various dilutions of HL647 hydrazide. The average intensity of a 1.6 μm by 1.6 μm by 1 μm volume element was measured at 10 nM HL647 hydrazide concentration increments from 0 nM to 60 nM (0 to 102 dye molecules per volume element). In this regime, intensity per number of molecules in a volume element

is linear, with a best-fit correlation coefficient of 0.996558. The slope of this line represents an intensity-per-molecule value that can be used to extract HL647-labeled Aβ oligomer size (Figure 2.4.1).

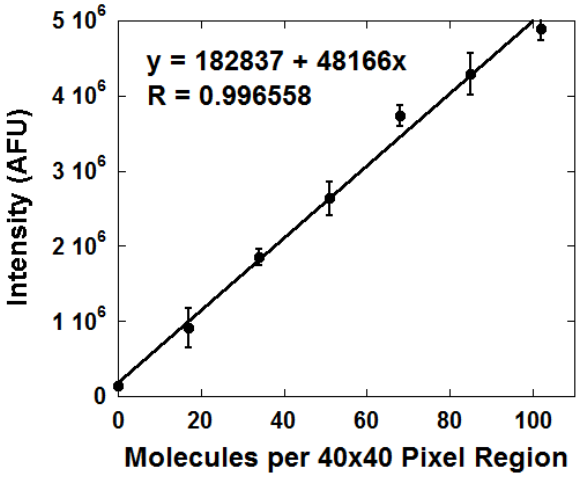

Figure 2.4.1 Confocal intensity calibration plot for single molecule studies.
Total fluorescence intensity in a 40 by 40 by 1 pixel (1.6 μm by 1.6 μm by 1 μm) volume element versus expected number of HiLyte Fluor 647 hydrazide molecules present in that element. Intensity measurements were made at dye concentrations of 0 nM to 60 nM. Error bars represent the standard deviation for four different experiments. The slope of this line represents the fluorescence intensity of a single dye molecule.

2.4.2 Fluorescence Lifetime Measurement

The validity of this calibration method requires the assumption that the fluorescence yields of HL647-labeled Aβ and free HL647 hydrazide in solution are identical. Collisional quenching from the attached peptide or differences in the local electronic environment might alter the efficiency of photon emission of the fluorophore in HL647-labeled Aβ. Fluorescence lifetime measurement was used to eliminate this possibility. For dynamic quenching, the ratio of intensity of the quenched fluorophore (I_q) to that of the unquenched fluorophore (I_0) is equal to the ratio of the fluorophore lifetimes (τ_q and τ_0, respectively) under each condition[85]:

$$\frac{I_q}{I_0} = \frac{\tau_q}{\tau_0} \qquad \text{Eq. 1}$$

Accordingly, fluorescence lifetimes of HL647 hydrazide and the HL647cAβ40 used in SH-SY5Y neurobastoma cell experiments were measured in imaging buffer on a custom-built fluorescence lifetime system, as described[70]. Fitting the fluorescence decay curves using the Exponential Series Method yielded lifetimes of 1.55 ± 0.24 ns for the free dye and 1.64 ± 0.09 ns for HL647cAβ40. Hence, the two lifetimes are equivalent within experimental error. Collisional quenching from Aβ40 does not alter the quantum yield of the dye in HL647cAβ40.

For primary hippocampal neuron studies, fluorescence lifetimes of HL647 hydrazide, HL647Aβ40, and HL647Aβ42 were assessed using the Time-Resolved Confocal Microscope ALBA system at the University of Michigan SMART (Single Molecule Analysis in Real Time) Center. Fitting the resulting decay curves yielded fluorescence lifetimes of 1.538 ± 0.009 ns for the HL647 hydrazide free dye, 1.646 ± 0.002 ns for the HL647Aβ40, and 1.688 ± 0.004 ns for the HL647Aβ42. The slightly increased lifetimes of the dye when bound to the peptide likely reflect slight changes to the local electronic environment. As these lifetimes are not equivalent within experimental error, the HL647 hydrazide fluorescence intensity per monomer was multiplied by 1.0702, the ratio of $\tau_{HL647AB40}$ to τ_{HL647}, obtain expected intensity per HL647Aβ40 monomer. For HL647Aβ42, the correction ratio (ratio of $\tau_{HL647AB42}$ to τ_{HL647}) was 1.0974, and for experiments with a 1:1 mix of the two peptides, the average of the two ratios, 1.0838, was used to determine expected monomer intensity.

Other factors may also affect the relative fluorescence efficiencies of the free dye and the peptide-bound dye when the fluorescently labeled peptide aggregates or associates with surfaces. One possibility is that oligomerization of the HL647-labeled Aβ peptide, its insertion into a biological membrane, or its interaction with a surface results in significant quenching. However, we have previously addressed these questions using Aβ40 N-terminally labeled with HiLyte Fluor 488 and established that oligomers up to 20 monomers in size have fluorescence decays that fit well to a single exponential, and fluorescence lifetime is not altered for aggregates of this size even after binding to (and insertion in) lipid bilayers[70]. As HL647cAβ40, HL647Aβ40, and HL647Aβ42, like HL488Aβ40, have N-terminally located fluorophores, it is reasonable that the

fluorophores on low-order oligomers also retain the lifetime of the dye attached to the free monomer under these conditions.

2.4.3 Single Molecule Photobleach Versus Integrated Intensity

To further verify the accuracy of this method, a distribution generated with our calibration was compared to one compiled from photobleach trajectories taken on a total internal reflection fluorescence (TIRF) microscope. Samples for both measurements were prepared by dilution of HL647cAβ40 to 50 nM in media over a kilned, autoclaved glass slide, which results in oligomers binding to the slide (Figure 3.5.1; Figure 2.4.2).

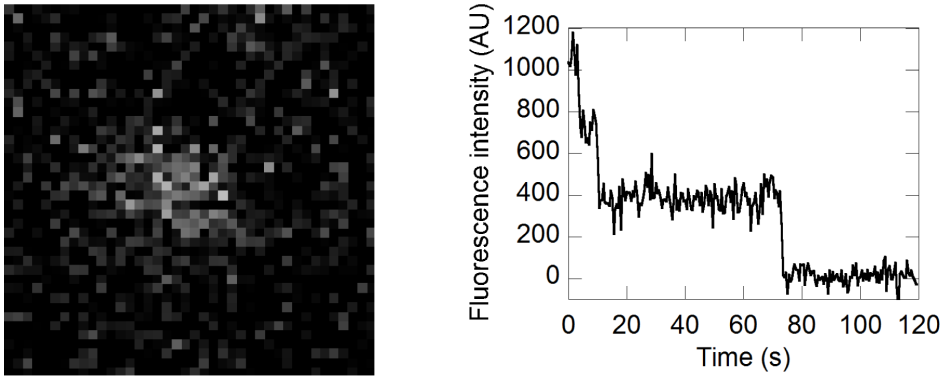

Figure 2.4.2 Data examples for confocal and TIRF single-molecule studies.
At left is an example of a 40 by 40 pixel (1.6 μm by 1.6 μm) region of interest (ROI) in the confocal mode; this ROI contains a slide-bound HL647cAβ40 particle with the integrated intensity of a trimer. To the right is an example photobleach trace taken from a Total Internal Reflection Fluorescence (TIRF) film. Three discrete photobleach steps can easily be identified, marking the particle as a trimer.

The oligomer size distributions obtained using the two methods were highly similar (Figure 2.4.3). In both samples, approximately 70% of oligomers fall in the monomer-to-dimer range, with roughly 30% trimers to hexamers.

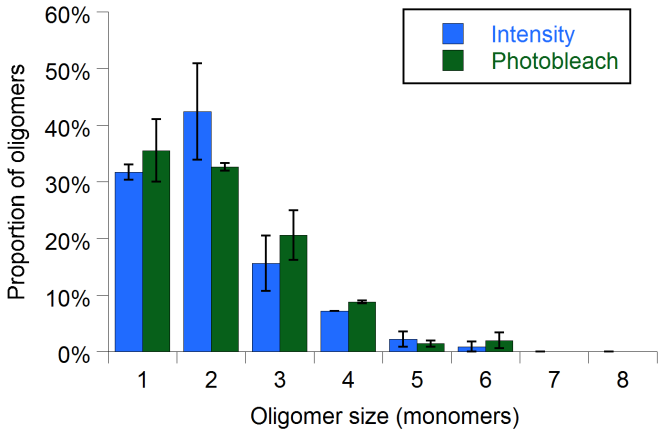

Figure 2.4.3 Confocal intensity and TIRF photobleaching produce similar results. HL647cAβ40 was diluted to 50 nM in media, bound a kilned glass slide, and imaged on the slide in solution, without cells present. Size was measured by confocal scan integrated intensity (*blue, N = 112 and 112 particles)* or by TIRF-mode single molecule photobleach step count (*green, N =100 and 117 particles*).

These distributions resemble those presented in the literature upon for Aβ40 in media or physiological buffers at nanomolar concentrations[8–10,86]. We note that unlike our earlier studies on dried samples[10], where we demonstrated significant variations in dipole orientation between monomers in a given oligomer, these measurements were made in solution. The data shows that this change allows orientational motion of the fluorophore emission dipoles, leading to the same time-averaged intensity for each monomer in an oligomer. The equal magnitudes of the photobleach steps for oligomers in solution observed here (Figure 2.4.2) support this assumption.

2.4.4 Confocal Microscopy: Data Acquisition and Analysis

Confocal laser scanning microscopy was performed on an Olympus FluoView 500 microscope mounted on an Olympus IX-71 frame. Images were acquired in line scan mode using an Olympus PlanAPO 60x, 1.42 NA oil immersion objective. The 488 nm line of an Argon laser was used to obtain FITC channel and Differential Interference Contrast (DIC) images, with illumination power of 140 μW, and a 633 nm HeNe red laser was used for HL647 excitation at a power of 28 μW. A BA660IF emission filter and Cy5 channel PMT settings of 850 volts, 6.0 gain, and 6% offset were used for all

single molecule experiments. Scans were taken at medium speed (10.67 seconds per scan). Scans of a 43 μm by 43 μm field of view were taken at 1024 by 1024 pixel resolution, yielding an image plane pixel size of 42 nm by 42 nm. Axial resolution (full width at half-maximum in the z-direction) was set to 1 μm by adjusting the confocal aperture diameter to 590 μm. Imaging was performed at 37°C under 5% CO_2 within 1 hour of exposure to Aβ.

For SH-SY5Y neuroblastoma cell data, an outline representing the cell membrane was drawn around the inner edge of the cell's image in the differential interference contrast (DIC) scan (Figure 2.4.4).

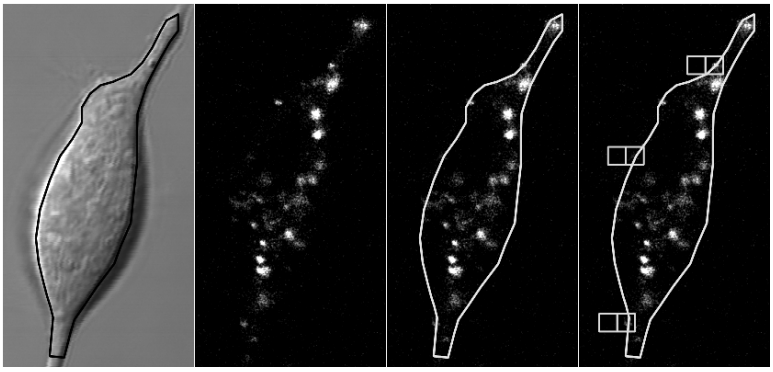

Figure 2.4.4 Data analysis for SH-SY5Y cell confocal single-molecule work.
From left to right: An outline was drawn onto the DIC image of each cell, just within the membrane. This outline was then pasted onto the corresponding fluorescence image. Edge-localized particles were identified as those spots whose maxima fell on or outside the outline and boxed with a 40 by 40 pixel region of interest. An adjacent off-cell 40 by 40 pixel region of interest was then identified as background.

This outline was then overlaid on the fluorescence scan. All diffraction-limited fluorescence spots whose maxima fell on or within 1 μm outside of this line were designated as "cell-bound oligomers". For primary hippocampal neurite studies, "cell-bound oligomers" were defined as those fluorescence spots whose maxima fell on or within 500 nm of a neurite. Irregularly shaped fluorescence spots, spots saturating the detector at four or more pixels, and spots associated with a clear non-membrane artifact (i.e., bigger than a resolution element) on the DIC image were rejected from the analysis. Remaining "cell-bound oligomers" were boxed with a 40 pixel by 40 pixel (approximately 1.6 μm by 1.6 μm) region of interest. The total photodetector output for such a square represents the intensity of a "volume element" containing the oligomer—a box 1.6 μm in length, 1.6 μm in width, and 1 μm in height with the oligomer at its center.

The total fluorescence counts for this region of interest were recorded. An adjacent off-cell square of the same dimensions was designated as "local background". The total counts for this box were then subtracted from the total counts present in the "oligomer" box to yield an integrated fluorescence intensity value for the oligomer. Dividing this value by the intensity per dye molecule (Figure 2.4.1) yields an oligomer size, in monomers, for each individual particle included in the analysis.

2.5 Additional Methods

While the majority of the data discussed in Chapters 3 and 4 was collected using single molecule microscopy, a number of other methods were utilized in preparing samples for these experiments and in conducting adjunct studies. Here we discuss peptide preparation and characterization, cell culture techniques, and fluorescence techniques used to study Aβ membrane permeabilization and binding location.

2.5.1 Amyloid-β(1-40) and (1-42) Preparation

Synthetic unlabeled amyloid-β(1-40), C2 maleimide HiLyte Fluor 647-labeled amyloid-β(1-40) (HL647cAβ40), N-terminally HiLyte Fluor 647-labeled amyloid-β(1-40) and (1-42) (HL647Aβ40 and 42, respectively), and HiLyte Fluor 647 hydrazide were from Anaspec. HL647cAβ40 was synthesized with an additional N-terminal cysteine residue, to which HiLyte Fluor 647 was attached by a C2 maleimide linkage. Amyloid-β (Aβ) peptides were dissolved in 1% NH_4OH at 0.1 mg/mL and vortexed for 30 seconds. Peptides were then lyophilized and stored at -20°C. To prepare fresh Aβ, single aliquots were dissolved in 10 mM sodium phosphate buffer, pH 7.4, at a concentration of 1 to 2 μM and pipetted 5 to 8 times to mix. Freshly prepared Aβ was used within 30 minutes to 1 hour. For spin-coated sample preparation, freshly solubilized HL647cAβ40, HL647Aβ40, or HL647Aβ42 was diluted to 0.5 nM in 10 mM sodium phosphate, pH 7.4, and a droplet of this was spin-coated onto a kilned glass slide.

2.5.2 SH-SY5Y Neuroblastoma Cell Culture and Imaging

SH-SY5Y neuroblastoma cells (ATCC) were maintained in phenol-red free 1:1 DMEM/Ham's F12 (Invitrogen) supplemented with 10% fetal bovine serum (Invitrogen) and 200 units/mL penicillin/streptomycin (Invitrogen). Prior to plating, 25 mm circular No. 1 cover glasses (Fisher Scientific) were kiln-baked at 500°C for 2 hours and then autoclaved. For live-cell imaging, cells were plated onto coverslips at a density of 28,000 cells per cm^2 and imaged 2 to 4 days following plating. Prior to imaging, cells were exposed to 50 nM HL647cAβ40 or unlabeled Aβ40 for 10 minutes at 37°C. Freshly dissolved peptide was added directly into media and pipetted over coverslips twice to mix. Following peptide exposure, coverslips were washed three times in Hanks' Balanced Salt Solution (HBSS), placed into a sampleholder and covered in 1 mL of HBSS for imaging.

2.5.3 Flow Cytometry

For flow cytometry experiments, adherent SH-SY5Y cells were grown to confluence in a 6-well plate, washed 1x with media, and treated for 90 minutes with 5μM peptide (one well each with HL488Aβ40, unlabeled Aβ40, HL488Aβ42 (lyophilized by Pamela Wong in 50% acetonitrile), or unlabeled Aβ42 (also lyophilized by Pamela Wong in 50% acetonitrile). Cells were then washed twice with D-PBS containing calcium and magnesium and removed from slides by 5 min incubation at 37°C with citric saline (1.35M potassium chloride, 0.15M sodium citrate). Cells were then resuspended in Annexin V binding buffer (10 mM HEPES, 140 mM NaCl, 2.5 mM $CaCl_2$, pH 7.4) at 2 x 10^6 cells/well and labeled with 10 μL per well Pacific Blue™ Annexin V (BioLegend) for 10 minutes in the dark. Cells were then resuspended in 300 μL/well PBS with 1% FCS for flow cytometry.

Flow cytometry was performed on a Becton-Dickinson LSR-II flow cytometer, using an Argon laser for 488 nm excitation and a vioflame laser for 405 nm excitation, with assistance from Bryan Petersen (Nicholas Lukacs laboratory, University of Michigan). PMT voltage settings were 410 V for FITC and 470 V for Pacific Blue channels. Data were gated by forward and side scatter to remove counts representing

clumped cells and debris. Data were also gated for Pacific Blue™ Annexin V staining, to reject dead cells from the analysis. A total of 94,000-98,000 cells per condition were counted.

2.5.4 HPLC

Gel filtration chromatography was performed at 23°C on a Shodex PROTEIN KW-802.5 size exclusion column. Injections of 20 µL of 8 µM labeled and unlabeled Aβ40 were run on the column in 10 mM sodium phosphate, 100 mM sodium chloride, pH 7.4, at a flow rate of 1 mL/minute. The column was calibrated for molecular weight under these conditions with the following protein standards: thyroglobulin (660 kDa), aldolase (158 kDa), bovine serum albumin (66 kDa), ovalbumin (43 kDa), peroxidase (40.2 kDa), adenylate kinase (32 kDa), myoglobin (17 kDa), RNAse A (13.7 kDa), and cyanocobalamin (1.35 kDa).

2.5.5 DiO Labeling and Colocalization

For membrane colocalization studies on HL647cAβ40, SH-SY5Y neuroblastoma cells were first incubated with or without 50nM HL647cAβ40 in 1 mL media for 10 minutes. An aliquot of 6 µL of 1 mM Vybrant DiO cell-labeling solution (Invitrogen) was then added and cells were swirled to mix. Cells were incubated at 37°C prior to washing and imaging as described above. Colocalization analysis was performed in ImageJ using an open-source macro entitled Colocalization (written by Pierre Bourdoncle, available on the web at http://rsbweb.nih.gov/ij/plugins/). Pixels where the ratio of HL647 to DiO fluorescence intensity was greater than 40% were designated "colocalized" regions.

2.5.6 Cell-bound Oligomer Quenching

For potassium iodide oligomer quenching, a 3 M solution of potassium iodide was prepared in HBSS and added onto SH-SY5Y cells to a final concentration of 300 mM. Cells were imaged before and after 2 minutes exposure to potassium iodide.

2.5.7 Calcium Leakage Experiments

SH-SY5Y cells were loaded with fluorescent calcium indicator Fluo4-AM (Invitrogen) at room temperature for 15 minutes at a concentration of 1.7 μM. Cells were then incubated in HBSS for an additional 15 minutes prior to washing and loading into sampleholders. 50 μL of 1 μM unlabeled Aβ40 or HL647cAβ40 were added by pipette to 950 μL HBSS in the sampleholder, for a final concentration of 50 nM. To induce maximal calcium leakage, ionomycin in HBSS was added by pipette to a final concentration of 6 μM. Fluo4-AM ΔF for each frame *n* was calculated as:

$$\Delta F = \frac{F_{c,n} - F_{bg,n}}{F_{c,i} - F_{bg,i}} \qquad \text{Eq. 2}$$

where $F_{c,n}$ represents cell body fluorescence in frame n, $F_{bg,n}$ represents fluorescence of an off-cell background region in frame n, $F_{c,i}$ represents initial cell body fluorescence, and $F_{bg,i}$ represents initial background fluorescence. Images were acquired in confocal mode on the microscope used for single molecule confocal studies or in epifluorescence mode on the microscope utilized for TIRF studies, using the 488 nm line of an Argon laser (Coherent) and a FITC filter cube.

2.5.8 Primary Rat Hippocampal Neuron Culture

Primary rat hippocampal neuron cultures were prepared in Michael Sutton's laboratory by Cynthia Carruthers and Christian Althaus, as described[87]. Cells were plated at 30,000/well on poly-D-lysine coated glass coverslips adhered to 35 mm wells (MatTek). Imaging experiments were performed between DIV 12 and DIV 18. For single

molecule oligomer size measurement experiments, cells were incubated for 10 minutes at 37°C in HBS (HEPES-Buffered Saline) containing 1 nM HL647Aβ, washed three times in HBS, and imaged at room temperature in HBS within an hour of exposure. For time course experiments, following initial incubation with 1 nM HL647Aβ, cells were placed back in the original media containing either no Aβ or 1 nM Aβ and incubated at 37°C for the time specified. Immediately prior to imaging, cells were washed three times in HBS and then imaged within an hour.

2.5.9 PSD95 Colocalization Experiments

To determine whether HL647Aβ oligomers localized to post-synaptic densities, HL647Aβ-exposed neurons were fixed and stained with an antibody for the post-synaptic density marker protein, PSD95. Cultures were treated with 10 nM HL647Aβ in HBS for 10 minutes, washed once in D-PBS, then fixed for 20 minutes in room temperature 2% paraformaldehyde / 2% sucrose. The cells were then washed three times in D-PBS, and cell membranes were permeabilized by 10 minutes exposure to 0.3% Tween 20 in D-PBS. Fixed, permeabilized cells were washed once in 0.3% Tween 20, stained for 1 hour with anti-PSD95 monoclonal mouse antibody 7E3-1B8 (Calbiochem, 1:400 dilution) or anti-Aβ monoclonal mouse antibody, clone W0-2 (Millipore, 1:2000 dilution), then stained for 1 hour with AlexaFluor488-labeled monoclonal anti-mouse antibody (Molecular Probes, 1:2000 dilution). Cells were then mounted in 1:9 D-PBS-glycerol and sealed with a coverslip.

Imaging was performed as described for single molecule confocal microscopy experiments, with illumination by 488 nm Argon laser, emission filtered with a BA 505-525 emission filter, and FITC channel PMT settings of 900V, 1.0x gain, and 5% offset.

2.5.10 HL647Aβ Binding Density on Axons and Dendrites

To assess HL647Aβ oligomer binding density on axons versus dendrites, HL647Aβ-treated neurons were fixed and stained with antibodies for the dendritic marker MAP2 and axonal neurofilament. Cultures were treated with 5 nM HL647Aβ40 or

HL647Aβ42 for 10 minutes, then washed three times in D-PBS. Fixation and permeabilization were performed as described in Section 2.5.9. Cells were then stained for 1 hour with anti-MAP2 mouse monoclonal antibody, clone HM-2 (Sigma, 1:2000 dilution), then for 1 hour with AlexaFluor488-labeled monoclonal anti-mouse antibody (1:2000 dilution). Pan-axonal neurofilament marker (clone SMI-312) mouse monoclonal antibody was labeled with the Zenon® 405 Mouse IgG Labeling Kit as per kit instructions (Molecular Probes). Cells were then stained with Zenon® 405-labeled anti-neurofilament antibody for 30-45 minutes in the dark, fixed for an additional 5 minutes in room temperature 2% paraformaldehyde / 2% sucrose, and mounted in 1:9 D-PBS-glycerol and sealed with a coverslip.

Imaging was performed as described for PSD95 experiments (Section 2.5.9), with additional illumination by a 405 nm diode laser. FITC channel PMT settings were 650V, 3.0x gain, and 5% offset, and CFP channel PMT settings were 650V (HL647AB40 experiment) or 700V (HL647AB42 experiment), 6x gain, and 5% offset.

2.5.11 eGFP Transfection and Spine Density Analysis

For preliminary studies on Aβ effects on spine density, DIV 11-12 primary rat hippocampal neurons were transfected with eGFP (provided by Amber McCartney, Sutton laboratory). Briefly, cells were placed in 500 µL fresh, prewarmed NGM (neuronal growth medium: Neurobasal A supplemented with 2% B27 and 1% GlutaMax) for 1-2 hours; conditioned media was saved. During incubation, eGFP was prepared as follows: eGFP plasmid was thawed at room temperature, and 0.5 µg eGFP plasmid (e.g. 1 µL for a 0.5µg/µL stock) per dish was added to ddH_2O, then 3.1 µL 2M calcium phosphate solution per dish was added to the DNA in water, to a final volume of 25 µL per dish. An equivalent volume of 2x HBS was then added to this in small amounts, vortexing at low speed for 3 seconds between additions. The plasmid solution was then incubated at room temperature for 20 minutes. 50 µL plasmid solution was then added dropwise to each dish of cells, and cells were incubated at 37°C, 5% CO_2 for 1-3 hours. Media containing plasmid was then removed and replaced with 1 mL fresh media (prewarmed at 37°C , in 10% CO_2). Cells were placed in a 37°C, 10% CO_2 incubator for

20 minutes, then washed 2x in prewarmed Neurobasal A and placed back in the original media.

After 24 hours, HL647Aβ42 was added to the media. Cells were incubated an additional 24 hours prior to imaging in confocal mode. Images were acquired in z-stack mode, with 20 scans per stack and a z-resolution of 0.4 µM, using 2x zoom with a 60x objective and PMT voltages in the FITC channel ranging from 400 V to 600 V. Images were analyzed manually for spine density per micron of neurite in ImageJ.

2.5.12 Single Particle Tracking and Lateral Diffusion Analysis

Particle tracking experiments with primary rat hippocampal neurons were performed on the same system used for TIRF mode studies, using a 300 ms exposure time. Coordinates of particles exhibiting motion were assessed by hand, and particle trajectories were obtained with the SpotTracker2D open-source macro for ImageJ, available at http://bigwww.epfl.ch/sage/soft/spottracker/ (courtesy of Daniel Sage, Biomedical Image Group, Ecole Polytechnique Federale de Lausanne, Switzerland)[88].

Diffusion coefficients were determined in LabView software custom-written by Chun-Chieh Chang (Gafni-Steel lab). Only trajectories with at least 15 consecutive frames were used with integration time of 300 ms. The mean square displacement (MSD) was calculated using the following formula:

$$\mathrm{MSD}(\mathrm{ndt}) = \frac{1}{\mathrm{N-n}} \sum_{i=1}^{\mathrm{N-n}} [(\mathrm{x_{(i+n)}} - \mathrm{x_i})^2 + (\mathrm{y_{(i+n)}} - \mathrm{y_i})^2] \qquad \text{Eq. 3}$$

where x_i and y_i are the coordinates of an object on frame i, N is the total number of frames of the trajectory, n is the number of intervals, dt is the time between two successive frames, and ndt is the time interval over which the displacement is averaged. The initial diffusion coefficient (D) was determined by fitting the first 2-5 points of the MSD plot versus time with $\mathrm{MSD(t)} = 4\mathrm{D_{2-5}t} + \mathrm{b}$, as referenced[67,73].

2.5.13 Primary Hippocampal Neuron Calcium Indicator Experiments

Calcium indicator experiments in primary hippocampal neurons were performed as described for SH-SY5Y cells (Section 2.5.7), with the exception that Fluo4-AM loading and imaging were performed in HBS rather than HBSS.

Chapter 3

Studies of Single Aβ Oligomers on SH-SY5Y Cells

3.1 Motivation for Live Cell Studies

Model membrane studies conducted by our lab and others have provided much mechanistic insight into amyloid-β's interactions with lipid membranes[28,29,70,76]. Experiments conducted in such model systems can yield quantitative data on binding affinity, association and dissociation rates, and dependence of binding on membrane charge and curvature. Additionally, these systems can be used to characterize the conditions under which amyloid peptides affect membrane conductance and to study the mechanism by which permeabilization occurs. However, the complexity of the membranes of hippocampal and cortical neurons with which extracellular Aβ likely interacts *in vivo* is difficult to approach with model systems. The lipid component of neuronal membranes alone includes sphingomyelin, phosphatidylcholine, phosphatidylethanolamine, inositol phospholipids, phosphatidylserine, cerebrosides, sulfatides, gangliosides, and free fatty acids[77]. Membrane integral proteins can also influence membrane fluidity and curvature, possibly affecting binding and insertion, and they provide a plethora of possible Aβ binding sites that are not represented in model membranes (see Introduction for details). In short, obtaining a complete picture of Aβ's interactions with membranes and how these phenomena relate to toxicity necessitates complementary studies on live cell membranes[89].

SH-SY5Y neuroblastoma cells are a commonly used model neuronal cell line. Composed of homogeneous N-type (neuronal-type) cells, this line was subcultured from SK-N-SH cells, a line taken from a neuroblastoma tumor in the 1970's; they exhibit several neuronal marker phenotypes and proliferate well in culture, making them highly suitable for *in vitro* live cell studies[90]. In recent years, these cells have been utilized frequently in the Alzheimer's research community for *in vitro* toxicity, permeabilization,

and uptake experiments[26,29,91]. We therefore chose to begin our development of live-cell single-molecule microscopy with SH-SY5Y cell experiments.

3.2 Autofluorescence Inhibits 488 nm Single Molecule Microscopy

Our previous work on the interaction of Aβ with model membranes has involved the use of a version of the peptide labeled with a single HiLyte Fluor 488 molecule (HL488Aβ40)[10,70]. However, initial attempts to perform single-molecule TIRF experiments with HL488Aβ40 on live cells were frustrated by extremely high autofluorescence levels in the 488 nm channel (Figure 3.2.1). With TIRF microscopy at this wavelength, determining whether Aβ bound to individual cells was problematic, due to the widespread and heterogeneous baseline fluorescence of the cells and the low number of individual cells which could be imaged over the course of a single experiment.

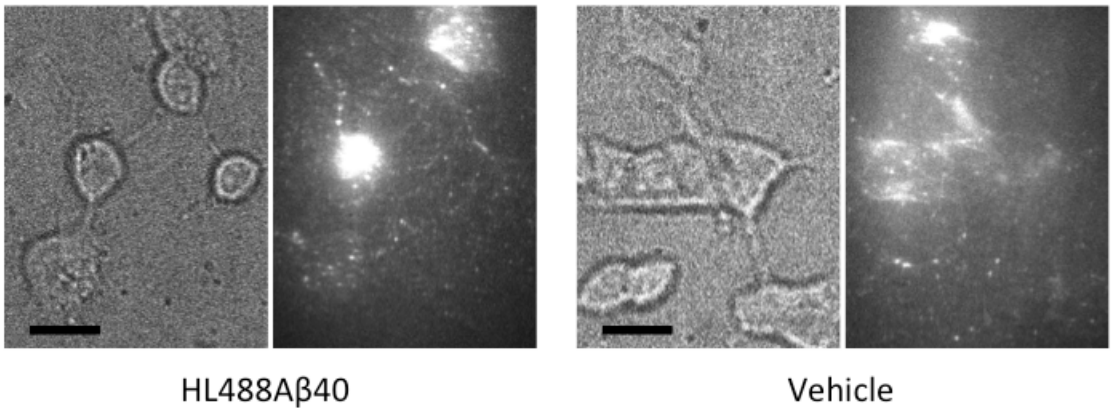

Figure 3.2.1 Autofluorescence obscures single molecule size determination at 488 nm. SH-SY5Y cells were treated with nanomolar HL488Aβ40 for several minutes; results are typical for concentrations up to 50 nM and treatment times of up to an hour. Scale bars, 10 μm.

Flow cytometry, by contrast, allows fluorescence measurements to be made on hundreds of thousands of individual cells during a single experiment. When SH-SY5Y cells were treated with 5 μM HL488Aβ for 90 minutes and a flow cytometry experiment was performed, results showed that on a population level, both HL488Aβ40 and HL488Aβ42 did bind to cells (Figure 3.2.2). Both peptides bound at two levels; cells in the main population exhibited only a small increase in fluorescence as compared to

controls, representing low-level binding, while less than 10% of cells in each sample exhibited high-level fluorescence, indicative of a high level of binding. Importantly, Annexin V staining was employed to screen out dead or dying cells, indicating that the cells exhibiting high-level binding do represent living cells.

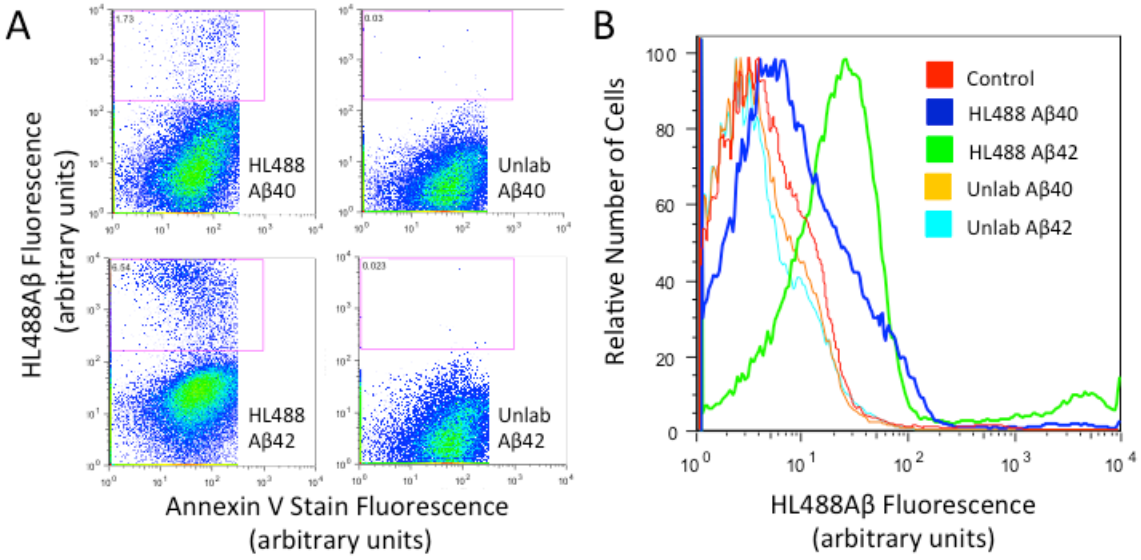

Figure 3.2.2 Flow cytometry demonstrates that HL488Aβ binds to SH-SY5Y cells. Low-level binding is seen in the main cell population in each group treated with the labeled peptide, and high-level binding is seen in a smaller population (roughly 2% of cells for HL488Aβ40, 7% for HL488Aβ42).

As these experiments indicated that binding was present on a population scale, autofluorescence appeared to be the main hindrance to single-molecule TIRF microscopy on live cells at 488 nM. This conclusion is consistent with the wide range of endogenous cellular fluorophores whose excitation maxima fall in the UV-to-low-visible range of the electromagnetic spectrum, three of which are listed in Table 3.2.1. These molecules have been implicated in autofluorescence studies as the main source of the strong mammalian cultured cell fluorescence emission observed in the 500 nm - 600 nm range[92,93].

Table 3.2.1 Endogenous cellular fluorophores may contribute to autofluorescence at 488 nm excitation [94].

Fluorophore	Excitation Maxima	Emission Maxima
NADH	340 nm	450 nm
Lipofuscin	340 nm - 395 nm	430 nm - 460 nm, 540 nm
FAD	450 nm	515 nm

In contrast, the far-red to infrared region of the electromagnetic spectrum has been recognized as a low-autofluorescence window, and probes at this wavelength have the advantage of lower competition from background fluorophores[95]. Therefore, some preliminary experiments were conducted in confocal mode as described in Chapter 2, using HiLyte Fluor 647-labeled Aβ. The autofluorescence level at this wavelength in confocal mode proved satisfactory for single-molecule studies, as discussed below (Figure 3.3.1; Figure 3.6.2).

3.3 Comparison of HL647cAβ40 and Unlabeled Aβ40

In order to examine the cell membrane binding behavior of Aβ40, nanomolar concentrations of Aβ40, labeled with HiLyte Fluor 647 at the N-terminus, were applied to SH-SY5Y neuroblastoma cells. The N-terminus of Aβ is solvent-exposed and therefore unlikely to be involved in the β-sheet formation which drives fibrillization[11,96]. Also, work done in our laboratory and others indicates that various forms of N-terminally labeled Aβ40 behave similarly to unlabeled Aβ40 in terms of fibrillization (Bateman, McLaurin, & Chakrabartty, 2007), ability to permeabilize synthetic membranes (Ding et al., 2009; Schauerte et al., 2010) as well as rat basophilic leukemia cell-derived membrane blebs (Figure 3.3.1), and toxicity to cultured cells[27].

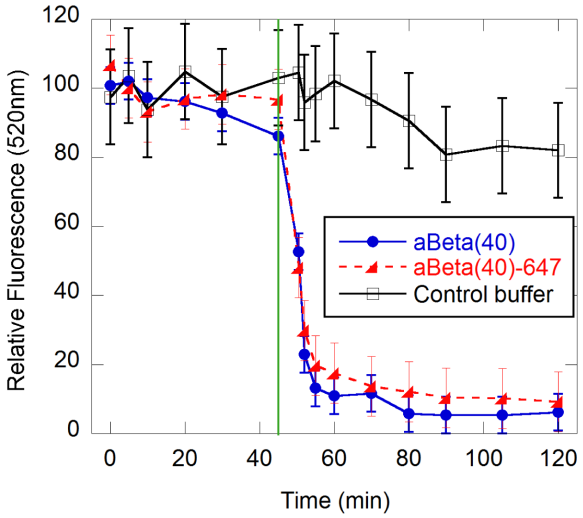

Figure 3.3.1: Unlabeled Aβ40 and HL647Aβ40 permeabilize cell-derived blebs.
Blebs are prepared from rat basophilic leukemia (RBL) cells. The blebs are first loaded with 5.7 µM calcein-AM. Blebs are then incubated on a kilned coverslip for 20 minutes, followed by gentle washing with buffer (10 mM HEPES, 150 mM NaCl, 2 mM $CaCl_2$, pH 7.4). Imaging begins after another 10 minutes. Then, 45 minutes after the blebs are first imaged (green line), 200 nM HL647Aβ40 (red), 200 nM unlabeled Aβ40 (blue), or buffer (black) is washed over the coverslip. Average bleb fluorescence for each sample is plotted over time. Error bars represent the standard deviation of 3 to 6 single blebs for each sample. Data courtesy of Kathleen Wisser and Joe Schauerte.

The current studies were performed using Aβ40 labeled with HiLyte Fluor 647 by a C2-maleimide linkage at the N-terminus. To confirm that this peptide behaves similarly to the unlabeled peptide on solubilization, we ran freshly prepared HL647cAβ40 and unlabeled Aβ40 on HPLC (Figure 3.3.2). Both peptides as a single peak with dimer-to-trimer molecular weight.

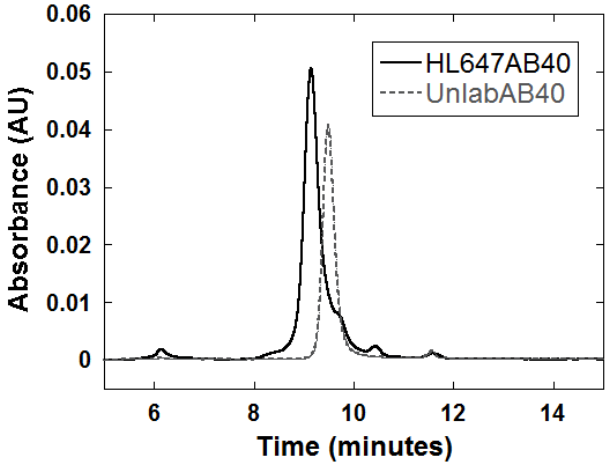

Figure 3.3.2: HPLC scans for 8 μM HL647cAβ40 and unlabeled Aβ40.
The 215 nm absorbance spectrum is shown (dark solid line, HL647AB40; gray dashed line, UnlabAB40). Both versions of the peptide elute primarily as a single peak with dimer-to-trimer molecular weight. An additional minor peak, visible in the void volume for the HL647cAβ0, may consist of peptide aggregates greater than 200 kDa; however, no fluorescent spots of the size and intensity expected for such large particles were observed in spin-coated samples examined by single molecule microscopy (see Figure 3.5.1). A limited number of large aggregates were detected in on-slide, in-solution samples, but these were a relatively small component (less than 10%) of the species observed.

3.4 HL647cAβ40 Binds Rapidly to SH-SY5Y Cells

To examine the questions of how Aβ40 binds to cell membranes and what species are present following binding, we applied HL647cAβ40 to live neuroblastoma cells at near physiological peptide concentrations and measured the integrated intensity of cell-bound particles. Cells were imaged following a 10-minute exposure to 50 nM HL647cAβ40 in media; in order to obtain cross-sections through the cell membranes, the objective was focused at a z-plane that fell halfway between the apical and basal portions of the cell membrane.

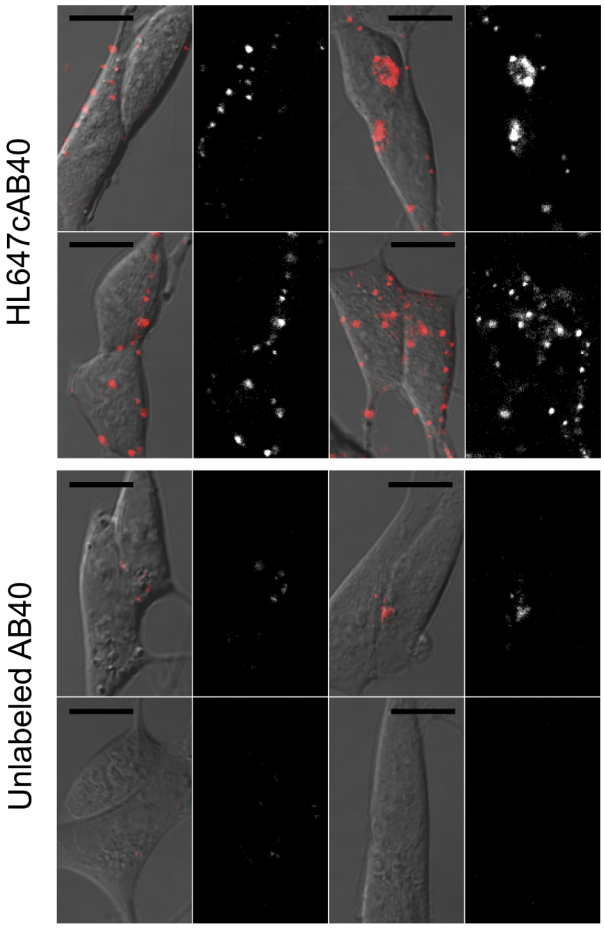

Figure 3.4.1: SH-SY5Y cells treated with HL647cAβ40 or unlabeled Aβ40.
Cells were treated with 50 nM Aβ for 10 minutes. Differential Interference Contrast images with confocal mode HL647 channel fluorescence overlaid in red are shown to the left of the corresponding HL647 channel only images. Scale bars, 10 μm.

Representative images of cells exposed to HL647cAβ40 and unlabeled Aβ40 (Figure 3.4.1) reveal both internal and surface-localized fluorescent particles in the HL647cAβ40 samples. Some form of membrane binding is believed to be a key step in toxicity directly mediated by Aβ40, and while several groups have observed internalization of fluorescently labeled Aβ40 and Aβ42 by neuroblastoma cell lines[27,91], only one has reported binding to live cells at physiological concentrations[72]. During analysis, we focused on measuring the size of those particles that were edge-localized (as this is where membrane-bound oligomers could be most clearly identified).

3.5 Fresh HL647cAβ40 Contains Primarily Monomers

To study how Aβ40 oligomerization and binding occur at physiological concentrations, we wished to begin with monomeric Aβ40. We therefore examined the size distribution of oligomers present in freshly dissolved HL647cAβ40 samples by recording photobleach trajectories on dry, spin-coated peptide (left image in Figure 3.5.1; Figure 3.5.2).

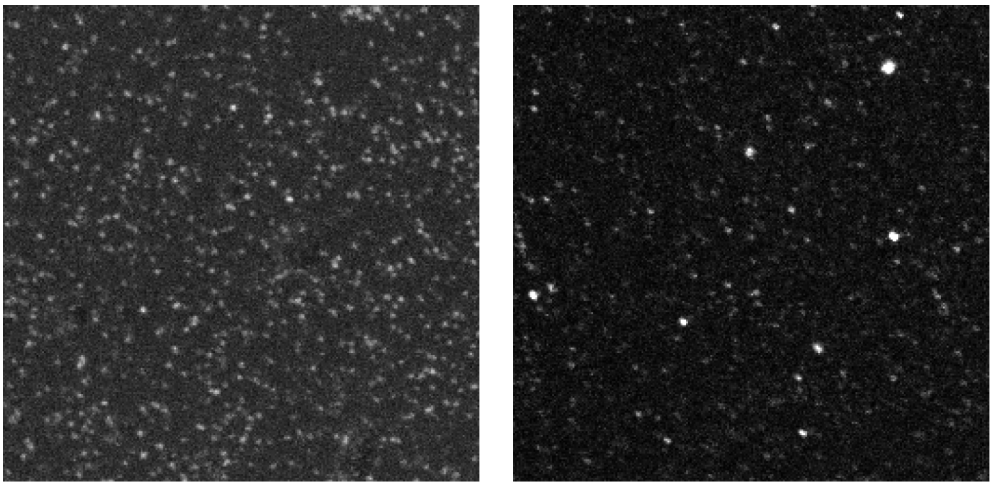

Figure 3.5.1 Spin-coated and on-slide, in solution HL647cAβ40.
The confocal image on the left depicts single molecules of dry HL647cAβ40. A droplet of 0.5 nM HL647Aβ40 in 10 mM sodium phosphate buffer, pH 7.4, was spin-coated onto a kilned glass slide. The confocal image on the right shows single molecules of HL647cAβ40 adhered to a glass slide after ten minutes' incubation of the slide with 50 nM peptide in media. Frames are 43 μm by 43 μm.

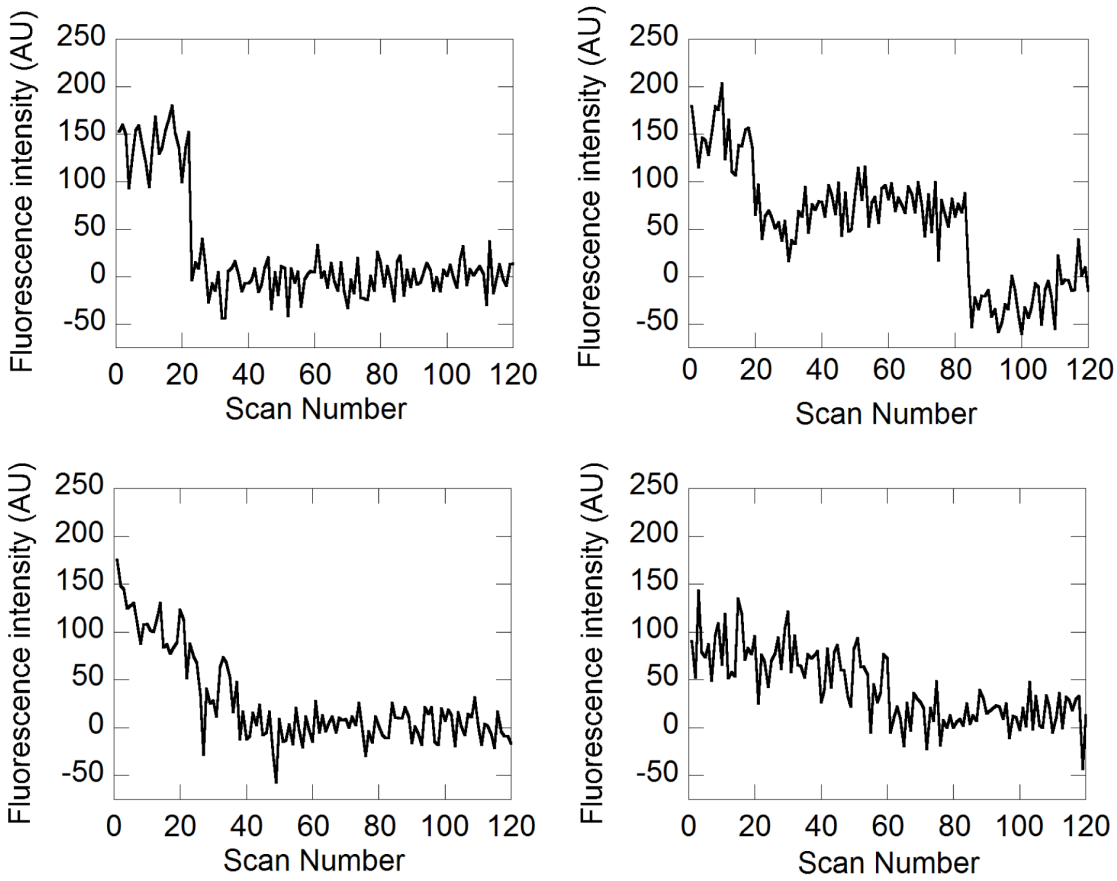

Figure 3.5.2 Typical confocal mode photobleach traces for HL647cAβ40.
Peptide was diluted to 0.5 nM and spin-coated onto a kilned glass coverslip. An example monomer trace is shown at top left; an example dimer is shown at top right. Example trajectories for two spots that do not photobleach in digital steps are shown at bottom left and right. Approximately 65% to 70% of particles bleached in clean, digital steps. Of these, 83% ± 3% bleach as monomers, and 15% ± 3% bleach as dimers. Of the particles that did not bleach in single steps, 5% ± 1% had intensities greater than was typical for observed monomers and dimers.

Of spots with clean photobleach traces, 83% ± 3% bleach as monomers and 15% ± 3% bleach as dimers (Figure 3.5.3). These results led us to conclude that the majority of freshly dissolved HL647cAβ40 is monomeric or dimeric.

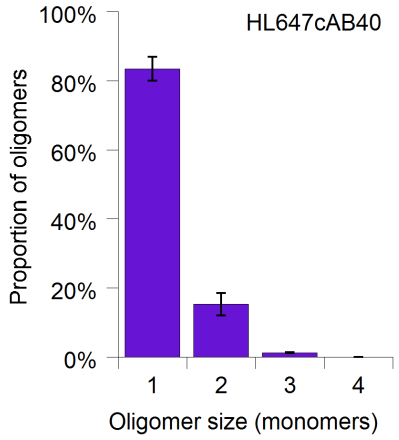

Figure 3.5.3 Oligomer size distribution for freshly solubilized HL647cAβ40.
Peptide was diluted to 0.5 nM in 10 mM phosphate buffer and spin-coated onto a kilned glass slide (*purple, N = 70 and 91 particles*). Size was measured by counting photobleach steps in sequences of confocal scans. Error bars represent the standard deviation for 2 experiments.

3.6 Small Oligomers Bind to the Membranes of SH-SY5Y Cells

Even a short incubation in media at 37°C results in some formation of oligomers in the trimer-to-hexamer size range. Interestingly, however, comparing the size distribution obtained for on-cell oligomers with the on-slide distribution (Figure 3.6.1) reveals a small decrease in the numbers of dimers and trimers observed on cells.

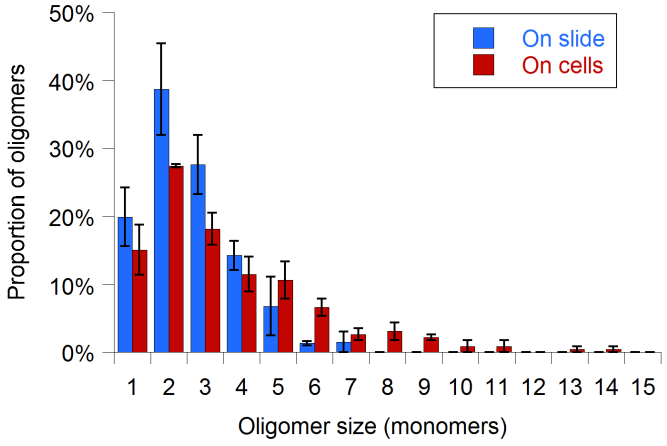

Figure 3.6.1 Oligomer size distributions for HL647cAβ40 on slide or on cells.
Peptide was diluted to 50 nM in media and bound to the slide in samples containing cells (*blue, N = 119 and 122 particles*) and bound to cells (*red, N = 114 and 112 particles*).

Conversely, particles with intensities corresponding to oligomer sizes from heptamers to 14-mers comprise a significant component of the on-cell distribution (10.6%), while the largest measurable oligomers observed on slides are heptamers (1.5% of the total on-slide distribution). The oligomer size distribution on the cell surface is thus shifted towards larger aggregates. (Note: These histograms exclude rarely detected spots with full width at half-maximum exceeding 250 nm and particles saturating the detector at more than three pixels—20-mers and larger by integrated intensity).

A prominent concern in live-cell single molecule microscopy involves signal contamination by autofluorescence. As an autofluorescence control, we performed our analysis on cells treated with unlabeled Aβ40. Figure 3.6.2 shows that the vast majority of detected spots in the HL647cAβ40 sample indeed represent fluorescently labeled peptide. Additionally, all of the autofluorescent spots detected by our analysis in the unlabeled Aβ40 sample have integrated fluorescence intensities that place them in the monomer-to-tetramer range.

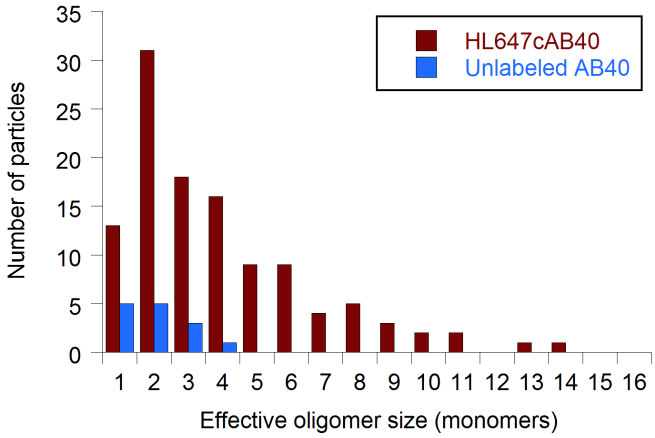

Figure 3.6.2 Raw oligomer size distributions for HL647cAβ40 and unlabeled Aβ40.
The analysis protocol was performed on similar numbers of cells treated with labeled (*crimson, N = 60 frames, 117 particles detected*) and unlabeled Aβ40 (*blue, N= 63 frames, 14 particles detected*). Both distributions were obtained using confocal mode integrated intensity.

3.7 Edge-localized HL647cAβ40 Oligomers are Membrane-bound

Potassium iodide quenching studies were performed to determine whether edge-localized HL647cAβ40 oligomers were solvent-accessible. Iodide, a well-known

collisional quencher, has formerly been used to characterize live cell-associated Aβ40 aggregates[71]. We imaged cells treated for 10 minutes with 50 nM HL647cAβ40 before and after the addition of 300 mM potassium iodide (Figure 3.7.1A).

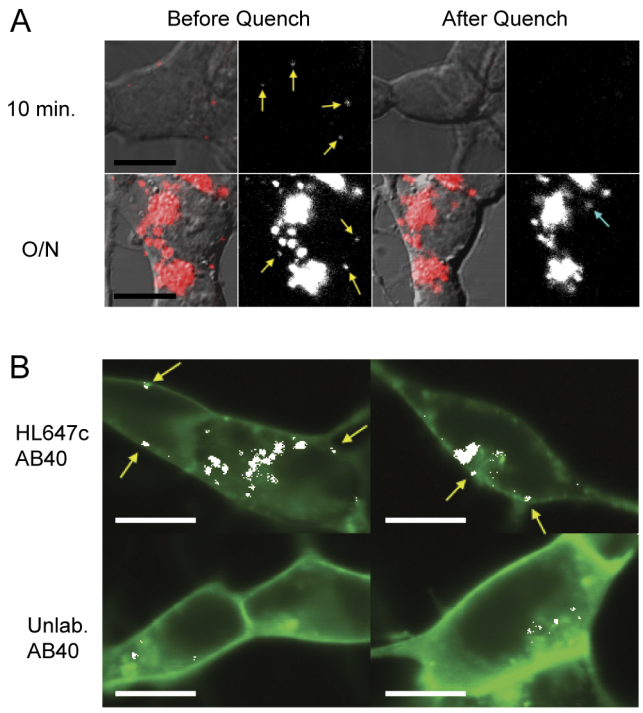

Figure 3.7.1: HL647cAβ40 is membrane bound.
(A) Colocalization images of cells treated with 50 nM labeled or unlabeled Aβ40 for 10 minutes prior to labeling with the lipophilic membrane marker, DiO. HL647 fluorescence is shown in red, DiO fluorescence in green, and pixels where the two are colocalized in white. Edge-localized fluorescent particles colocalizing with DiO are marked with yellow arrows. Scale bars, 10 µm. (B) Cells treated for 10 minutes or overnight with 50 nM HL647cAβ40 were imaged before and 2 minutes after addition of 300 mM potassium iodide. HL647cAβ40 oligomers that quench are marked with yellow arrows. New fluorescence spot (marked with teal arrow) presumably represents an endosome containing HL647cAβ40 which has migrated into the image plane during the incubation period. Scale bars, 10 µm.

Under these conditions, cell-perimeter localized peptide was highly susceptible to quenching. Interestingly, the majority of large internalized aggregates in cells exposed to 50 nM peptide overnight did not quench. Subsequent experiments verified that potassium iodide is able to permeate cells and quench fluorophores localized to the cytoplasm (Figure 3.7.2).

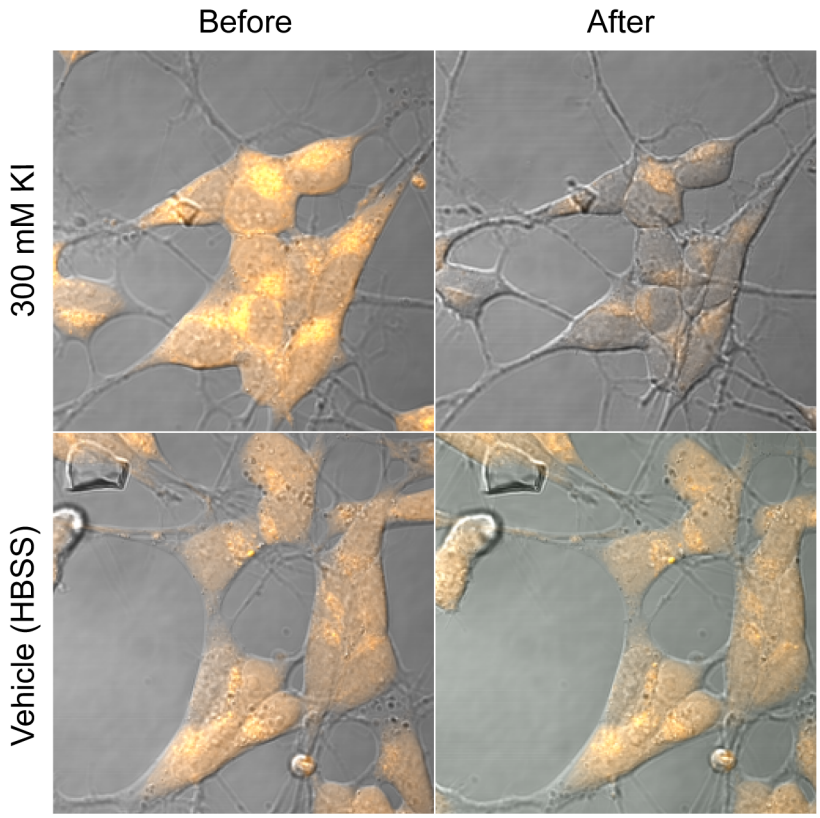

Figure 3.7.2: Potassium iodide permeates quenches internal fluorophores.
Confocal images of cells loaded with the cytoplasmic marker CellTracker™ Orange CMTMR (5- (and-6) - (((4-chloromethyl) benzoyl) amino) tetramethylrhodamine) (Invitrogen), before and after addition of potassium iodide to a final concentration of 300 mM (top row) or vehicle (Hanks' Balanced Salt Solution) (bottom row). The collisional quencher potassium iodide permeates the cell membrane quenches internal (cytoplasmic) fluorescence. Images are 43 μm by 43 μm.

Late stage aggregate quenching resistance may represent a fundamental change in aggregate structure[71] or an inability of iodide ions to permeate the endosome-lysosome system.

We also stained cell membranes with a lipophilic membrane dye, DiO, and performed colocalization studies. The vast majority of the HL647cAβ40 signal is colocalized with DiO (Figure 3.7.1B), suggesting that HL647cAβ40 in and on the cell is nearly all membrane-associated, bound to membrane-associated proteins, or enclosed in membrane-bound vesicles.

3.8 HL647cAβ40 and Unlabeled Aβ40 Induce Little Calcium Leakage

Application of either extracellular Aβ at supraphysiological concentrations or of chemically prepared oligomers[26,97] has previously been shown to result in dramatic calcium influx (3-fold or greater increases in calcium indicator fluorescence), and this effect was observed within seconds in a majority of cells. To test whether freshly prepared Aβ permeabilized cell membranes to calcium at physiological Aβ levels, SH-SY5Y cells were loaded with the fluorescent calcium indicator Fluo4-AM and exposed to 50 nM Aβ. The calcium ionophore ionomycin was used as a permeabilization control. Only a small proportion (roughly 10%) of cells treated with unlabeled Aβ40 (Figure 3.8.1A) or HL647cAβ40 (Figure 3.8.1B) exhibited any increase in fluorescence as compared to controls (Figure 3.8.1C). Observed fluorescence increases were less than 2-fold and occurred gradually over the course of 3 to 5 minutes.

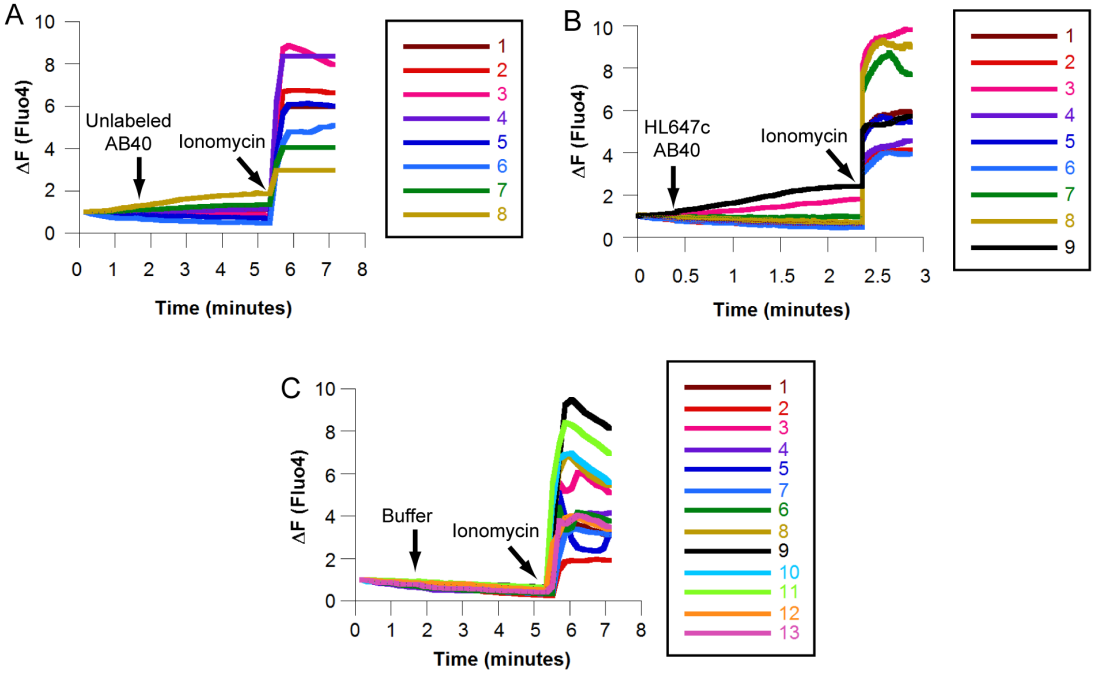

Figure 3.8.1: Physiological Aβ40 levels induce low level calcium leakage.
(A) Fluo4 fluorescence intensity plot for 8 cells treated with unlabeled Aβ40 and imaged by sequential confocal scans. Unlabeled Aβ40 was added to 50 nM after 1 minute and 40 seconds; ionomycin was added to 6 µM after 5 minutes and 20 seconds. (B) Plot for 9 cells treated with HL647cAβ40 and imaged in epifluorescence. HL647cAβ40 was added to 50 nM after 25 seconds; ionomycin was added to 6 µM after 2 minutes and 20 seconds. (C) Plot for 13 cells treated with vehicle and imaged by sequential confocal scans. 10 mM sodium phosphate was added to 50 nM after 1 minute and 40 seconds; ionomycin was added to 6 µM after 5 minutes and 20 seconds.

3.9 Fresh HL647cAβ42 Contains Primarily Monomers

As Aβ42 is generally acknowledged to be both more fibrillogenic and more neurotoxic than Aβ40, we wanted to compare the size distribution of Aβ42 oligomers on neuroblastoma cells to that obtained for Aβ42. To determine the size distribution of HL647Aβ42 oligomers in freshly prepared peptide, newly dissolved HL647Aβ42 was spin-coated onto a kilned glass slide and imaged in TIRF mode. Oligomer sizes were measured by single-molecule photobleach step counting .

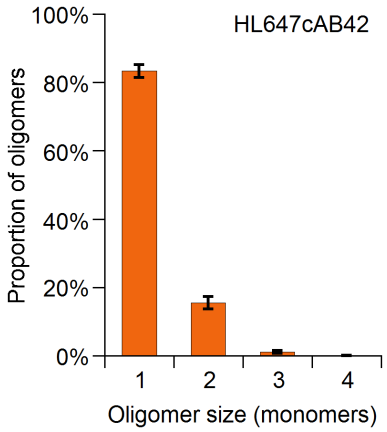

Figure 3.9.1 Oligomer size distributions for freshly solubilized HL647cAβ42.
Peptide was diluted to 0.5 nM in 10 mM phosphate buffer and spin-coated onto a kilned glass slide (*orange, N = 471, 255, and 364 particles*). Size was measured by counting photobleach steps in TIRF mode image sequences. Error bars represent the standard deviation for 3 experiments.

As shown in Figure 3.9.1, 83% of analyzable traces bleached as monomers, and 15% as dimers, indicating that the majority of freshly solubilized HL647cAβ42 is exists as monomer.

3.10 HL647cAβ42 Binds Sparsely to SH-SY5Y Cells

When SH-SY5Y cells were treated for 10 minutes with 50 nM HL647cAβ42 and imaged in single-molecule confocal mode, single particles were visualized both inside cells and along the cells periphery. As seen in the representative images in Figure 3.10.1, while the edge-localized oligomers observed were generally comparable in brightness those seen in the HL647cAβ40 samples, the overall number of edge-localized oligomers

per cell was greatly reduced. Autofluorescence was therefore slightly higher in comparison to the number of observed "cellbound" oligomers.

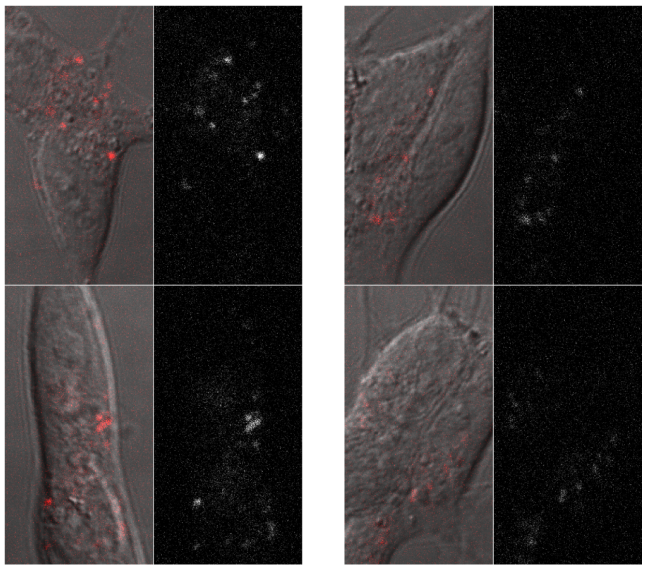

Figure 3.10.1 SH-SY5Y cells treated with HL647cAβ42 or unlabeled Aβ42.
Cells were treated with 50 nM peptide for 10 minutes and then imaged in single-molecule confocal mode. Fewer particles were detected per cell in comparison to experiments with HL647cβ40 (see Figure 3.4.1).

Furthermore, a greater proportion of these edge-localized particles saturated the detector, reducing the overall number of measurable edge-localized oligomers from roughly 2 per cell in HL647cβ40-treated cells (Figure 3.6.2) to slightly over one per cell in HL647cAβ42-treated samples (Figure 3.10.2).

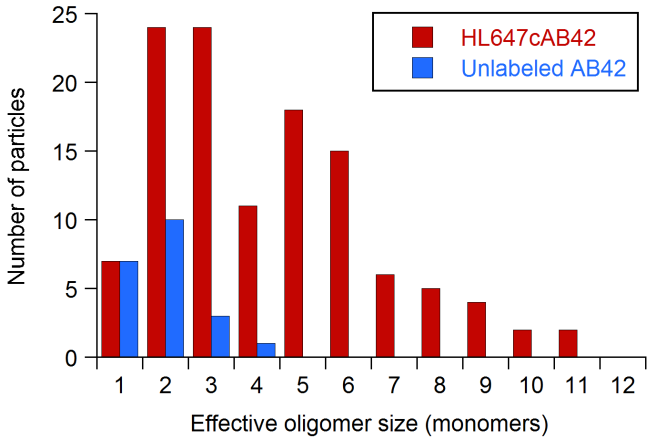

Figure 3.10.2 Raw oligomer size distributions for HL647cAβ42 and unlabeled Aβ42. The analysis protocol was performed on similar numbers of cells treated with HL647cAβ42 (*red, N = 104 frames, 118 particles detected*) and unlabeled Aβ42 (*blue, N= 104 frames, 21 particles detected*). Data is compiled from 3 separate experiments. Both distributions were obtained using confocal mode integrated intensity.

Due to the reduced yield of these experiments in terms of data per image and the difficulty of interpreting these distributions in the context of higher levels of internalized peptide, SH-SY5Y neuroblastoma cells studies with HL647cAβ42 were concluded after the 3 trials shown above. However, these results do show that HL647cAβ42 and HL647cAβ40 form similarly sized oligomers on SH-SY5Y cells, with the mode of the distribution falling in the dimer-to-trimer range for both peptides. Decamers to 14mers were the largest measurable oligomers detected in both samples and comprised a small portion (less than 10%) of the overall population.

Calcium indicator experiments were also conducted on Fluo4-AM-loaded SH-SY5Y cells treated with concentrations ranging from 1 nM up to 1 μM unlabeled Aβ42. Results were similar to those obtained with labeled and unlabeled Aβ40 (data not shown), with a small minority (<10%) of cells exhibiting transient, low-level calcium leakage on exposure to the peptide (data not shown).

3.11 Chapter Summary

We used single particle fluorescence intensity measurements to obtain direct optical evidence that small Aβ oligomers bind to living SH-SY5Y neuroblastoma cells at

near physiological (50 nM) Aβ concentrations. Results indicate that cell-bound Aβ40 and Aβ42 species range in size from monomers to hexamers and greater, with the majority of bound oligomers falling in the dimer-to-tetramer range. Furthermore, while low-molecular weight oligomeric species do form in solution, the membrane-bound oligomer size distribution is shifted towards larger aggregates, indicating either that bound Aβ oligomers can rapidly increase in size or that these oligomers cluster at specific sites on the membrane. Calcium indicator studies demonstrate that small oligomer binding at physiological concentrations induces only mild, sporadic calcium leakage in SH-SY5Y neuroblastoma cells.

Chapter 4

Studies of Aβ40 and Aβ42 on Primary Neuron Neurites

4.1 Motivation for Primary Rat Hippocampal Cell Studies

Single-molecule investigation of HL647Aβ40 oligomer size on SH-SY5Y neuroblastoma cells demonstrates that oligomers grow or cluster rapidly following binding to live cells, even at near physiological concentrations. However, the paucity of Aβ-induced calcium leakage in these cells suggested that toxicity may be associated with features unique to neurons. Interest in Aβ oligomer effects on structures and functions particular to neuronal cells has skyrocketed in the past 10 years, in part because synaptic loss is one of the earliest markers of AD[98]. While studies in immortalized neuronal cell lines provide useful insight into biophysical interactions of the peptide with real cell membranes, their similarity to real neurons is limited. In particular, these cells generally do not form active electrical signaling networks, axonal or dendritic polar morphology, dendritic spines, or functioning synapses.

By contrast, neurons in primary hippocampal cell cultures share many more morphological and functional traits with neurons in the brain. Measures of synaptic plasticity such as long-term potentiation have been found to be dampened by Aβ exposure in brain slices[30] and can also be studied in primary cell cultures[99]. The level of complexity reached by neurites in these preparations enables their use in studies of Aβ's effects on neurite structure and composition. Dendritic spines can be visualized in primary hippocampal cell cultures by labeling with fluorescent proteins or specific post-synaptic density markers, and several groups have utilized this technique to demonstrate that Aβ can decrease spine density[35,100] Finally, many possible synapse-specific Aβ receptor proteins have been identified on cells in primary hippocampal cultures[65,67,68]. Importantly, organotypic brain slices also offer the abililty to observe all of these effects. Fluorescence microscopy in living slices is notably more difficult, however, and two-

photon methods are often necessary to obtain low enough background fluorescence to visualize the desired fluorophores[101]. Here we show that single-molecule microscopy of HL647Aβ is feasible on the neurites of primary hippocampal neurons in culture. Evidence is presented for interesting differences between HL647Aβ40, HL647Aβ42, and 1:1 mixed oligomers' binding to and evolution on neurites. Initial neurite-bound HL647Aβ40 and HL647Aβ42 oligomers are larger than those bound nonspecifically to coverslips, and grow little over the course of an additional 48 hours. A 1:1 mix of the two peptides, however, binds initially to neurites as very small oligomers, and these oligomers grow substantially over the next 2 days. These results have important implications for Alzheimer's disease. Familial AD-associated mutations in presenilins 1 and 2 significantly increase Aβ42: Aβ40 ratio in transfected cultured cells and transgenic mice[102–104], and higher Aβ42:Aβ40 ratio is correlated with earlier age-of-onset in humans with these mutations[105,106]. Our results imply that localized increases in the Aβ42:Aβ40 ratio, independently of changes in overall Aβ concentration, significantly alter the kinetics of on-membrane oligomer growth.

We also demonstrate that these early oligomers do not preferentially bind to synapses. Finally, we present preliminary experiments that illustrate how working in this system opens up prospects for studying oligomer stoichiometry and evolution in combination with synaptotoxicity and changes in neuronal calcium homeostasis.

4.2 Fresh HL647Aβ40 and Aβ42 Contain Primarily Monomers

For experiments with primary rat hippocampal neurons, we utilized Aβ40 and Aβ42 N-terminally labeled with HiLyte Fluor 647 (HL647Aβ40 and HL647Aβ42). According to a recent report, HL647Aβ40 aggregates at the same rate as unlabeled Aβ40 in ThT assays, and fibrils formed from mixed HL647Aβ40 and HL488Aβ40 have similar morphology to fibrils formed from unlabeled peptide[107]. As with SH-SY5Y cell experiments, we began our study of Aβ oligomer growth and binding by ascertaining that freshly prepared labeled peptide contained primarily monomeric peptide. Accordingly, spin-coated samples were imaged in TIRF mode, and oligomer size was measured by the

single-molecule photobleach step counting method. Over 85% of particles bleached as monomers in both samples.

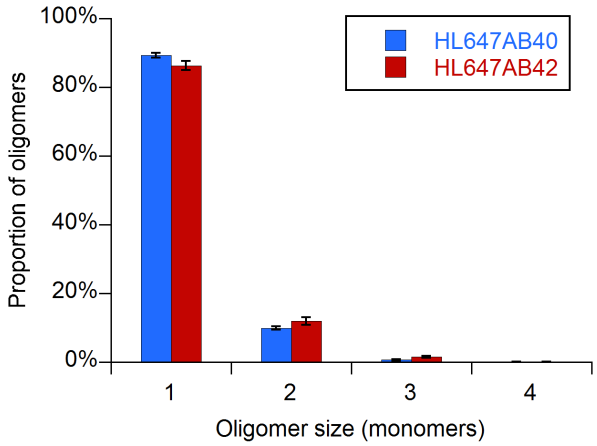

Figure 4.2.1 Oligomer size distributions for freshly prepared HL647Aβ40 and Aβ42. The majority of both are present as monomer. Measurements were made in TIRF mode, using single-molecule photobleach step count to determine oligomer size, and proportions represent the averages for three separate films *(N = 326, 225, and 227 particles for HL647Aβ40; N = 522, 464, and 408 particles for HL647Aβ42)*. Error bars represent S.E.M.

We conclude from these data that freshly prepared HL647Aβ40 and HL647Aβ42 contain mostly monomeric peptide.

4.3 Neurite Autofluorescence is Negligible

Initial studies of HL647Aβ40-treated and control primary rat hippocampal cells indicated cell bodies exhibited prohibitive levels of autofluorescence at single-molecule sensitivity settings. Neurites, however, had exceedingly low autofluorescence levels, and HL647Aβ40 appeared to have an extremely high affinity for these structures. Approximately 10 minutes' exposure at 50 nM HL647Aβ40 produced images with too high a binding density for measurement of single oligomer size. Exposure concentration was hence titrated to produce appropriate fluorescent particle density for single molecule studies. We found that 10 minutes exposure at only 1 nM HL647Aβ40 resulted in significant binding at a low enough density for single oligomer size measurements to be performed.

To quantify autofluorescence in these experiments, we compared single oligomer size data from equal numbers of confocal images of neurites treated with 1 nM HL647Aβ40 and 1 nM unlabeled Aβ40 (Figure 4.3.1).

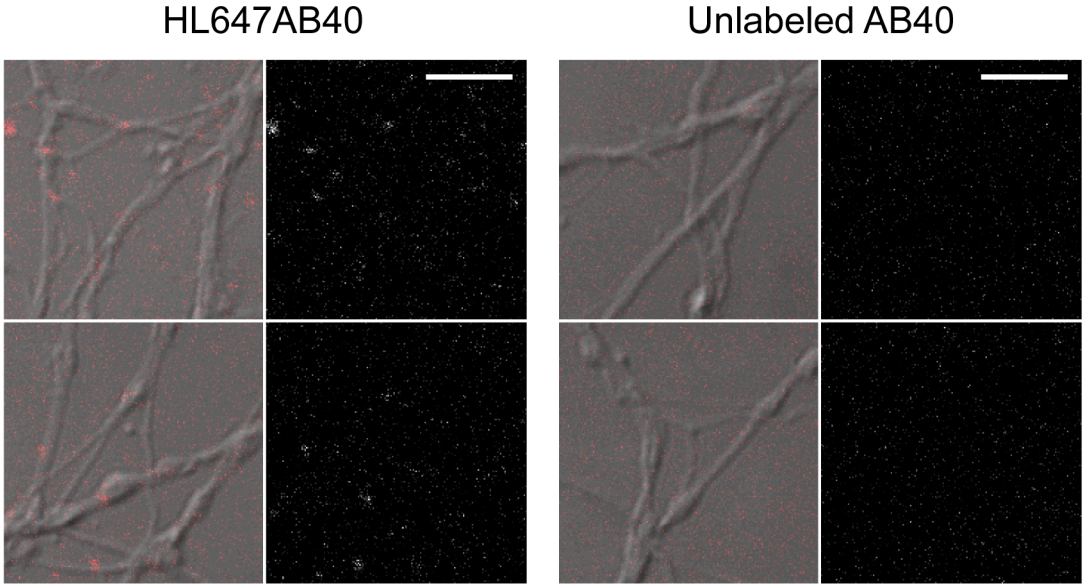

Figure 4.3.1 Neurites treated with HL647Aβ40 or unlabeled Aβ40.
Primary rat hippocampal cells were treated for 10 minutes with 1 nM Aβ. Overlays with brightfield are shown to the left, with corresponding HL647 fluorescence images on the right. Scale bars, 5 μm.

While 237 particles were detected on HL647Aβ40-treated neurites, only 2 were detected on neurites in cultures treated with unlabeled Aβ40, and both of these had monomer-equivalent fluorescence intensities (Figure 4.3.2).

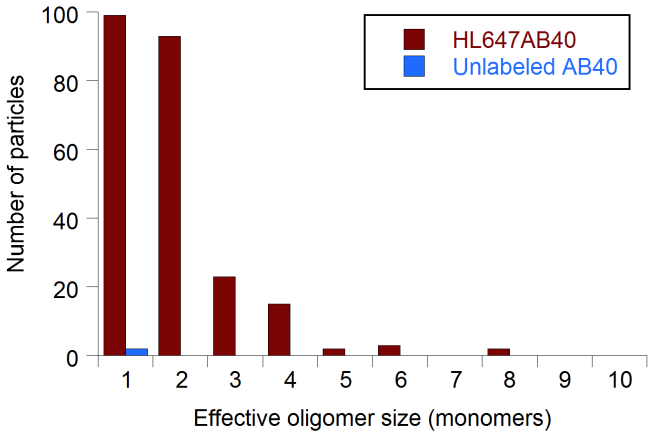

Figure 4.3.2 Neurites have low autofluorescence levels.
Analysis of 20 frames of neurites in cultures treated for 10 minutes with 1 nM HL647Aβ40 yielded a total of 237 diffraction-limited fluorescent particles, while only 2 particles were detected in 20 frames from cultures treated with 1 nM unlabeled Aβ40.

These data imply that less than 1% of detected particles in HL647Aβ-treated samples represent autofluorescent contamination or "false" oligomers, rendering rat primary hippocampal cell neurites an excellent model system for single molecule studies.

4.4 Size Differences between Neurite and Slide-bound Oligomers

We began our study of the population of oligomers bound to primary rat hippocampal cell neurites by obtaining separate size distributions for slide-bound and neurite-bound oligomers. As SH-SY5Y experiments provided evidence that rapid growth or clustering of HL647Aβ40 oligomers occurs on binding cell membranes, we hypothesized that similar results would be observed on neurites. Representative images from these experiments are shown in Figure 4.4.1.

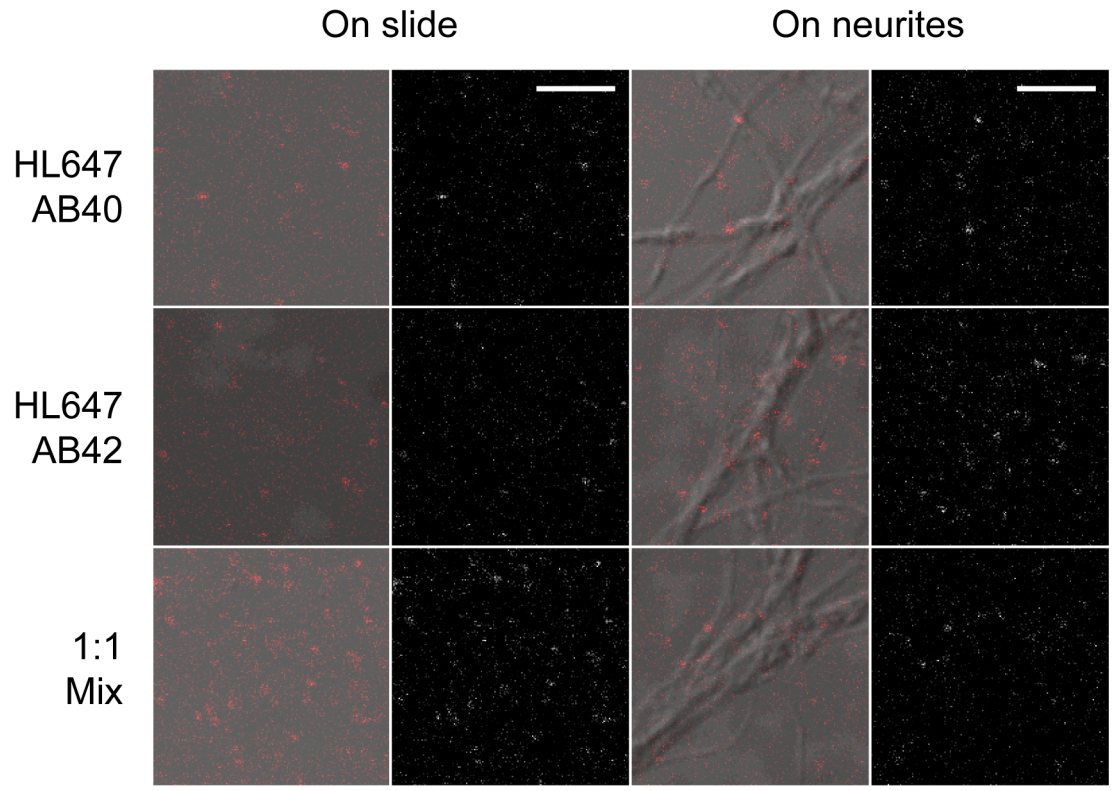

Figure 4.4.1 HL647Aβ binds both to poly-D-lysine coated slides and to neurites. Cultures were treated for 10 minutes with 1 nM HL647Aβ40, HL647Aβ42, or a 1:1 mix of the two. Overlays with brightfield are shown to the left, with corresponding HL647 fluorescence images on the right. Scale bars, 5 μm.

For both HL647Aβ40 and HL647Aβ42 nonspecifically bound to slides, around half the total monomer was present as monomer, and roughly 35% was present as dimers (Figure 4.4.2). As with SH-SY5Y cell experiments (Chapter 3), larger oligomers were observed on-slide in physiological buffer than were detected in spin-coated, dry samples of freshly solubilized peptide (Figure 4.2.1). This again indicates that significant oligomer growth occurs for Aβ upon dilution into physiological buffers or culture media and exposure to surfaces. HL647Aβ40 oligomers detected on slide were slightly smaller than slide-bound HL647Aβ42 oligomers. The neurite-bound populations of both peptides contained significantly larger oligomers than the slide-bound population, with the largest proportion of monomer present as dimers.

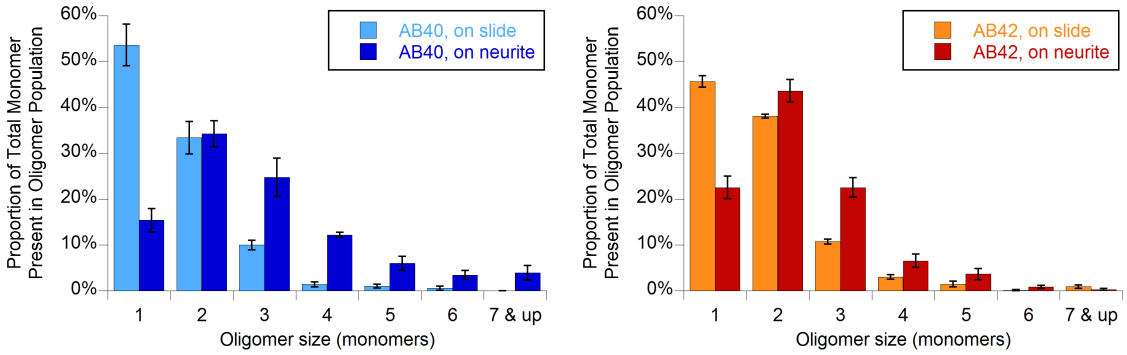

Figure 4.4.2 On-neurite HL647Aβ40 and Aβ42 oligomers are larger than those on-slide. Distributions are shown as percentage of total monomer present as oligomer of each size for HL647Aβ40 and HL647Aβ42, nonspecifically bound to slides or bound to primary rat hippocampal neurites. Proportions represent the average percentage for three separate experiments, 20 images per experiment *(Aβ40 on slide, N = 627, 301, and 281 particles; Aβ40 on neurites, N = 303, 218, and 237 particles; Aβ42 on slide, N = 728, 887, and 1030 particles; Aβ42 on neurites, N = 403, 778, and 612 particles)*. Error bars represent S.E.M.

Surprisingly, HL647Aβ42 formed slightly smaller oligomers on cells than did HL647Aβ40. Whereas 25% of Aβ40 monomers on the neurites had aggregated to form tetramers or larger, only 11% of total Aβ42 monomers fell in the same region of the distribution. This may indicate that initially membrane binding has a slightly greater pro-aggregation effect on Aβ40 than on Aβ42. This result is unexpected, given that Aβ42 has generally been found to aggregate more rapidly than Aβ42 and forms larger initial oligomers[108]. However, overall, the results were as predicted by our hypothesis.

We also examined the on-slide and on-neurite distributions of a 1:1 mixture of the two peptides (Figure 4.4.3). The on-neurite population interestingly contains smaller oligomers than the distributions for either peptide alone. For mixed on-neurite oligomers, 80% of the peptide shows up in the monomer-dimer populations. Only 50% and 66% of HL647Aβ40 and 42, respectively, are present as monomers-dimers. This result is not unexpected, given that Aβ40 and Aβ42 have been shown to inhibit each other's oligomerization[109]. Perhaps more surprisingly, the size distribution of mixed oligomers observed on the slides is shifted towards larger oligomers as compared to what is seen for either peptide alone. This may indicate that interaction with the poly-D-lysine coated coverslip is facilitating oligomerization of the mixed peptide, at least more so than it does for Aβ40 or Aβ42 individually.

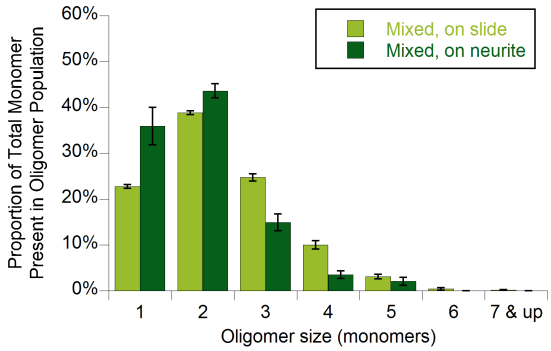

Figure 4.4.3 On neurite 1:1 HL647Aβ40:Aβ42 are smaller than those on-slide. Distributions are shown as percentage of total monomer present as oligomer of each size for a 1:1 HL647Aβ40 and HL647Aβ42 mixture nonspecifically bound to slides or bound to primary rat hippocampal neurites. Proportions represent the average percentage for three separate experiments for neurite-bound and 2 separate experiments for slide-bound, 20 images per experiment *(Mixed, on slide, N = 1330 and 1221 particles; Mixed, on neurites, N = 299 (only 15 frames), 328, and 307 particles).* Error bars represent S.E.M.

These two trends combined result in the neurite-bound population of mixed oligomers containing smaller aggregates than the slide-bound population.

4.5 Oligomer Growth of HL647Aβ40, Aβ42, and a 1:1 Mix

We assessed the stability of these distributions over time by performing experiments in which cultures were treated with HL647Aβ for a brief binding period (10 minutes, as in the above experiments) and then either (a) placed back into conditioned media containing no Aβ, for 6 to 48 hours ("washout") or (b) placed into conditioned media containing 1 nM Aβ for 6 to 48 hours ("1 nM"). Representative images for the 48 hour time points in each culture are shown in Figure 4.5.1.

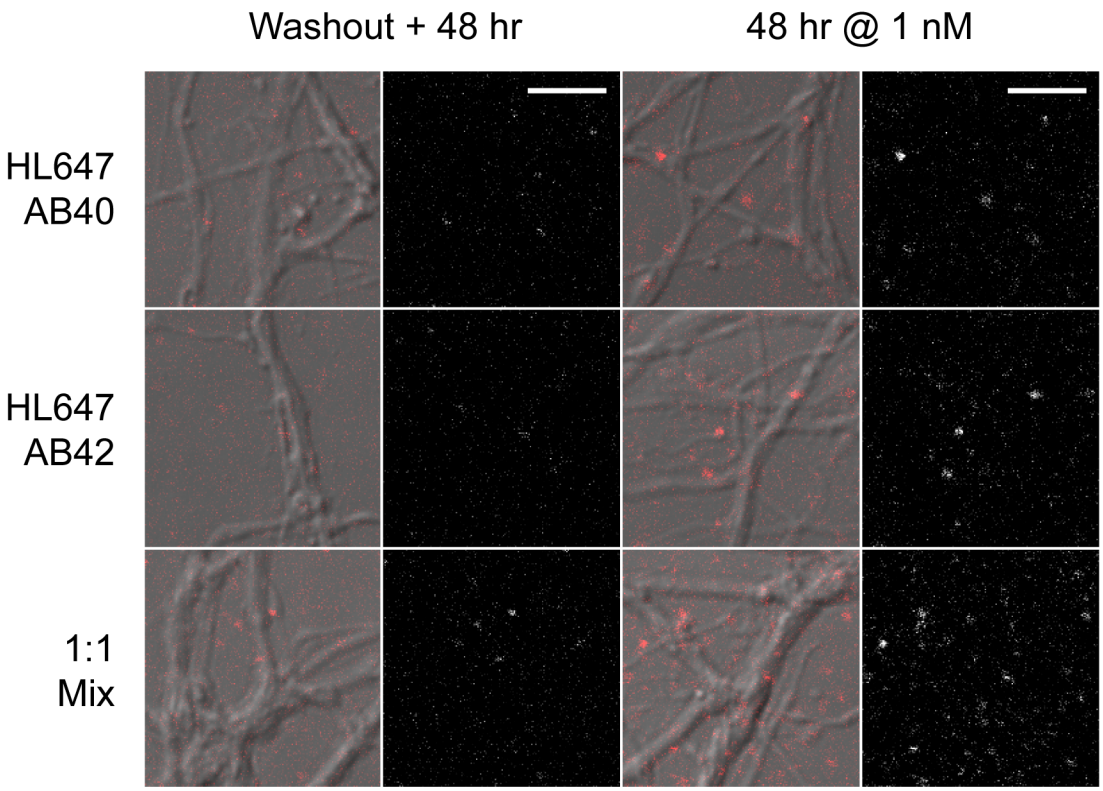

Figure 4.5.1 In general, on-neurite oligomer growth requires HL647Aβ in solution. Primary rat hippocampal cell cultures were treated for 10 minutes with HL647Aβ and then placed into media not containing HL647Aβ (Washout + 48 hr) or into media containing 1 nM HL647Aβ (48 hr @ 1 nM). Cultures were then incubated another 48 hours prior to imaging. Overlays with brightfield are shown to the left, with corresponding HL647 fluorescence images on the right. Scale bars, 5 μm.

As experiments with model membranes have indicated that on-membrane oligomer growth requires the presence of solution peptide (Hao Ding, unpublished results; Chun-Chieh Chang, unpublished results), we hypothesized that this would also be the case on neurites. The results of the washout experiment with each peptide individually are shown in Figure 4.5.2. Neither distribution exhibits substantial changes over the course of 48 hours without peptide in solution. Slight increases are present in the proportion of peptide present as monomer and dimer in the HL647Aβ40 distribution and as monomer in the HL647Aβ42 distribution.

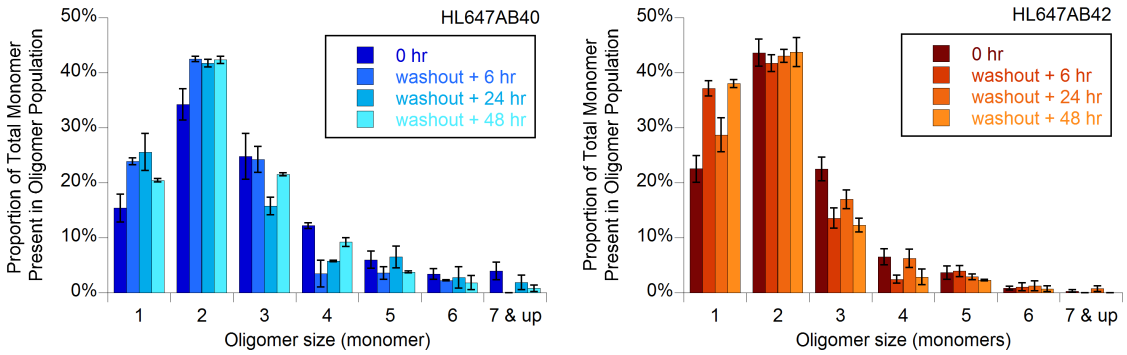

Figure 4.5.2 HL647Aβ40 or 42 washout decreases on-neurite oligomer size.
Primary rat hippocampal cell cultures were treated with 1 nM HL647Aβ40 or 42 for 10 minutes, then incubated a further 6, 24, or 48 hours in media containing no Aβ. On-neurite distributions from Figure 4.4.2 (0 hr bars) are shown for comparison. Results are plotted as proportion of total monomer present as oligomers of each size. Data represent the average of proportions from two separate experiments, 30 images per experiment *(HL647Aβ40: 6 hr N = 141 and 155 particles; 24 hr N = 157 and 111 particles; 48 hr N = 222 and 258 particles. HL647Aβ42: 6 hr N = 173 and 524 particles; 24 hr N = 254 and 255 particles; 48 hr N = 258 and 324 particles)*. Error bars represent S.E.M.

This may be due to dissociation of large oligomers into monomers on the membrane once the solution pool of Aβ has been removed. In other words, the oligomer size equilibrium on the membrane is slightly perturbed by the removal of solution Aβ. Another possible explanation is that larger oligomers may be more easily or quickly cleared from the membrane via endocytosis, shifting the distribution towards monomers over time. As we observed no oligomer growth, these results are in agreement with our initial hypothesis.

We performed a similar experiment with a 1:1 mix of the two peptides, including only 24 and 48 hour time points. Interestingly, the 1:1 mixed oligomers appear to exhibit slight oligomer growth in the absence of solution peptide, with greater proportions of the total peptide showing up in the trimer and tetramer populations after 24 and 48 hours.

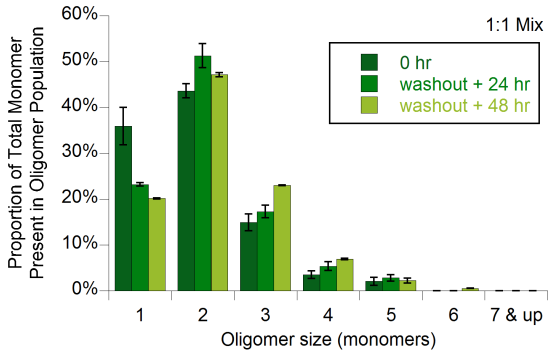

Figure 4.5.3 On neurite 1:1 HL647Aβ40:42 oligomer size increase slightly after washout. Primary rat hippocampal cell cultures were treated with 1 nM 1:1 HL647Aβ40:42 for 10 minutes, then incubated a further 24 or 48 hours in media containing no Aβ. On-neurite distribution from Figure 4.4.3 (0 hr) is included for reference. Results are plotted as proportion of total monomer present as oligomers of each size. Data represent the average of proportions from two separate experiments, 30 images per experiment *(24 hr N = 725 and 632 particles; 48 hr N = 552 and 623 particles)*. Error bars represent S.E.M.

Again, mixing the two peptides appears to cause substantial differences in behavior. These results may simply indicate that a 1:1 mix of the two peptides requires more time (hours instead of minutes) for the oligomer size distribution to reach equilibrium on the membrane. In other words, initial membrane-facilitated oligomerization occurs more slowly for the 1:1 mix of the two peptides than for either Aβ40 or Aβ42 alone.

We next assessed oligomer growth in the presence of 1 nM Aβ by first treating cells for 10 minutes with each peptide and then placing the cells back into media containing Aβ for 1 nM 6 to 48 hours. We anticipated that substantial on-membrane growth would be observed for all three of the treatment conditions. Interestingly, Aβ40 on the membrane appears to maintain the same size distribution for at least 48 hours in the presence of 1 nM peptide (Figure 4.5.4).

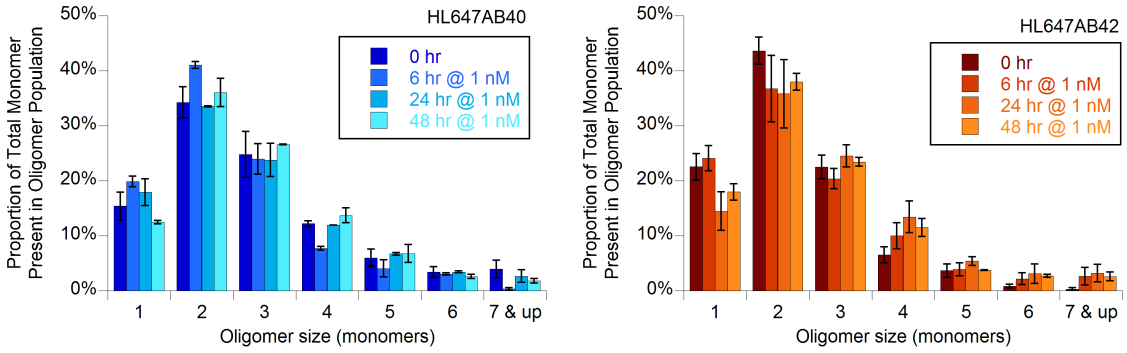

Figure 4.5.4 On-neurite HL647Aβ40 or 42 oligomers grow little in 48 hours at 1 nM. Primary rat hippocampal cell cultures were treated with 1 nM HL647Aβ40 or 42 for 10 minutes, then incubated a further 6, 24, or 48 hours in media containing 1 nM HL647Aβ40 or 42. On-neurite distributions from Figure 4.4.2 (0 hr bars) are shown for comparison. Results are plotted as proportion of total monomer present as oligomers of each size. Data represent the average of proportions from two separate experiments, 30 images per experiment *(HL647Aβ40: 6 hr N = 378 and 547 particles; 24 hr N = 469 and 749 particles; 48 hr N = 502 and 675 particles. HL647Aβ42: 6 hr N = 392 and 521 particles; 24 hr N = 425 and 492 particles; 48 hr N = 491 and 615 particles)*. Error bars represent S.E.M.

HL647Aβ42, however, does exhibit some slight growth in oligomer size over this time period. The portion of peptide present as monomers decreases after 24 to 48 hours, while the proportion in tetramers, hexamers, and heptamers and larger increases. These trends are consistent with the widely cited observation that HL647Aβ40 is the more slowly aggregating of the two versions of the peptide.

Possibly the most intriguing result to emerge from this set of experiments comes from the 1 nM time lapse 1:1 mixed peptide data (Figure 4.5.5). While changes in the size distribution for either peptide alone over up to 48 hours are small, the 1:1 mixed peptide oligomer size distribution exhibits a substantial shift towards larger structures. These results are deeply interesting, considering the recent observation that increases from the physiological 1:9 Aβ40:Aβ42 ratio can substantially decrease neuronal firing rate, possibly to a greater degree than Aβ42 alone[110].

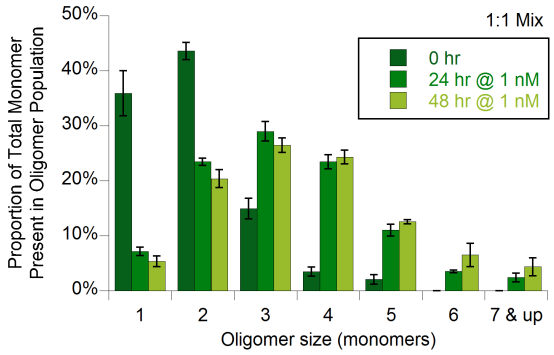

Figure 4.5.5 On-neurite 1:1 HL647Aβ40:42 oligomers are larger after 48 hours at 1 nM. Primary rat hippocampal cell cultures were treated with 1 nM 1:1 HL647Aβ40:42 for 10 minutes, then incubated a further 24 or 48 hours in media containing 1 nM 1:1 HL647Aβ40:42. On-neurite distribution from Figure 4.4.3 (0 hr) is shown for comparison. Results are plotted as proportion of total monomer present as oligomers of each size. Data represent the average of proportions from two separate experiments, 30 images per experiment *(24 hr N = 1081 and 618 particles; 48 hr N = 930 and 659 particles)*. Error bars represent S.E.M.

The oligomer population containing the largest quantity of peptide changes from dimers to trimers. At time zero, only 20% of the total neurite-bound peptide is present as trimers or larger, but after 24 hours, these larger oligomers account for 70% of the total peptide.

Some additional insight into the mechanisms behind these changes can be gained by displaying the data in a slightly different manner. The number of each oligomer detected per 30 images at each time point is plotted for HL647Aβ40 and HL647Aβ42 (Figure 4.5.6).

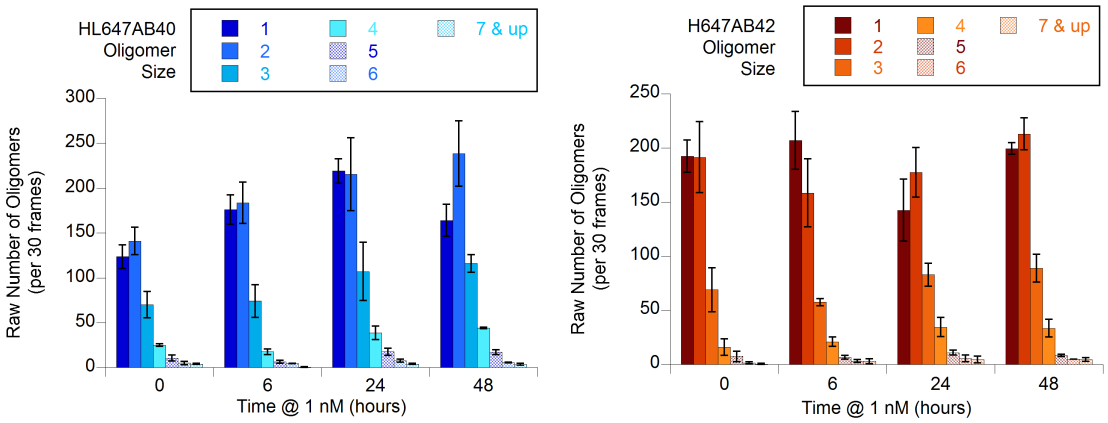

Figure 4.5.6 Average numbers of HL647Aβ40 or 42 oligomers across 48 hours at 1 nM. Average raw oligomers of each size per 30 frames at each time point for HL647Aβ40 oligomers on neurites (left) and HL647Aβ42 oligomers on neurites (right) are shown, over 48 hours in 1 nM peptide.

By examining the plot for HL647Aβ40, we see that in general, the raw number of oligomers of each size on the membrane increases slightly over time during incubation at 1 nM peptide. When looked at with Figure 4.5.4, these data would indicate that while the size distribution of small oligomers remains constant over time for HL647Aβ40, the overall quantity of peptide bound does not remain constant. On the contrary, for HL647Aβ42, the raw numbers of monomers and dimers on the membrane remain relatively constant within experimental error for up to 48 hours. However, increases are seen in the trimer and tetramer counts. The shift towards larger HL647Aβ42 oligomers observed in Figure 4.5.4 is therefore purely due to an increase in the number of large oligomers over time, not to a depletion of monomers and dimers.

Again, however, the most interesting results are seen with the 1:1 mix of the two peptides (Figure 4.5.7).

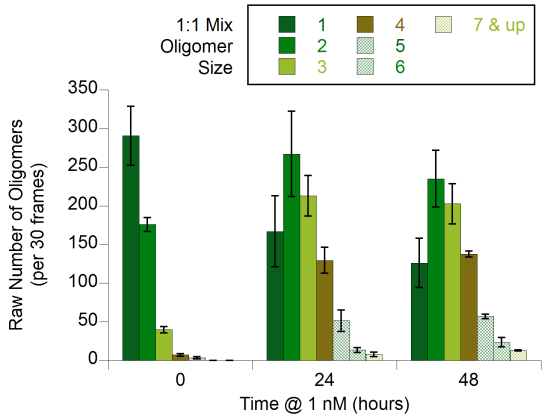

Figure 4.5.7 Average numbers of 1:1 HL647Aβ40:42 oligomers across 48 hours at 1 nM. Changes in the average raw number of each oligomer per 30 frames on neurites over time are shown for a 1:1 mix of HL647Aβ40:42. Cultures were incubated for 0, 24, or 48 hours in media containing 1 nM peptide.

The raw number of monomers bound to neurites decreases significantly over the course of 48 hours, and the dimer count increases slightly. Very large increases are observed in the numbers of trimers and larger oligomers. The shift in overall distribution shown in Figure 4.5.5 can thus be partially attributed to a roughly 50% decrease in the number of on-neurite monomers and partially to large increases in the numbers of trimers, tetramers, and pentamers on the neurites.

In order to form final conclusions about these data, it is helpful to examine the total quantities of peptide bound to the neurites at each time point (Figure 4.5.8).

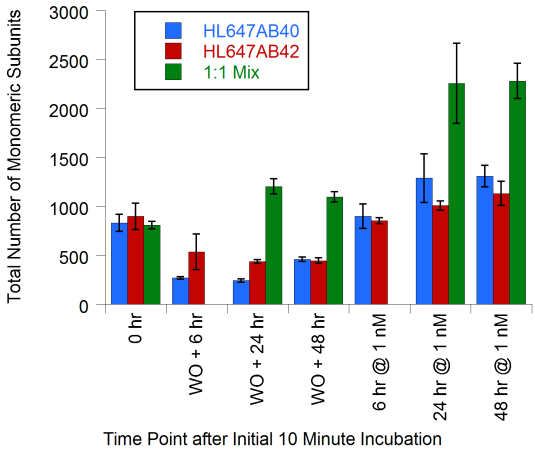

Figure 4.5.8 Total quantities of monomeric HL647Aβ present on neurites over time. Raw number of monomeric subunits on neurites is shown for 6 hours, 24 hours, and 48 hours following an initial 10 minute incubation. Bars labeled with "WO" represent "washout" samples incubated without peptide in the media; bars labeled "@ 1 nM" represent samples incubated with 1 nM peptide in the media.

Interestingly, the total quantity of peptide bound after a 10 minute incubation at 1 nM is equivalent for all three conditions. Under washout and 1 nM incubation conditions, HL647Aβ40 and HL647Aβ42 total peptide follow similar trends: total neurite-bound peptide decreases significantly over time when no peptide is present in solution and increases slightly on incubation with 1 nM. The 1:1 mix of the two peptides, however, shows an unexpected *increase* in total peptide bound when no peptide is present in solution. How is this possible? One explanation may be that slide-bound 1:1 peptide dissociates over time, acting as a source of new solution peptide after the cultures have been placed into saved media that does not contain peptide. Images shown in Figure 4.5.9 illustrate that approximately 50% of the slide-bound 1:1 HL647Aβ40:42 oligomers are lost after 24 to 48 hours' incubation without peptide in solution. Similar degrees of dissocation are noted for both HL647Aβ40 and HL647Aβ42 alone, but the on-slide oligomer density is lower for each of these (20 ± 5 oligomers per frame for HL647Aβ40 and 44 ± 4 oligomers per frame for HL647Aβ42, versus 64 ± 2 oligomers per frame for the mixed peptide).

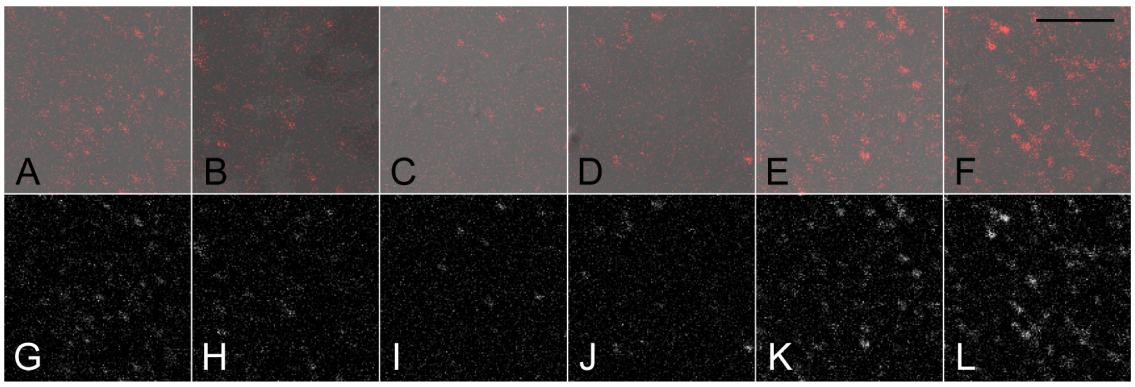

Figure 4.5.9 Loss of slide-bound peptide when slides are incubated after washout.
Images of 1:1 HL647Aβ40:42 oligomers on a Poly-D-Lysine coated slide at various time points show that dissociation occurs. Cultures were incubated with 1 nM peptide, then incubated for 24 or 48 hours in peptide-free media (washout) or media containing 1 nM peptide. A, B, G, & H, 0 hours; C & I, 24 hours after washout ; D & J, 48 hours after washout; E & K, 24 hours' incubation with 1 nM peptide; F & L, 48 hours' incubation with 1 nM peptide. Scale bar, 5 μm.

Assuming that half the slide-bound peptide dissociates into solution results in a concentration of approximately 2 fM 1:1 HL647Aβ40:42. The binding affinity of the 1:1 mixed oligomers for the membrane would have to be extremely high for the neurites to bind peptide under these conditions. However, the 1:1 mixed oligomers appear to aggregate rapidly enough on the membrane to reduce the overall number of neurite-bound monomers over time, possibly opening up monomer "binding sites" to solution peptide. Additionally, possibly due to their increased size, oligomers formed from 1:1 HL647Aβ40:42 may have unique effects on the neurite membrane composition which increase the Aβ-membrane affinity (enrichment in externalized phosphatidylserine, for instance).

4.6 Motion of a Small Portion of Neurite-Bound Oligomers

To obtain preliminary data on the motion of neurite-bound oligomers, 10-frame xyt scans were performed on cultures treated with 1 nM HL647Aβ40, HL647Aβ42, or HL647Aβ40:42 for 10 minutes. Kymographs were then assembled to determine whether oligomers exhibited significant motion over the 2 minutes during which the scans were acquired. Oligomers were sorted into categories based on whether they exhibited

significant motion. Examples of kymographs for oligomers falling in each category are shown in Figure 4.6.1.

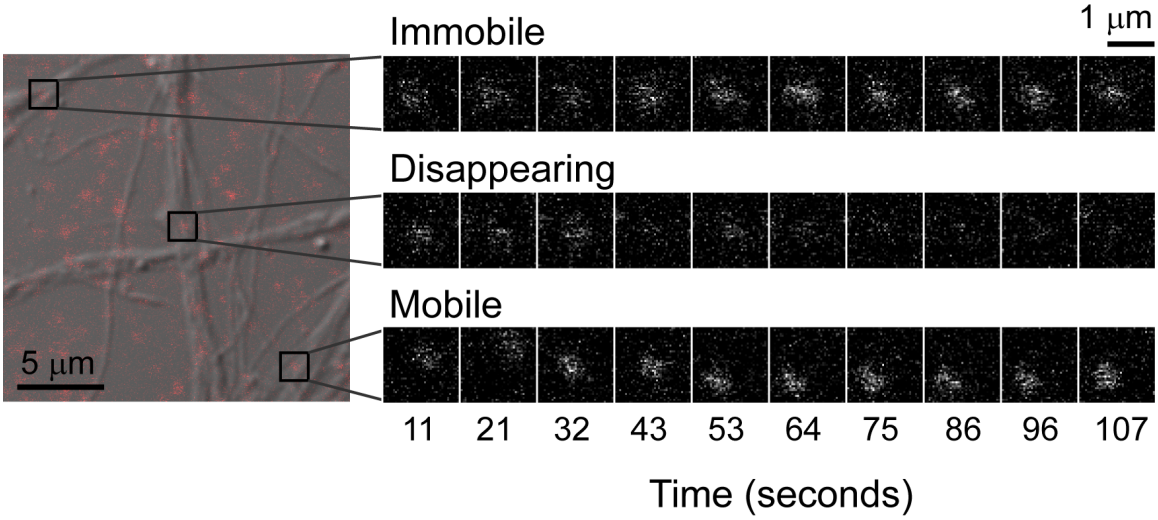

Figure 4.6.1 Kymographs of HL647Aβ imaged in confocal mode show oligomer motion. Three different neurite-bound 1:1 HL647Aβ40:42 oligomers classified according to the motion they exhibit over 10 sequential frames (roughly 2 minutes). Included are kymographs for a particle which disappears (top row), a particle which is immobile (middle row), and a particle which exhibits motion (bottom row). Boxes are 40 x 40 pixels, or roughly 1.6 μm x 1.6 μm.

Overall, 60% to 70% of particles did not exhibit detectable motion over the course of 10 scans (Figure 4.6.2). This value is consistent with the proportion of cell-bound oligomers exhibiting "confined" motion in a recent single-particle tracking study of Aβ42 on SH-SY5Y cells (52% to 77%, depending on type of oligomer)[73]. Between 10% and 20% of particles in each sample bleached or moved out of the z-plane of the image by the end of the series of images, making their motion impossible to classify, and 20% to 30% of particles were mobile. Mobility was defined as (a) moving more than 0.25 μm within a 1.6 μm x 1.6 μm region of interest during the image series, (b) moving out of the 1.6 μm x 1.6 μm region of interest over the image series, or (c) appearing to split or merge with another particle over the course of the image series.

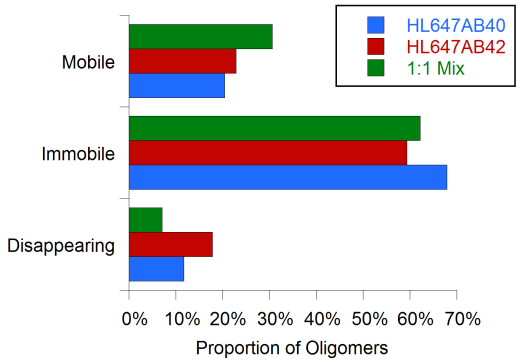

Figure 4.6.2 Most oligomers are immobile, according to kymographs.
Oligomers were classified by their behavior in kymographs. A total of 137 particles were analyzed in 4 frames of neurites treated with 1 nM HL647Aβ40. A total of 118 particles were analyzed in 4 frames of neurites treated with 1 nM HL647Aβ42. A total of 98 particles were analyzed in 2 frames of neurites treated with 1 nM 1:1 HL647Aβ40:40.

These data confirmed that a majority of detected neurite-bound oligomers remain motionless on a time scale of minutes but also identified a population of oligomers which exhibited movement.

To further study the movement of this subset of oligomers, we performed single-particle tracking experiments in TIRF mode. As the proportions of particles falling in each category were similar across the three samples, it is likely that the mechanisms of membrane binding and motion on the membrane do not differ among HL647Aβ40, HL647Aβ42, and 1:1 mixed peptide oligomers. As extensive study of neurite-bound particle motion is beyond the scope of this thesis, particle-tracking experiments were only conducted on neurite-bound HL647Aβ40 oligomers. It is expected, however, that results for oligomers in the other two samples will be similar. Representative TIRF images of neurites treated with HL647Aβ40 and unlabeled Aβ40 are shown in Figure 4.6.3. While autofluorescence levels again prohibited definitive identification of HL647Aβ40 oligomers on cell somas, autofluorescence levels on neurites were quite low.

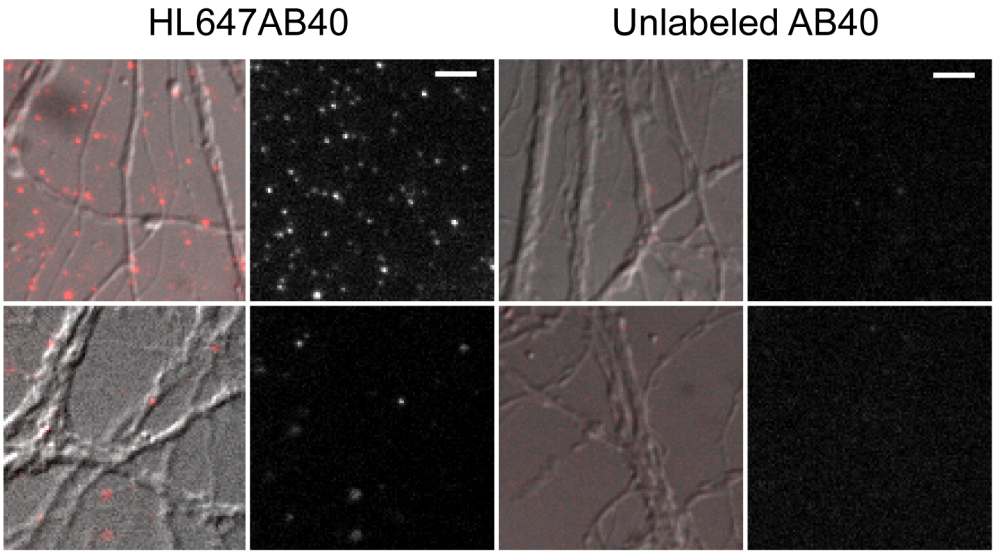

Figure 4.6.3 TIRF-mode neurite autofluorescence is low.
Primary rat hippocampal cell cultures were treated for 10 minutes with 1 nM HL647Aβ40 (left) or unlabeled Aβ40 (control, right). Variations in density of bound HL647Aβ40 particles are representative of the full range of binding density across two experiments. Scale bars, 5 μm. Data obtained in cooperation with Chun-Chieh (Andrew) Chang.

Accordingly, analysis of particle motion was restricted to those particles identified on neurites. In 2 separate experiments, a total of 89 particles overlapping with a membrane region in the brightfield image exhibited motion; only 2 moving particles were detected that were not obviously associated with a neurite. Example trajectories for three mobile neurite-bound HL647Aβ40 oligomers are shown in Figure 4.6.4. Of total particles detected bound to neurites in the initial frames of 3 separate films, 17% ± 3% of particles exhibited motion (N = 37, 34, and 45 total oligomers, error is standard deviation). This result is slightly lower than the expected proportion of mobile particles from confocal mode imaging kymographs (Figure 4.6.2) but is consistent with the observation that the majority of bound particles do not exhibit detectable motion on a seconds-to-minutes time scale.

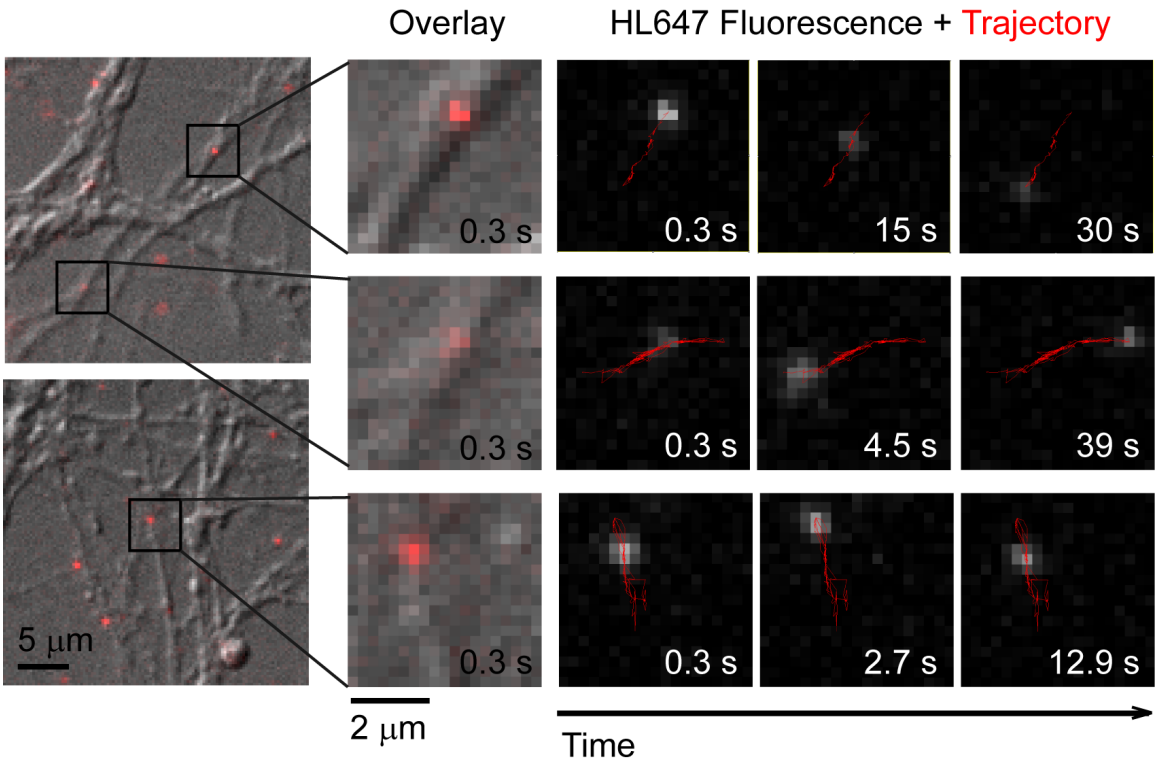

Figure 4.6.4 TIRF mode trajectories for HL647Aβ40 oligomer in motion on neurites. Time-stamped stills from TIRF-mode films of neurite-bound HL647Aβ40 oligomers illustrate the motion of three different particles (A, B, and C). The first image in each sequence is an overlay of brightfield (DIC) and the first frame of the film, with HL647Aβ40 oligomer shown in red. For the following fluorescence images, the particle's overall trajectory over the course of the sequence is shown in red. Frames are time-stamped in seconds. Data obtained in cooperation with Chun-Chieh (Andrew) Chang.

Particles in motion generally exhibited trajectories aligned with the membrane of the neurite to which they were bound, with many reversals of direction. Example trajectories are shown in Figure 4.6.4. We note that many of the plotted trajectories appear unidirectional at first glance, but this has much to do with the restrictive tubular geometry of the neurites. On closer examination, for instance, the trajectory of the particle in the bottom row of Figure 4.6.4 records significant motion perpendicular to the neurite axis as well as parallel to it. Trajectories were plotted and diffusion coefficients were obtained for a total of 83 neurite-bound HL647Aβ40 oligomers (Figure 4.6.5). While we note that these values are likely 25-50% lower than the actual diffusion coefficients, due to the effects of projecting cylindrical trajectories onto a flat plane[111], they are useful in terms of classifying the motion of the particles and placing their movement in context with previous Aβ oligomer tracking studies.

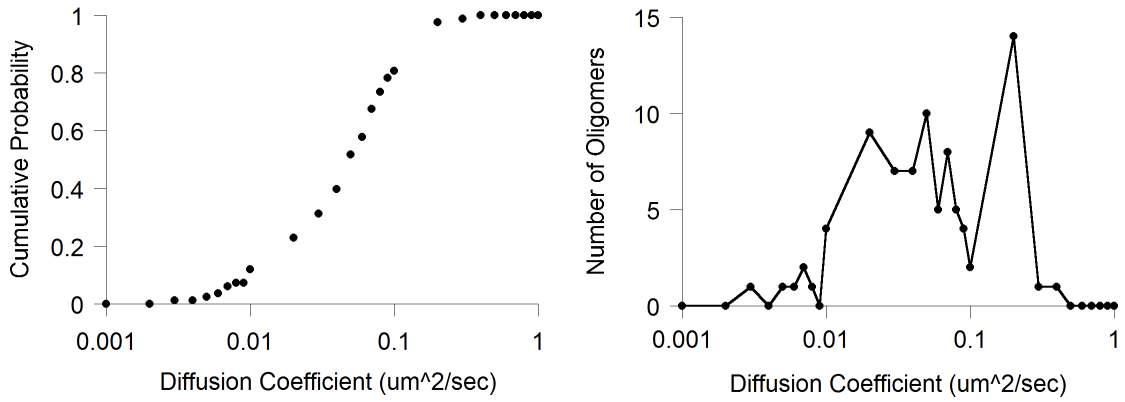

Figure 4.6.5 Cumulative probability plot and histogram for HL647Aβ40 oligomers. A total of 83 neurite-bound HL647Aβ40 exhibited motion in 14 TIRF-mode films. Diffusion coefficients were obtained from a LabView program written by Chun-Chieh (Andrew) Chang.

The median diffusion coefficient for neurite-bound HL647Aβ particles was 0.044 μm^2 per second. This value is in good agreement with a median diffusion coefficient obtained for extrasynaptic Aβ42 oligomers by Renner and colleagues (0.0341 μm^2 per second) [67]. It is an order of magnitude higher than that recently measured by Calamai and Pavone (0.0040 μm^2 per second)[73], but Calamai and Pavone included highly "confined" oligomers in their data set, which by and large exhibited very slow diffusion. Interestingly, examination of the histogram in Figure 4.6.5 reveals two peaks, one located at 0.01 to 0.08 μm^2 per second and one at 0.1 to 0.2 μm^2 per second. It is possible that these two peaks represent two distinct populations of oligomers which interact with the membrane in different ways. Fast-moving oligomers may represent freely diffusing particles that are loosely associated with the outer leaflet of the lipid bilayer. The slower-moving population may represent oligomers which are actually inserted into the bilayer and therefore exhibit restricted diffusion. The diffusion coefficients of this group are similar to those measured for a number of other membrane integral proteins and receptors using the single-particle tracking method [112–114]. However, more statistical power would be required to determine whether these peaks truly represent two distinct populations.

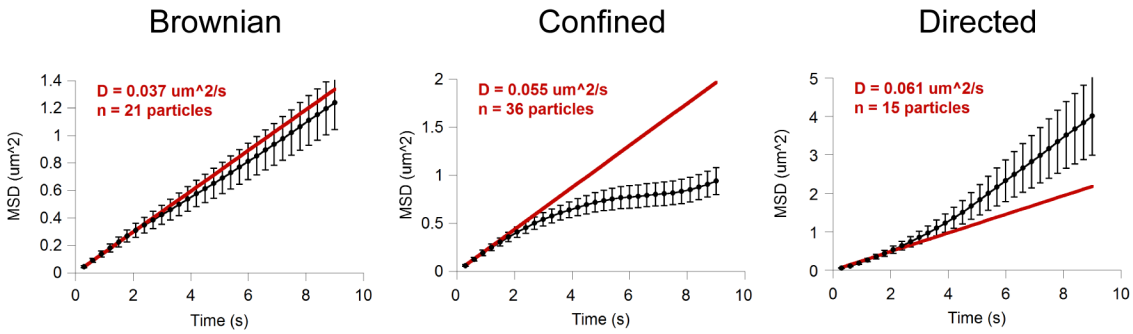

Figure 4.6.6 Mean-square displacement (MSD) vs. time plots for moving oligomers. HL647Aβ40 oligomers in motion were classified as exhibiting Brownian diffusion, confined diffusion, or directed motion plus diffusion by their individual MSD vs. time plots. Particles were classified based on whether MSD vs. time plot (a) aligned with the linear plot predicted for Brownian motion (Brownian), (b) plateaued underneath the linear plot (confined or corralled motion) or (c) sloped upwards from the linear plot (directed motion in combination with diffusion). MSD plots for each type of particle were then averaged and plotted along with the linear MSD vs. time curve predicted by the mean diffusion coefficient of the group. Error bars represent S.E.M.

We plotted mean-square displacement (MSD) versus time curves to fully understand the modes of diffusion exhibited by the particles[115] (see Section 2.5.12 for details). We found that of 71 particles with trajectories long enough to be included in the analysis, 80% exhibited MSD versus time plots characteristic of Brownian or confined/corralled motion. Only 20% of oligomers exhibited directed motion (far right plot in Figure 4.6.6). These particles may represent endocytosed oligomers being actively transported within neurites, as proposed by Calamai et al[73]. Average velocities for this population were measured over at least 8 seconds (mean trajectory length 20.9 seconds, or 70 frames). Interestingly, average velocity values for these particles fell in the range of 0.05 to 0.5 μm/s, with a mean value of 0.25 μm/s. If these oligomers are being actively transported, their motion lies on the slow end of a fairly wide range of observed rates for axonal transport (0.01 μm/s to 3 μm/s)[116] and is roughly an order of magnitude slower than has been observed for axonal vesicular transport in rat neurons[117].

Half of the analyzed particles exhibit MSD plots characteristic of confined or corralled motion. Plateau level of MSD plots has in the past been used as an estimate of corral size[115,118]. Examination of the middle plot in Figure 4.6.6 indicates that mean corral size for detected "confined" oligomers is roughly 0.8 microns, or 900 nm on a side if a region of particle confinement is modeled as a square. This confinement is likely partially

a result of particles' diffusion being restricted to the flat projection of the neurite membrane. Neurites in these experiments range from under 200 nm in diameter to nearly 2 μm. However, other factors are also likely contributors. Recent years have seen the emergence of a new model of the cell membrane as a "partitioned" fluid bilayer, as multiple investigators have obtained evidence of diffusional barriers for membrane-integral proteins in cell membranes[112,118]. Posited corrals have dimensions ranging from tens of nanometers to over a micron. Such restriction to diffusion may result from molecular crowding in the membrane[112], presence of micro- or nanodomains[118], or interaction of bilayer-spanning proteins with other protein complexes or cytoskeletal networks[113,119]. Thus, if oligomers actually insert into the lipid bilayer, as discussed above, they have a high probability of exhibiting this type of restricted diffusion.

As less than 100 particles were classified, and classification of diffusion mode was performed by eye, we note that these results are preliminary in nature. In order to determine whether the observed MSD plots actually represent atypical diffusion modes, simulations could be performed to generate MSD vs. time plots for a similar number of particles taking "random walks" on tubular membranes. If similar numbers of particles exhibiting "confined" and "directed" motion were observed in such a simulation, we could conclude that these plots merely represent statistical deviation about a linear (Brownian) MSD vs. time plot, rather than particles exhibiting true confinement or directed motion.

4.7 Oligomers Do Not Exhibit Synapse-Localized Binding

A number of groups have observed that Aβ oligomers localize to synapses[34,67,120]. Importantly, most of these studies have been performed using anti-Aβ oligomer antibody to label endogenous Aβ aggregates or by applying oligomers which have been prepared *in vitro* to cultured cells. Whether the large cell-bound Aβ oligomers observed *in vivo* form directly from Aβ in solution or are seeded by dissociation from fibrils is unknown. The relationship of physiological concentrations of soluble, low-molecular weight Aβ aggregates to these synaptically targeted larger aggregates is therefore poorly understood. To determine whether small oligomers formed on the membrane from freshly prepared

HL647Aβ40 and HL647Aβ2 bind preferentially to post-synaptic membranes, neurites treated with 5 nM peptide were stained for PSD-95, a post-synaptic membrane marker protein, or for Aβ (as a positive control) (Figure 4.7.1).

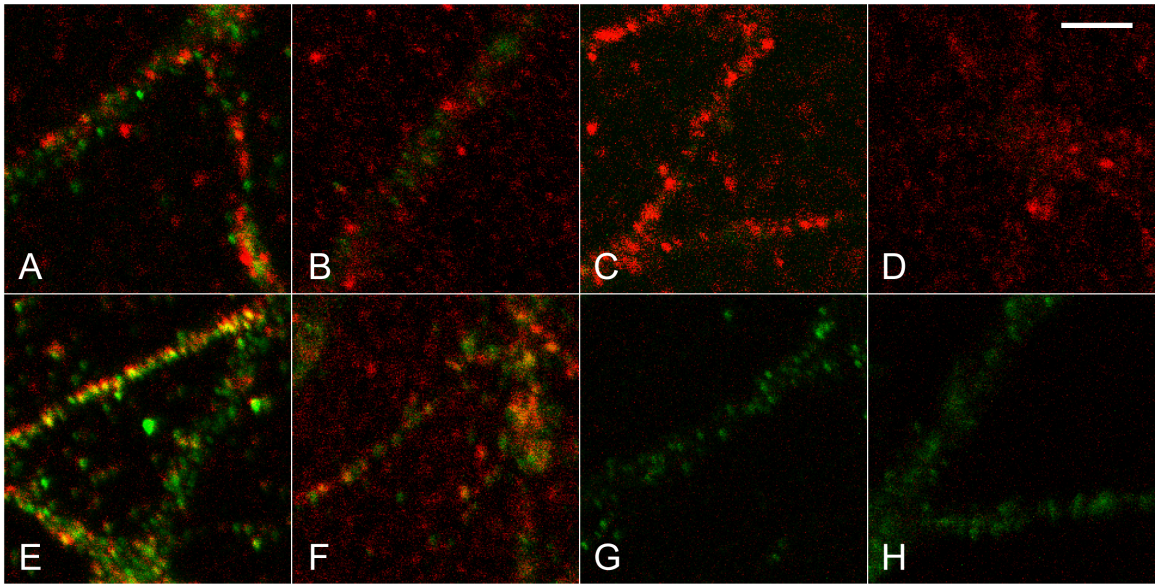

Figure 4.7.1 Neurite-bound HL647Aβ does not colocalize with PSD-95.
Primary rat hippocampal cell cultures were treated for 10 minutes with 5 nM HL647Aβ40 or HL647Aβ42 (red) and then stained for the post-synaptic membrane marker protein PSD-95 (green). A, HL647Aβ40 + anti-PSD-95; B, HL647Aβ42 + anti-PSD-95; C, HL647Aβ40 only (negative control); D, HL647Aβ42 only (negative control); E, HL647Aβ40 + anti-Aβ (positive control); F, HL647Aβ42 + anti-Aβ (positive control); G, anti-PSD-95 + unlabeled Aβ40 (negative control); H, anti-PSD-95 alone (negative control). Regions of colocalization appear yellow. Scale bar, 5 μm.

While significant colocalization is observed for neurites treated with HL647Aβ and stained with an anti-Aβ antibody, comparatively little overlap is visible between PSD-95 and HL647Aβ. This data does indicates that small oligomers formed at physiological concentrations of HL647Aβ do not preferentially bind to synapses.

If HL647Aβ is binding to a specific pre-synaptic or post-synaptic membrane protein or receptor, it might be expected to bind differentially to a particular type of neurite, e.g. to exhibit a preference for dendrites over axons or vice versa. Surface density of certain posited Aβ receptors or target proteins is site-specific, with mGluR5, NMDA receptors, and cellular prion protein all more strongly concentrated on dendrites or at the post-synaptic membrane than on axons[65,121,122]. To determine whether HL647Aβ oligomer binding was stronger on axons or dendrites, we assessed bound oligomer

density on neurites treated with 1 nM HL647Aβ and then stained with specific markers for axons and dendrites (Figure 4.7.2).

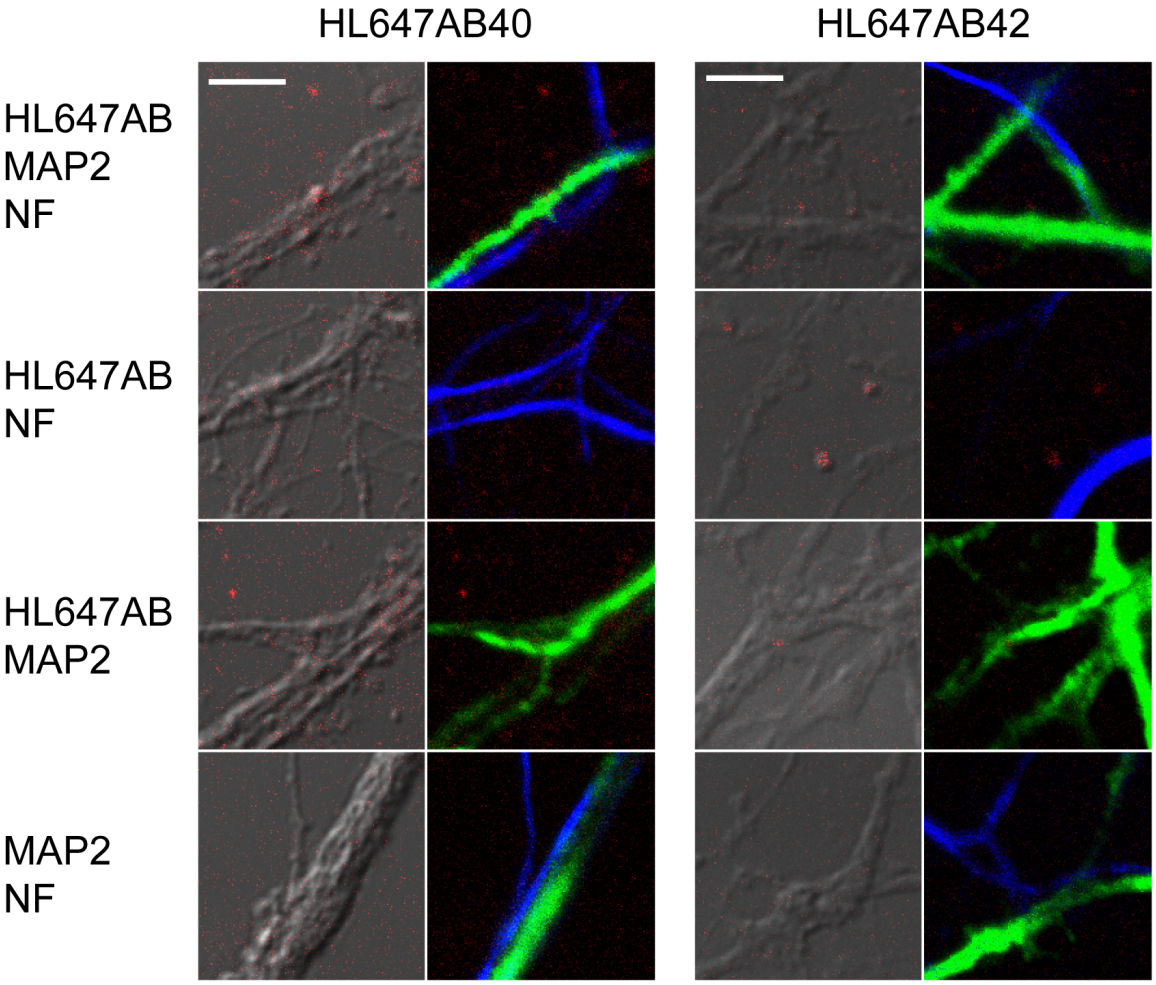

Figure 4.7.2 Neurites treated with HL647Aβ and stained for axons and dendrites.
Primary rat hippocampal cell cultures were treated for 10 minutes with 10 nM HL647Aβ40 or HL647Aβ42 (red) and then stained for the axonal marker neurofilament (NF, blue) or the dendritic marker MAP2 (green). Brightfield and HL647Aβ overlays are shown on the left, and HL647Aβ, MAP2, and NF overlays are shown on the right for each image. Scale bar, 5 μm.

HL647Aβ oligomer binding density per length was then measured on axons and dendrites. The values were compared to determine whether oligomers exhibited any preference for one type of neurite over the other. Results were normalized and plotted in Figure 4.7.3.

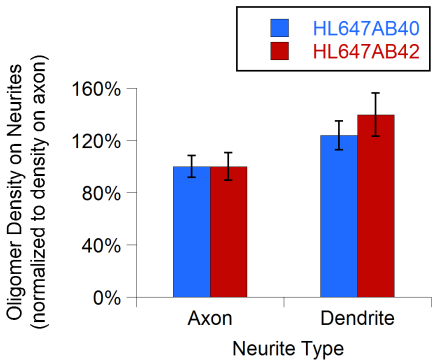

Figure 4.7.3 Oligomer density is slightly higher on dendrites than on axons.
HL647Aβ40 and HL647Aβ42 oligomer density is only slightly higher on dendrites as compared to axons. Oligomer density per micron of neurite was assessed in 30 images of neurites treated with either HL647Aβ40 or HL647Aβ42, then stained with anti-MAP2 (dendritic marker) and anti-NF (axonal marker). Results were then normalized to oligomer density on axons. Images containing no axon-bound or dendrite-bound oligomers were excluded from analysis. Error bars represent S.E.M. across images for each experiment (Aβ40 on axons, N = 23 images; Aβ40 on dendrites, N = 19 images; Aβ42 on axons, N = 20 images; Aβ42 on dendrites, N = 17 images).

Both HL647Aβ40 and HL647Aβ42 oligomers bound to dendrites at slightly higher density than to axons. No significant difference is observed between the results for the two peptides. This implies that if HL647Aβ40 and HL647Aβ42 bind to different sites or receptors on neurites, these binding sites must have very similar distributions on the cell. Furthermore, these results indicate that binding sites for the peptide are present on both axonal and dendritic processes. If oligomers are binding to a specific membrane protein rather than directly to the lipid bilayer, this "receptor" must be present at nearly equivalent levels on both types of neurites. A more plausible explanation is that HL647Aβ40 and HL647Aβ42 oligomers bind directly to the lipid bilayer and that small differences in membrane composition and morphology between axons and dendrites result in the slight preference of the oligomers for dendrites over axons. Oligomers may also be exploiting more than one binding mechanism. For instance, a large population may be binding at fairly uniform density to the lipid bilayer of all neurites, with a smaller subpopulation (5% to 10% of particles) binding to a specific postsynaptic membrane protein, present only on dendrites.

These results do not eliminate the possibility that Aβ oligomer neurotoxicity is mediated by interference with a specific membrane protein. They do, however, suggest

that any functional changes in membrane integral receptors of neurons exposed to the oligomers may be triggered indirectly, by changes in the structure of the local membrane, consistent with the explanation of Li, et al.[32] In other words, oligomer binding may occur generally and nonspecifically, but toxic effects may be restricted to certain sites in the cell (e.g., synapses). Further studies will be necessary to determine which specific hypothesis best explains these data.

4.8 Future Work: Functional Effects of Aβ on Neurons

Aβ has been shown to have deleterious effects on multiple aspects of cell physiology in the brain. Application of Aβ to cultured cells has been shown to decrease dendritic spine density[35,123], and expression of human Aβ in rodent brain also results in lowered spine number[101,100]. The potential of single molecule microscopy in the context of these observations is that by expressing fluorescent proteins localized to the cytoplasm and studying neurite-bound oligomers, it may be possible to identify particular Aβ oligomers associated with the loss of specific spines. Obtaining meaningful results from such experiments would require extensive exploration of the parameter space involved. We have, however, begun to develop neuronal experiments in this direction by transfecting primary rat hippocampal neurons with eGFP and examining spine density after treatment with freshly prepared Aβ42. Results were only obtained on a small number of cells (n = 1 per treatment group in each of 2 separate experiments) and are preliminary in nature. Representative data are shown in Figure 4.8.1.

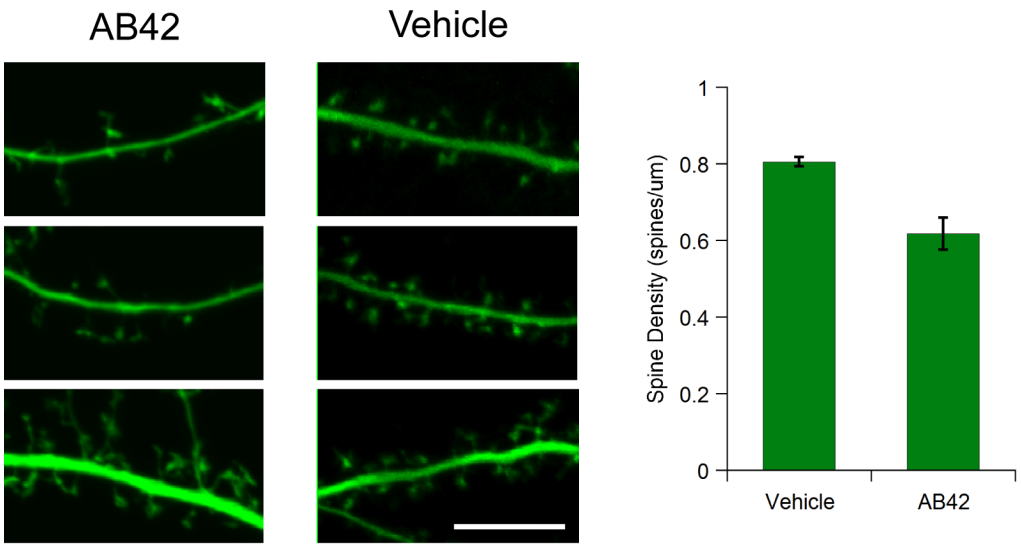

Figure 4.8.1 Example data in an assay for Aβ42-induced reductions in spine density. Primary rat hippocampal cell cultures were transfected with eGFP on DIV 12 and incubated in 100 nM freshly prepared unlabeled Aβ42 in media (images at left) or vehicle-treated media (images in center). eGFP-labeled neurites were then imaged in confocal mode and spine density was assessed. Example data is shown for one experiment (one cell per condition). Error bars represent standard deviation across images in each sample (n = 5 images in each sample). Total dendrite length analyzed was 999 μm for vehicle, 994 μm for Aβ42.

Even were this data replicated with a larger sample size, the observations would not be novel, as Smith et al. obtained nearly identical results[123]. These results do, however, demonstrate that examining HL647Aβ oligomer binding and dendritic spine density in parallel should be feasible for our group.

Disruption of neuronal or astrocytic calcium homeostasis has also been widely cited as a primary mechanism for Aβ neurotoxicity. Most recently, two groups separately observed that the regions around amyloid plaques in the brains of Alzheimer's model mice contain increased numbers of both hyperactive neurons[124], and of hyperactive astrocytes[125], as measured by calcium transient frequency. Events termed "intercellular calcium waves", oscillations or waves of increased intracellular calcium which move through sequential regions of astrocytes within a network, were also observed in astrocytes[125]. To assess Aβ effects on cultured primary rat hippocampal cell calcium homeostasis, we loaded cultures with the calcium indicator Fluo4-AM and imaged cells before and after treatment with Aβ. Results (not shown) were difficult to interpret and to quantify due to the cultures' sensitivity to fluid addition and due to the high frequency of

spontaneous calcium transients. We did however observe an enhanced level of wavelike increases in indicator fluorescence moving across the cultures following addition of Aβ. Coincidently, Riera and colleagues have recently developed a method for describing and quantifying these phenomena[126]. Correlating such increases with the presence of specific HL647Aβ oligomers on cells could prove an interesting direction for further study.

4.9 Chapter Summary

Primary neurons provide opportunities to explore questions about the size and evolution of Aβ oligomers on neuronal membranes, the motion of these oligomers, and the sites to which they bind. We demonstrate here that primary hippocampal cell neurites are a suitable system for single-molecule microscopy, with very low autofluorescence levels in the red region of the spectrum. We show that HL647Aβ40 and Aβ42 oligomers on neurites, as on neuroblastoma cells, are significantly larger than oligomers that bind nonspecifically to slides, while neurite-bound oligomers formed from a 1:1 mix of the two peptides are smaller than the slide-bound population. Furthermore, we demonstrate that while neurite-bound size distributions change little in the absence of peptide, with 1 nM Aβ in solution, neurite bound oligomers grow to varying degrees within 24 to 48 hours. Degree of growth is dependent upon the identity of the peptide, with HL647Aβ40 oligomers remaining the same size, HL647Aβ42 oligomers growing very slightly, and 1:1 mixed oligomers exhibiting a substantial increase in oligomer size over time. We examine the motion of these oligomers and show that while most remain immobile, roughly 20% of neurite-bound species exhibit motion on the neurites. Colocalization studies illustrate HL647Aβ40 and HL647Aβ42 oligomers formed on the membrane do not localize to synapses and exhibit only a slight preference for dendrites over axons. Finally, spine density assays and calcium indicator experiments are discussed as potential methods for linking toxicity with specific neurite-bound oligomers. These may be promising directions for the future of this project.

Chapter 5

Discussion and Conclusions

5.1 Introduction

Physiologically meaningful experiments on Aβ binding to live cells and the resulting toxicity have historically been difficult due to low endogenous concentrations of the peptide, the dynamic nature of Aβ aggregates, and the complex nature of Aβ interactions with biological membranes. Emerging single molecule techniques represent one avenue for overcoming these barriers. Here, we adapt a conventional confocal laser scanning microscope to perform single molecule measurements on slide-localized and cell-bound single Aβ40 and Aβ42 oligomers. By optimizing our imaging parameters, we identified a linear regime in which integrated intensity level for a given volume element was directly proportional to number of molecules present. We confirmed the accuracy of this method by another technique commonly used for measuring oligomer size, total internal reflection fluorescence (TIRF) single molecule photobleaching[83,127].

Using this calibration, we find that HL647Aβ rapidly forms oligomers in the trimer to hexamer range upon dilution to low nanomolar concentrations in physiological buffers and exposure to surfaces. Importantly, our treatment did not utilize harsh solvents, unnaturally high peptide concentrations, or chemical modification of oligomer structure, and our initial freshly prepared Aβ40 and Aβ42 samples for all experiments contained over 80% monomers (Figure 3.5.3, Figure 3.8.1, Figure 4.2.1).

SH-SY5Y neuroblastoma cells proved to be a suitable cell line for development of live-cell single molecule imaging techniques. While high autofluorescence levels in the blue region of the spectrum prohibited identification of cell-bound HL488Aβ oligomers, endogenous fluorescence at the red wavelengths was sufficiently low for single HL647Aβ detection. Primary hippocampal cell neurites, as well, had extremely low autofluorescence.

Occasional very high-intensity fluorescent structures are visible in our images of SH-SY5Y cells and of primary neurites (Figure 3.4.1, Figure 4.5.1). These probably represent peptide aggregates containing many more than 20 monomers. Such large species have not been rejected as possible mediators of Aβ toxicity (see Chapter 1 for a complete discussion). However, given the relative rarity of these species and the lack of obvious morphologic abnormalities in the cells to which they are bound, we focused our analysis on oligomers of measurable size.

5.2 HL647cAβ40 Binding to SH-SY5Y Cells

SH-SY5Y cells exposed to 50 nM HL647cAβ both bind the peptide and internalize it, as previously reported[27,91]. For HL647cAβ42, the level of internalization and the sizes of the few detected cell-bound aggregates were determined to be too large for single-molecule studies to be practical. Accordingly, we limited our quantitative study of SH-SY5Y cell-associated Aβ to cell perimeter-localized HL647cAβ40 particles.

Significantly, cell-bound HL647cAβ40 oligomers include a small number of aggregates (roughly 10%) that are greater in size than the largest particles present on slides (Figure 3.6.1). Decreases of approximately 20% in both monomers/dimers and trimers/tetramers are observed on cells as compared to the on-slide data. These decreases reflect a 140% increase in pentamers/hexamers and an 8-fold increase in heptamers to 14-mers. The largest "oligomers" may simply be smaller aggregates clustered in specific, high-density peptide binding domains. Alternatively, these structures may represent large oligomers formed from the on-membrane association of several slow-moving, smaller oligomers or from addition of single monomers to bound oligomers. Our recent data indicates that at low (2 nM) Aβ40 concentrations, oligomers form slowly on supported anionic lipid bilayers from self-association of diffusing monomers. However, at 100 nM, large oligomers appear much more quickly (within 2 hours), which may indicate that small oligomers binding directly from solution can recruit other species both from solution and from on the membrane (Hao Ding, unpublished observations).

We found no evidence for a rapidly diffusing, uniformly distributed population of monomers and dimers on SH-SY5Y cells. However, if the binding of mobile labeled

monomers to the membrane surface is nonuniform, or densities are lower than approximately 1 monomer per 3 μm^2, our analysis will not detect such monomers above cellular autofluorescence. Nag et al. recently reported the presence of diffusible, membrane-bound fluorescein-labeled Aβ40 on PC12 cells exposed to near-physiological peptide concentrations[72]. Our laboratory has also observed uniformly bound pools of diffusible Aβ40 at densities up to 5 to 8 monomers per μm^2 on synthetic lipid bilayers[70]. This disparity may result from our use of a different cell line and a lower concentration of Aβ40 than Nag et al. (50 nM vs. 150 to 350 nM) and from differences in membrane composition between living cells and model membranes.

The majority of cell-bound oligomers appear to be immobile on a time scale of several seconds. This immobility is likely related both to the limited temporal resolution of confocal mode imaging and to Aβ40 binding or insertion sites on the membrane, a number of which are discussed in Chapter 1 of this thesis[55,56,58,61,62]. Aβ oligomers may bind to specific lipid microdomains, such as regions enriched in externalized phosphatidylserines[55], cholesterol-rich regions[58], or lipid rafts[56]. Whether such mechanisms would preclude detectable diffusion of cell-bound Aβ in confocal mode is unclear. Lipid microdomains are dynamic nanoscale structures[128], with lipid confinement times in the tens to hundreds of milliseconds. High-affinity Aβ40 binding to such sites may stabilize microdomains, possibly by interacting with intracellular anchor proteins. Another likely explanation is that oligomers bind to or associate with specific membrane-integral proteins or receptors[30,61,62,68] that are temporarily restricted to specific locations within the cell membrane[129,130], immobilizing the Aβ within an area small enough that positional fluctuations are difficult to detect by the methods used here. Some of these receptors are expressed in SH-SY5Y cells and could be the binding sites of the small oligomers we observe on cells (e.g. NMDA NR1[131], α7nAChR[132], and EphB2[133]).

Substantial evidence supports the hypothesis that Aβ-induced toxicity stems from the formation of calcium-permeable Aβ pores in cell membranes. Interestingly, treatment of SH-SY5Y cells with 50 nM fresh unlabeled Aβ40 or HL647Aβ40 and with similar Aβ42 concentrations results in minimal, sporadic calcium leakage (Figure 3.8.1, Section 3.10). Superficially, these findings may seem contrary to the massive, immediate calcium influxes observed by other groups[26,51,97]. However, such studies have in general been

performed at micromolar Aβ42 concentrations[55,97] or using Aβ42 prepared with solvents known to destabilize membranes[26,29]. Our own studies of Aβ40-liposome interactions indicate that membrane binding and permeabilization occur in separate stages and depend on distinct membrane characteristics[76]. The low-level calcium leakage seen here may simply reflect how extracellular Aβ at physiological levels interacts with healthy cell membranes.

5.3 HL647Aβ on Primary Rat Hippocampal Cell Neurites

Similarly to HL647Aβ40 oligomers detected on SH-SY5Y neuroblastoma cells, neurite-bound HL647Aβ40 and HL647Aβ42 oligomers were significantly larger than those detected on slides. Interestingly, exposing the neurites to 1 nM HL647Aβ for only 10 minutes produced binding at an appropriate density for single-molecule experiments, implying that the peptide has a higher affinity for neurites than for SH-SY5Y cell somas. These results are in line with those acquired by Renner et al., who were able to visualize single neuron-bound particles after only 5 minutes' exposure to 20 nM Aβ oligomers[67]. The neurite-bound HL647Aβ40 size distribution at this early stage unexpectedly contains larger oligomers than that of HL647Aβ42; fully 25% of the total HL647Aβ40 monomers present on cells are part of tetramers or larger, while only 11% of HL647Aβ42 monomers are contained in oligomers of this size (Figure 4.4.2). When samples with peptide bound were incubated for up to 48 hours without peptide in solution, both distributions shifted very slightly towards smaller oligomers, but the above imbalance remained (Figure 4.5.2). The total quantity of peptide bound decreased significantly over the course of 48 hours following washout for neurites treated with HL647Aβ40 or HL647Aβ42 alone (Figure 4.5.8). These results would indicate that one or more of the following processes are occurring: (1) reversible binding (oligomers are released into solution when solution Aβ is low), (2) preferential clearance of large oligomers are from the cell surface over time, and/or (3) dissociation of large oligomers into smaller ones on the cell membrane.

When neurites treated with either peptide were incubated for a further 6 to 48 hours with 1 nM peptide in solution, no significant changes were observed in the

HL647Aβ40 distribution (Figure 4.5.4), implying that Aβ40 oligomers on the membrane reached a stable size equilibrium and were in equilibrium with oligomers in solution within minutes of binding. For HL647Aβ42, a slight shift towards larger oligomers was observed over the same time scale. After 24 to 48 hours in solution at 1 nM HL647Aβ42, 20% to 25% of the monomeric peptide is contained in the tetramers-and-larger population. These results would seem to indicate that while the two peptides reach a similar oligomer size equilibrium on the membrane eventually, Aβ42 requires hours-to-days to reach this equilibrium, while for Aβ40, membrane-catalyzed oligomer growth occurs within minutes upon binding to membranes. Aβ42 typically forms larger oligomers in solution than Aβ40—hexamers and dodecamers of Aβ42 are observed, whereas Aβ40 populates oligomeric states ranging from monomers to tetramers[8,108]. The contrast between these results implies that oligomerization on membranes proceeds through different pathways than oligomerization in solution, as proposed by Zhang et al.[47]

Both peptides exhibited small increases in the total amount of peptide bound on this time scale with 1 nM peptide in solution (Figure 4.5.8). These observations are consistent with the theory that Aβ oligomer growth on membranes requires the presence of solution Aβ, a trend we have observed in our single-molecule studies of Aβ oligomers on planar model membranes (Hao Ding and Chun-Chieh Chang, unpublished observations).

The most interesting size distribution dynamics in this study were observed for oligomers formed from a 1:1 mix of HL647Aβ40 and HL647Aβ42. To begin with, slide-bound oligomers in the 1:1 mix were larger than those detected on the surface for either peptide alone (Figure 4.4.2, Figure 4.4.3); *dimers* constituted the largest percentage of total peptide in this sample (39%) whereas for HL647Aβ40 and HL647Aβ42 individually, the largest proportions were present as monomers (53% and 45%, respectively). Conversely, initial neurite-bound oligomers were smaller than both those bound to the slide and oligomers of either peptide alone on neurites (Figure 4.4.3), with only 5% of the peptide forming tetramers or larger. Unexpectedly, oligomer growth was observed on neurites over 24 to 48 hours even when the solution peptide was ostensibly gone (Figure 4.5.3). The total quantity of peptide bound to neurites increased in the

apparent absence of solution Aβ (Figure 4.5.8). This result might be explained by recruitment of slide-bound peptide into solution (dissociation of slide-bound Aβ from the slide) over the course of the hours following the initial 10-minute incubation. The observed increase in neurite-bound peptide could then occur if 1:1 oligomers bound to the membrane with extremely high affinity. Such an interpretation is consistent with the observation that over 24 to 48 hours at 1 nM, twice as many total monomeric peptide units bind to the neurites of cells treated with a 1:1 mix as compared to cells treated with either peptide alone (Figure 4.5.8). Significantly, when incubated for 24 to 48 hours in the presence of 1 nM 1:1 HL647Aβ40:Aβ42, oligomers grow substantially, with over 40% of the total peptide eventually existing in tetramers or larger structures (Figure 4.5.5).

Recent surface plasmon resonance experiments have indicated that Aβ40 and Aβ42 bind to each other, albeit more weakly than either peptide self-associates[134]. In the same study, Aβ40 was demonstrated to slow Aβ42 fibril formation, with fibrillization proceeding at the same rate for both peptides in a 1:1 mix of the two. These results were interpreted as strong evidence for formation of mixed fibrils. Another group also recently showed that incubating Aβ40 at a 1:1 ratio with Aβ42 inhibits Aβ42 fibril formation, but the authors of the study explicitly state that formation of high-order prefibrillar structures is not slowed[135]. Conclusive evidence for mixed oligomer formation has not to our knowledge been previously demonstrated, decidedly not at physiological concentrations (1 nM). However, the most logical explanation for our current results is the formation of hetero-oligomers of the two peptides. The data presented in the plots in Chapter 4 is summarized in Table 5.3.1; mean oligomer size for each distribution is listed to simplify comparison of the samples.

Table 5.3.1 Mean oligomer sizes (in monomeric subunits) over time.

Peptide	On slide	On neurites (initially)	Washout, 48 hr	48 hr @ 1 nM
Aβ40	1.38	2.19	1.91	2.22
Aβ42	1.44	1.87	1.53	2.04
1:1 Mix	1.87	1.57	1.86	2.87

Mixed peptide forms smaller oligomers on neurites and larger ones on the slide, but either peptide alone forms larger neurite-bound oligomers than those it forms on the slide. This result again demonstrates that oligomerization in solution proceeds along a distinct biophysical pathway in solution as compared to on surfaces. While neurite membrane appears to catalyze the formation of larger oligomers (or selectively bind larger oligomers) for each peptide individually, it initially has smaller oligomers of the 1:1 mix. However, the total initial quantities of all three peptide combinations bound following 10 minutes at 1 nM are equivalent within experimental error. A mechanism in which monomers and dimers of the peptides bind to the neurites at the same initial rate but have dissociation constants, oligomer growth rates, and clearance rates dependent upon the peptide identity would explain this (Figure 5.3.1). Perhaps on-neurite growth proceeds very rapidly—within minutes—to a stable size equilibrium for Aβ40 and to a lesser degree, for Aβ42, but formation of larger oligomers on the membrane is quite slow for the mixed peptide, translating to a longer incubation period for reaching equilibrium. The increased size of the mixed oligomers once equilibrium has been reached may indicate that the cell's ability to clear large mixed oligomers is reduced as compared to aggregates of either peptide separately. This reaction scheme is almost certainly oversimplified in comparison to the real interactions but is useful in interpreting our observations.

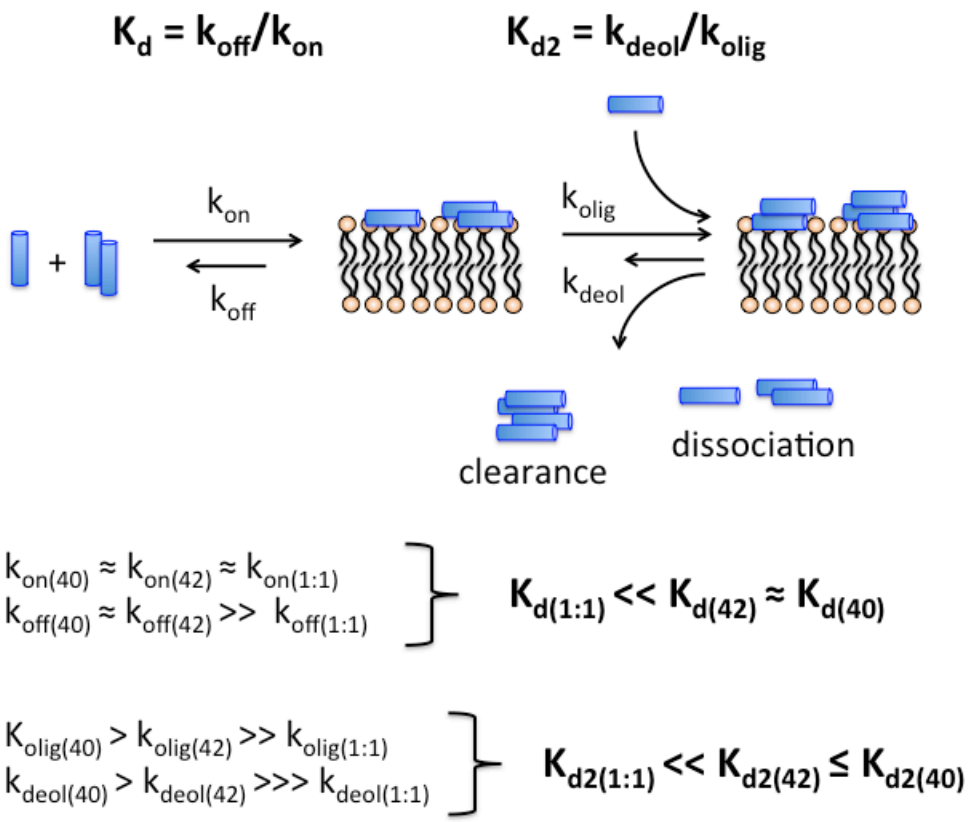

Figure 5.3.1 Binding and on-membrane oligomerization schematic for HL647Aβ.
A kinetic explanation is proposed for observed oligomer interactions with neurite membranes. K_d, dissociation constant for initial binding to membrane; K_{d2}, dissociation constant for on-membrane oligomerization; k_{on}, rate constant for monomers and dimers binding to membrane; k_{off}, rate constant for monomer and dimer dissociation from membrane; k_{olig}, rate constant for on-membrane oligomerization; k_{deol}, rate constant for "deoligomerization" (a group of processes including dissociation of large oligomers into small ones, dissociation of oligomers from the membrane, and cellular clearance of membrane-bound oligomers).

Understanding the functional effects of these oligomers over time will require further study. Jan and colleagues observed higher viability levels in rat cortical neurons treated with a 1:1 mix of initially monomeric Aβ40 and Aβ42 than with equimolar amounts of either peptide alone, but these studies were performed at 10 μM peptide (10,000 times the level used here) and did not assess subtle measures of neurophysiology[135]. More recently, Kuperstein et al. treated neurons with 1 μM peptide for only 2 hours and demonstrated that under these conditions, a 3:7 ratio of Aβ42 to Aβ40 reduced neuronal firing rate to a greater degree than Aβ42 alone[110]. If oligomer neurotoxicity or modulation of synaptic function increase with oligomer size, as some

have suggested[25,31], the current results might help explain the observations of Kuperstein and colleagues.

We do not observe initial binding of Aβ40 or Aβ42 at low nanomolar concentrations to be synaptically localized (Figure 4.7.1), and on-neurite oligomers are only slightly more densely distributed on dendrites than on axons after a 10 minute exposure (Figure 4.7.2). While a number of studies have reported that Aβ preferentially binds to synapses[34,67,120], these have all to our knowledge utilized pre-aggregated oligomers or stained for endogenous oligomers in model mice, using an anti-oligomer antibody. These studies may therefore overlook low-molecular weight oligomers formed in contact with the membrane, the behavior of which is the focus of the current work. The oligomers described here may represent precursor structures to pre-aggregated oligomers or a structurally distinct set of Aβ aggregates which can only form in contact with neuronal membranes. We note, however, that confocal mode kymographs (Figure 4.6.1, Figure 4.6.2) identified a small portion of neurite-bound oligomers which are mobile (20% to 30%) and that migration of these oligomers to cell membrane regions containing specific receptors or even to synapses could occur given sufficient time. Diffusion coefficients measured here for HL647Aβ40 oligomers are consistent with those recently reported for pre-aggregated HL647Aβ42 oligomers on primary neurons[67]. Renner et al. reported increased oligomer confinement, clustering, and binding to mGluR5 receptors over time. Further experiments will be necessary to determine whether similar phenomena are occurring in our system but are beyond the scope of the current study. The work presented here points to a mechanism by which, at physiological concentrations, very small Aβ oligomers bind to the membrane and grow on the membrane over time, with kinetics dependent upon the local Aβ42:Aβ40 ratio (Figure 5.3.2).

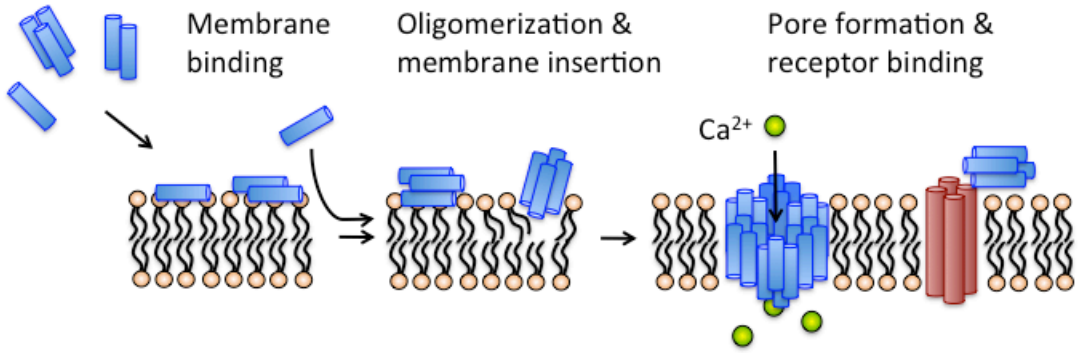

Figure 5.3.2 Mechanism for oligomer formation and toxicity at low concentrations. At physiological Aβ concentrations, addition of solution subunits to small membrane-bound oligomers likely leads to formation of larger potentially neurotoxic oligomers over time. Our data indicates that Aβ42:40 ratio may affect the kinetics of this process.

Such oligomers may gradually localize to synapses and interfere with function of specific membrane proteins or aggregate further to directly form toxic pores in biological membranes. Recent work in our laboratory has demonstrated that oligomers must contain at least 6 monomeric subunits of Aβ40 to induce significant conductivity in model membranes[70], and the quantities of such structures observed on the time scales examined here are minimal and probably result in only subtle changes to neuronal function. Preliminary assessments of Aβ42 effects on spine density (Figure 4.8.1) and neuronal calcium homeostasis in cultured neurons can be considered groundwork for future studies combining single-molecule oligomer size measurement with these techniques.

5.4 Conclusions

We have developed a single-molecule microscopy method for the measurement of fluorescently labeled Aβ oligomers on living cells. We use the integrated intensity of individual particles to determine oligomer size and show that oligomers of HL647Aβ40 and Aβ42 grow on cell membranes, with kinetics dependent on peptide identity. We demonstrate that while most oligomers are confined, some do exhibit motion and that these oligomers do not initially preferentially associate with synapses. These results provide new insight into the dynamics and mechanism of Aβ binding and oligomer

formation on membranes at physiological concentrations. They also provide a foundation for future studies into the time, concentration, and Aβ42:Aβ40 ratio dependence of oligomer growth and the correlation of these factors with neurotoxicity.

References

1. 2010 Alzheimer's disease facts and figures. *Alzheimer's & Dementia : The Journal of the Alzheimer's Association* **6**, 158-94 (2010).

2. Cipriani, G., Dolciotti, C., Picchi, L. & Bonuccelli, U. Alzheimer and his disease: a brief history. *Neurological Sciences* **32**, 275-9 (2011).

3. Crouch, P.J., Harding, S.-M.E., White, A.R., Camakaris, J., Bush, A.I. & Masters, C.L. Mechanisms of Aβ mediated neurodegeneration in Alzheimer's disease. *The International Journal of Biochemistry & Cell Biology* **40**, 181-98 (2008).

4. McLean, C.A., Cherny, R.A., Fraser, F.W., Fuller, S.J., Smith, M.J., Beyreuther, K., Bush, A.I. & Masters, C.L. Soluble pool of Aβ amyloid as a determinant of severity of neurodegeneration in Alzheimer's disease. *Annals of Neurology* **155**, 853-866 (1999).

5. Lue, L., Kuo, Y., Roher, A. & Brachova, L. Soluble amyloid β peptide concentration as a predictor of synaptic change in Alzheimer's disease. *American Journal of Pathology* **155**, 853-862 (1999).

6. Lazo, N.D., Grant, M.A., Condron, M.C., Rigby, A.C. & Teplow, D.B. On the nucleation of amyloid β-protein monomer folding. *Protein Science* **14**, 1581-1596 (2005).

7. Vivekanandan, S., Brender, J.R., Lee, S.Y. & Ramamoorthy, A. A partially folded structure of amyloid-beta(1-40) in an aqueous environment. *Biochemical and Biophysical Research Communications* **411**, 312-6 (2011).

8. Bitan, G., Kirkitadze, M.D., Lomakin, A., Vollers, S.S., Benedek, G.B. & Teplow, D.B. Amyloid β-protein (Aβ) assembly : Aβ40 and Aβ42 oligomerize through distinct pathways. *Proceedings of the National Academy of Sciences of the United States of America* **100**, 330-335 (2003).

9. Bitan, G., Lomakin, A. & Teplow, D.B. Amyloid β-protein oligomerization: prenucleation interactions revealed by photo-induced cross-linking of unmodified proteins. *The Journal of Biological Chemistry* **276**, 35176-84 (2001).

10. Ding, H., Wong, P.T., Lee, E.L., Gafni, A. & Steel, D.G. Determination of the oligomer size of amyloidogenic protein β-amyloid(1-40) by single-molecule spectroscopy. *Biophysical Journal* **97**, 912-21 (2009).

11. Luhrs, T., Ritter, C., Adrian, M., Riek-Loher, D., Bohrmann, B., Dobeli, H., Schubert, D. & Riek, R. 3D structure of Alzheimer's amyloid-β(1–42) fibrils. *Proceedings of the National Academy of Sciences of the United States of America* **102**, 17342-17347 (2005).

12. Tycko, R. Solid-state NMR studies of amyloid fibril structure. *Annual Review of Physical Chemistry* **62**, 279-99 (2011).

13. Puzzo, D., Privitera, L., Fa', M., Staniszewski, A., Hashimoto, G., Aziz, F., Sakurai, M., Ribe, E.M., Troy, C.M., Mercken, M., Jung, S.S., Palmeri, A. & Arancio, O. Endogenous amyloid-β is necessary for hippocampal synaptic plasticity and memory. *Annals of Neurology* **69**, 819-30 (2011).

14. Lee, K.J., Moussa, C.E.H., Lee, Y., Sung, Y., Howell, B.W., Turner, R.S., Pak, D.T.S. & Hoe, H.S. Beta amyloid-independent role of amyloid precursor protein in generation and maintenance of dendritic spines. *Neuroscience* **169**, 344-56 (2010).

15. Puzzo, D., Privitera, L. & Palmeri, A. Hormetic effect of amyloid-beta peptide in synaptic plasticity and memory. *Neurobiology of Aging* (2012).

16. Yu, J.-T., Chang, R.C.-C. & Tan, L. Calcium dysregulation in Alzheimer's disease: from mechanisms to therapeutic opportunities. *Progress in Neurobiology* **89**, 240-255 (2009).

17. Cerf, E., Gustot, A., Goormaghtigh, E., Ruysschaert, J.-M. & Raussens, V. High ability of apolipoprotein E4 to stabilize amyloid-β peptide oligomers, the pathological entities responsible for Alzheimer's disease. *FASEB Journal* **25**, 1585-95 (2011).

18. Castellano, J.M., Kim, J., Stewart, F.R., Jiang, H., DeMattos, R.B., Patterson, B.W., Fagan, A.M., Morris, J.C., Mawuenyega, K.G., Cruchaga, C., Goate, A.M., Bales, K.R., Paul, S.M., Bateman, R.J. & Holtzman, D.M. Human apoE isoforms differentially regulate brain amyloid-β peptide clearance. *Science Translational Medicine* **3**, 89ra57 (2011).

19. Klein, W.L., Krafft, G.A. & Finch, C.E. Targeting small Aβ oligomers: the solution to an Alzheimer's disease conundrum? *Trends in Neurosciences* **24**, 219-224 (2001).

20. Walsh, D.M. & Selkoe, D.J. Aβ oligomers - a decade of discovery. *Journal of Neurochemistry* **101**, 1172-84 (2007).

21. Benilova, I., Karran, E. & De Strooper, B. The toxic Aβ oligomer and Alzheimer's disease: an emperor in need of clothes. *Nature Neuroscience* **15**, 349-57 (2012).

22. Davis, D.G., Schmitt, F.A. & Wekstein, D.R. Alzheimer neuropathologic alterations in aged cognitively normal subjects. *Journal of Neuropathology and Experimental Neurology* **58**, 376-388 (1999).

23. Terry, R.D., Masliah, E., Salmon, D.P., Butters, N., DeTeresa, R., Hill, R., Hansen, L. a & Katzman, R. Physical basis of cognitive alterations in Alzheimer's disease: synapse loss is the major correlate of cognitive impairment. *Annals of Neurology* **30**, 572-80 (1991).

24. De Meyer, G., Shapiro, F., Vanderstichele, H., Vanmechelen, E., Engelborghs, S., De Deyn, P.P., Coart, E., Hansson, O., Minthon, L., Zetterberg, H., Blennow, K., Shaw, L. & Trojanowski, J.Q. Diagnosis-independent Alzheimer disease biomarker signature in cognitively normal elderly people. *Archives of Neurology* **67**, 949-956 (2010).

25. Ono, K., Condron, M.M. & Teplow, D.B. Structure-neurotoxicity relationships of amyloid β-protein oligomers. *Proceedings of the National Academy of Sciences of the United States of America* **106**, 14745-50 (2009).

26. Demuro, A., Mina, E., Kayed, R., Milton, S.C., Parker, I. & Glabe, C.G. Calcium dysregulation and membrane disruption as a ubiquitous neurotoxic mechanism of soluble amyloid oligomers. *The Journal of Biological Chemistry* **280**, 17294-300 (2005).

27. Chafekar, S.M., Baas, F. & Scheper, W. Oligomer-specific Aβ toxicity in cell models is mediated by selective uptake. *Biochimica et Biophysica Acta* **1782**, 523-31 (2008).

28. Sokolov, Y., Kozak, J.A., Kayed, R., Chanturiya, A., Glabe, C. & Hall, J.E. Soluble amyloid oligomers increase bilayer conductance by altering dielectric structure. *The Journal of General Physiology* **128**, 637-47 (2006).

29. Capone, R., Quiroz, F.G., Prangkio, P., Saluja, I., Sauer, A.M., Bautista, M.R., Turner, R.S., Yang, J. & Mayer, M. Amyloid-β-induced ion flux in artificial lipid bilayers and neuronal cells: resolving a controversy. *Neurotoxicity Research* **16**, 1-13 (2009).

30. Shankar, G.M., Li, S., Mehta, T.H., Garcia-Munoz, A., Shepardson, N.E., Smith, I., Brett, F.M., Farrell, M.A., Rowan, M.J., Lemere, C.A., Regan, C.M., Walsh, D.M., Sabatini, B.L. & Selkoe, D.J. Amyloid-β protein dimers isolated directly from Alzheimer's brains impair synaptic plasticity and memory. *Nature Medicine* **14**, 837-42 (2008).

31. O'Nuallain, B., Freir, D.B., Nicoll, A.J., Risse, E., Ferguson, N., Herron, C.E., Collinge, J. & Walsh, D.M. Amyloid β-protein dimers rapidly form stable synaptotoxic protofibrils. *The Journal of Neuroscience* **30**, 14411-9 (2010).

32. Li, S., Hong, S., Shepardson, N.E., Walsh, D.M., Shankar, G.M. & Selkoe, D. Soluble Oligomers of Amyloid β Protein Facilitate Hippocampal Long-Term Depression by Disrupting Neuronal Glutamate Uptake. *Neuron* **62**, 788-801 (2009).

33. Klein, W.L. Aβ toxicity in Alzheimer's disease : globular oligomers (ADDLs) as new vaccine and drug targets. *Neurochemistry International* **41**, 345-352 (2002).

34. Lacor, P.N., Buniel, M.C., Chang, L., Fernandez, S.J., Gong, Y., Viola, K.L., Lambert, M.P., Velasco, P.T., Bigio, E.H., Finch, C.E., Krafft, G.A. & Klein, W.L. Synaptic targeting by Alzheimer's-related amyloid β oligomers. *The Journal of Neuroscience* **24**, 10191-200 (2004).

35. Lacor, P., Buniel, M. & Furlow, P. Aβ oligomer-induced aberrations in synapse composition, shape, and density provide a molecular basis for loss of connectivity in Alzheimer's disease. *The Journal of Neuroscience* **27**, 796 - 807 (2007).

36. Zempel, H., Thies, E., Mandelkow, E. & Mandelkow, E.-M. Aβ oligomers cause localized Ca(2+) elevation, missorting of endogenous Tau into dendrites, Tau phosphorylation, and destruction of microtubules and spines. *The Journal of Neuroscience* **30**, 11938-50 (2010).

37. Lesné, S., Koh, M.T., Kotilinek, L., Kayed, R., Glabe, C.G., Yang, A., Gallagher, M. & Ashe, K.H. A specific amyloid-beta protein assembly in the brain impairs memory. *Nature* **440**, 352-7 (2006).

38. McDonald, J.M., Savva, G.M., Brayne, C., Welzel, A.T., Forster, G., Shankar, G.M., Selkoe, D.J., Ince, P.G. & Walsh, D.M. The presence of sodium dodecyl sulphate-stable Aβ dimers is strongly associated with Alzheimer-type dementia. *Brain : A Journal of Neurology* **133**, 1328-41 (2010).

39. Arispe, N., Rojas, E. & Pollard, H.B. Giant multilevel cation channels formed by Alzheimer disease. *Proceedings of the National Academy of Sciences of the United States of America* **90**, 10573-10577 (1993).

40. Kawahara, M., Arispe, N., Kuroda, Y. & Rojas, E. Alzheimer's disease amyloid β-protein forms Zn(2+)-sensitive, cation-selective channels across excised membrane patches from hypothalamic neurons. *Biophysical Journal* **73**, 67-75 (1997).

41. Lashuel, H.A., Hartley, D., Petre, B.M., Walz, T., Jr, P.T.L., Turner, J., King, J.C., Lachlan-cope, T.A. & Jones, P.D. Amyloid pores from pathogenic mutations. *Nature* **418**, 291 (2002).

42. Lashuel, H.A. & Lansbury, P.T. Are amyloid diseases caused by protein aggregates that mimic bacterial pore-forming toxins? *Quarterly Reviews of Biophysics* **39**, 167-201 (2006).

43. Quist, A., Doudevski, I., Lin, H., Azimova, R., Ng, D., Frangione, B., Kagan, B., Ghiso, J. & Lal, R. Amyloid ion channels: a common structural link for protein-misfolding disease. *Proceedings of the National Academy of Sciences of the United States of America* **102**, 10427-10432 (2005).

44. Laganowsky, A., Liu, C., Sawaya, M.R., Whitelegge, J.P., Park, J., Zhao, M., Pensalfini, A., Soriaga, A.B., Landau, M., Teng, P.K., Cascio, D., Glabe, C. & Eisenberg, D. Atomic View of a Toxic Amyloid Small Oligomer. *Science* **335**, 1228-1231 (2012).

45. Kayed, R., Pensalfini, A., Margol, L., Sokolov, Y., Sarsoza, F., Head, E., Hall, J. & Glabe, C. Annular protofibrils are a structurally and functionally distinct type of amyloid oligomer. *The Journal of Biological Chemistry* **284**, 4230-7 (2009).

46. Dahlgren, K.N., Manelli, A.M., Stine, W.B., Baker, L.K., Krafft, G.A. & LaDu, M.J. Oligomeric and fibrillar species of amyloid-β peptides differentially affect neuronal viability. *The Journal of Biological Chemistry* **277**, 32046-53 (2002).

47. Zhang, Y.-J., Shi, J.-M., Bai, C.-J., Wang, H., Li, H.-Y., Wu, Y. & Ji, S.-R. Intra-membrane Oligomerization and Extra-membrane Oligomerization of Amyloid-β Peptide Are Competing Processes as a Result of Distinct Patterns of Motif Interplay. *The Journal of Biological Chemistry* **287**, 748-56 (2012).

48. Kawahara, M. & Kuroda, Y. Molecular mechanism of neurodegeneration induced by Alzheimer's β-amyloid protein : Channel formation and disruption of calcium homeostasis. *Brain Research* **53**, 389 -397 (2000).

49. Arispe, N. Architecture of the Alzheimer's AβP Ion Channel Pore. *The Journal of Membrane Biology* **197**, 33-48 (2004).

50. Arispe, N., Diaz, J.C. & Simakova, O. Aβ ion channels . Prospects for treating Alzheimer's disease with Aβ channel blockers. *Biochimica et Biophysica Acta* **1768**, 1952 - 1965 (2007).

51. Sepulveda, F.J., Parodi, J., Peoples, R.W., Opazo, C. & Aguayo, L.G. Synaptotoxicity of Alzheimer Beta Amyloid Can Be Explained by Its Membrane Perforating Property. *PLoS one* **5**, e11820 (2010).

52. Demuro, A., Smith, M. & Parker, I. Single-channel Ca(2+) imaging implicates Aβ1-42 amyloid pores in Alzheimer's disease pathology. *The Journal of Cell Biology* **195**, 515-24 (2011).

53. Bezprozvanny, I. Calcium signaling and neurodegenerative diseases. *Trends in Molecular Medicine* **15**, 89-100 (2009).

54. Lee, G., Pollard, H.B. & Arispe, N. Annexin 5 and apolipoprotein E2 protect against Alzheimer's amyloid-β-peptide cytotoxicity by competitive inhibition at a common phosphatidylserine interaction site. *Peptides* **23**, 1249-1263 (2002).

55. Simakova, O. & Arispe, N.J. The cell-selective neurotoxicity of the Alzheimer's Aβ peptide is determined by surface phosphatidylserine and cytosolic ATP levels. Membrane binding is required for Aβ toxicity. *The Journal of Neuroscience* **27**, 13719-13729 (2007).

56. Williamson, R., Usardi, A., Hanger, D.P. & Anderton, B.H. Membrane-bound β-amyloid oligomers are recruited into lipid rafts by a fyn-dependent mechanism. *FASEB Journal* **22**, 1552-1559 (2008).

57. Zampagni, M., Evangelisti, E., Cascella, R., Liguri, G., Becatti, M., Pensalfini, A., Uberti, D., Cenini, G., Memo, M., Bagnoli, S., Nacmias, B., Sorbi, S. & Cecchi, C. Lipid rafts are primary mediators of amyloid oxidative attack on plasma membrane. *Journal of Molecular Medicine* **88**, 597-608 (2010).

58. Nicholson, A.M. & Ferreira, A. Increased membrane cholesterol might render mature hippocampal neurons more susceptible to β-amyloid-induced calpain activation and tau toxicity. *The Journal of Neuroscience* **29**, 4640-4651 (2009).

59. Bateman, D.A., McLaurin, J. & Chakrabartty, A. Requirement of aggregation propensity of Alzheimer amyloid peptides for neuronal cell surface binding. *BMC Neuroscience* **8**, 29 (2007).

60. Snyder, E.M., Nong, Y., Almeida, C.G., Paul, S., Moran, T., Choi, E.Y., Nairn, A.C., Salter, M.W., Lombroso, P.J., Gouras, G.K. & Greengard, P. Regulation of NMDA receptor trafficking by amyloid-β. *Nature Neuroscience* **8**, 1051-8 (2005).

61. Decker, H., Jürgensen, S., Adrover, M.F., Brito-Moreira, J., Bomfim, T.R., Klein, W.L., Epstein, A.L., De Felice, F.G., Jerusalinsky, D. & Ferreira, S.T. N-methyl-D-aspartate receptors are required for synaptic targeting of Alzheimer's toxic amyloid-β peptide oligomers. *Journal of Neurochemistry* **115**, 1520-1529 (2010).

62. Wang, H.-yan, Lee, D.H.S., Andrea, M.R.D., Peterson, P.A., Shank, R.P. & Reitz, A.B. β-Amyloid 1–42 Binds to α7 Nicotinic Acetylcholine Receptor with High Affinity. *The Journal of Biological Chemistry* **275**, 5626 -5632 (2000).

63. Hernandez, C.M., Kayed, R., Zheng, H., Sweatt, J.D. & Dineley, K.T. Loss of α7 nicotinic receptors enhances β-amyloid oligomer accumulation, exacerbating early-stage cognitive decline and septohippocampal pathology in a mouse model of Alzheimer's disease. *The Journal of Neuroscience* **30**, 2442-53 (2010).

64. Dziewczapolski, G., Glogowski, C.M., Masliah, E. & Heinemann, S.F. Deletion of the α7 nicotinic acetylcholine receptor gene improves cognitive deficits and synaptic pathology in a mouse model of Alzheimer's disease. *The Journal of Neuroscience* **29**, 8805-15 (2009).

65. Laurén, J., Gimbel, D.A., Nygaard, H.B., Gilbert, J.W. & Strittmatter, S.M. Cellular prion protein mediates impairment of synaptic plasticity by amyloid-β oligomers. *Nature* **457**, 1128-32 (2009).

66. Kessels, H.W., Nguyen, L.N., Nabavi, S. & Malinow, R. The prion protein as a receptor for amyloid-β. *Nature* **466**, E3-E5 (2010).

67. Renner, M., Lacor, P.N., Velasco, P.T., Xu, J., Contractor, A., Klein, W.L. & Triller, A. Deleterious effects of amyloid β oligomers acting as an extracellular scaffold for mGluR5. *Neuron* **66**, 739-54 (2010).

68. Cisse, M., Halabisky, B., Harris, J., Devidze, N., Dubal, D.B., Sun, B., Orr, A., Lotz, G., Kim, D.H., Hamto, P., Ho, K., Yu, G.-Q. & Mucke, L. Reversing EphB2 depletion rescues cognitive functions in Alzheimer model. *Nature* **469**, 47-52 (2011).

69. Li, S., Jin, M., Koeglsperger, T., Shepardson, N.E., Shankar, G.M. & Selkoe, D.J. Soluble Aβ Oligomers Inhibit Long-Term Potentiation through a Mechanism Involving Excessive Activation of Extrasynaptic NR2B-Containing NMDA Receptors. *Journal of Neuroscience* **31**, 6627- 6638 (2011).

70. Schauerte, J.A., Wong, P.T., Wisser, K.C., Ding, H., Steel, D.G. & Gafni, A. Simultaneous single-molecule fluorescence and conductivity studies reveal distinct classes of Aβ species on lipid bilayers. *Biochemistry* **49**, 3031-3039 (2010).

71. Bateman, D.A. & Chakrabartty, A. Two distinct conformations of Aβ aggregates on the surface of living PC12 cells. *Biophysical Journal* **96**, 4260-4267 (2009).

72. Nag, S., Chen, J., Irudayaraj, J. & Maiti, S. Measurement of the Attachment and Assembly of Small Amyloid-β Oligomers on Live Cell Membranes at Physiological Concentrations Using Single-Molecule Tools. *Biophysical Journal* **99**, 1969-1975 (2010).

73. Calamai, M. & Pavone, F.S. Single molecule tracking analysis reveals that the surface mobility of amyloid oligomers is driven by their conformational structure. *Journal of the American Chemical Society* **133**, 12001-8 (2011).

74. Lord, S.J., Lee, H.D. & Moerner, W.E. Single-molecule spectroscopy and imaging of biomolecules in living cells. *Analytical Chemistry* **82**, 2192-203 (2010).

75. Walter, N.G., Huang, C., Manzo, A.J. & Sobhy, M.A. Do-it-yourself guide : how to use the modern single-molecule toolkit. *Nature Methods* **5**, 475-489 (2008).

76. Wong, P.T., Schauerte, J.A., Wisser, K.C., Ding, H., Lee, E.L., Steel, D.G. & Gafni, A. Amyloid-β membrane binding and permeabilization are distinct processes influenced separately by membrane charge and fluidity. *Journal of Molecular Biology* **386**, 81-96 (2009).

77. Calderon, R.O., Attema, B. & DeVries, G.H. Lipid composition of neuronal cell bodies and neurites from cultured dorsal root ganglia. *Journal of Neurochemistry* **64**, 424-9 (1995).

78. Okabe, S. Molecular anatomy of the postsynaptic density. *Molecular and Cellular Neurosciences* **34**, 503-18 (2007).

79. von Bohlen Und Halbach, O. Structure and function of dendritic spines within the hippocampus. *Annals of Anatomy* **191**, 518-31 (2009).

80. Dukes, K.D., Rodenberg, C.F. & Lammi, R.K. Monitoring the earliest amyloid-β oligomers via quantized photobleaching of dye-labeled peptides. *Analytical Biochemistry* **382**, 29-34 (2008).

81. Paige, M.F., Bjerneld, E.J. & Moerner, W.E. A Comparison of Through-the-Objective Total Internal Reflection Microscopy and Epi- fluorescence Microscopy for Single-Molecule Fluorescence Imaging. *Single Molecules* **2**, 191-201 (2001).

82. Steyer, J.A. & Almers, W. A real-time view of life within 100 nm of the plasma membrane. *Nature Reviews. Molecular Cell Biology* **2**, 268-75 (2001).

83. Ulbrich, M.H. & Isacoff, E.Y. Subunit counting in membrane-bound proteins. *Nature Methods* **4**, 319-321 (2007).

84. Leake, M.C., Chandler, J.H., Wadhams, G.H., Bai, F., Berry, R.M. & Armitage, J.P. Stoichiometry and turnover in single, functioning membrane protein complexes. *Nature* **443**, 355-8 (2006).

85. Lacowicz, J.R. *Principles of Fluorescence Spectroscopy*. 241 (Kluwer Academic/Plenum Publishers: New York, 1999).

86. Podlisny, M.B., Ostaszewski, B.L., Squazzo, S.L., Koo, E.H., Rydell, R.E., Teplow, D.B. & Selkoe, D.J. Aggregation of secreted amyloid β-protein into sodium dodecyl sulfate-stable oligomers in cell culture. *The Journal of Biological Chemistry* **270**, 9564-9570 (1995).

87. Jakawich, S.K., Nasser, H.B., Strong, M.J., McCartney, A.J., Perez, A.S., Rakesh, N., Carruthers, C.J.L. & Sutton, M.A. Local presynaptic activity gates homeostatic

changes in presynaptic function driven by dendritic BDNF synthesis. *Neuron* **68**, 1143-58 (2010).

88. Sage, D., Neumann, F. & Hediger, F. Automatic tracking of individual fluorescence particles: application to the study of chromosome dynamics. *IEEE Transactions on Image Processing* **14**, 1372-1383 (2005).

89. Sani, M.-A., Separovic, F. & Gehman, J.D. The lipid network. *Biophysical Reviews* (2012).doi:10.1007/s12551-012-0071-1

90. Xie, H., Hu, Li. & Li, G. Sh-SY5Y human neuroblastoma cell line: in vitro cell model of dopaminergic neurons in Parkinson's disease. *Chinese Medical Journal* **123**, 1086-1092 (2010).

91. Hu, X., Crick, S.L., Bu, G., Frieden, C., Pappu, R.V. & Lee, J.-M. Amyloid seeds formed by cellular uptake, concentration, and aggregation of the amyloid-β peptide. *Proceedings of the National Academy of Sciences of the United States of America* **106**, 20324-20329 (2009).

92. Benson, R.C., Meyer, R.A., Zaruba, M.E. & McKhann, G.M. Cellular autofluorescence--is it due to flavins? *Journal of Histochemistry & Cytochemistry* **27**, 44-48 (1979).

93. Aubin, J.E. Autofluorescence of viable cultured mammalian cells. *Journal of Histochemistry & Cytochemistry* **27**, 36-43 (1979).

94. Richards-Kortum, R. & Sevick-Muraca, E. Quantitative optical spectroscopy for tissue diagnosis. *Annual Review of Physical Chemistry* **47**, 555-606 (1996).

95. Egawa, T., Hanaoka, K., Koide, Y., Ujita, S., Takahashi, N., Ikegaya, Y., Matsuki, N., Terai, T., Ueno, T., Komatsu, T. & Nagano, T. Development of a far-red to near-infrared fluorescence probe for calcium ion and its application to multicolor neuronal imaging. *Journal of the American Chemical Society* **133**, 14157-9 (2011).

96. Kheterpal, I., Williams, A., Murphy, C., Bledsoe, B. & Wetzel, R. Structural features of the Aβ amyloid fibril elucidated by limited proteolysis. *Biochemistry* **40**, 11757-11767 (2001).

97. Simakova, O. & Arispe, N.J. Early and Late Cytotoxic Effects of External Application of the Alzheimer's Aβ Result from the Initial Formation and Function of Aβ Ion Channels. *Biochemistry* **45**, 5907-5915 (2006).

98. Koffie, R.M., Hyman, B.T. & Spires-Jones, T.L. Alzheimer's disease: synapses gone cold. *Molecular Neurodegeneration* **6**, 63 (2011).

99. Molnár, E. Long-term potentiation in cultured hippocampal neurons. *Seminars in Cell & Developmental Biology* **22**, 506-13 (2011).

100. Wu, H.-Y., Hudry, E., Hashimoto, T., Kuchibhotla, K., Rozkalne, A., Fan, Z., Spires-Jones, T., Xie, H., Arbel-Ornath, M., Grosskreutz, C.L., Bacskai, B.J. & Hyman, B.T. Amyloid β induces the morphological neurodegenerative triad of spine loss, dendritic simplification, and neuritic dystrophies through calcineurin activation. *The Journal of Neuroscience* **30**, 2636-49 (2010).

101. Wei, W., Nguyen, L.N., Kessels, H.W., Hagiwara, H., Sisodia, S. & Malinow, R. Amyloid beta from axons and dendrites reduces local spine number and plasticity. *Nature Neuroscience* **13**, 190-6 (2010).

102. Duff, K., Eckman, C., Zehr, C., Yu, X. & Prada, C. Increased amyloid-β42(43) in brains of mice expressing mutant presenilin 1. *Nature* **383**, 710-713 (1996).

103. Citron, M., Westaway, D., Xia, W. & Carlson, G. Mutant presenilins of Alzheimer's disease increase production of 42-residue amyloid β-protein in both transfected cells and transgenic mice. *Nature Medicine* **3**, 67-72 (1997).

104. Borchelt, D.R., Thinakaran, G., Eckman, C.B., Lee, M.K., Davenport, F., Ratovitsky, T., Prada, C.-mihail, Kim, G., Seekins, S., Yager, D., Slunt, H.H., Wang, R., Seeger, M., Levey, A.I., Gandy, S.E., Copeland, N.G., Jenkins, N.A., Price, D.L., Younkin, S.G. & Sisodia, S.S. Familial Alzheimer's Disease – Linked Presenilin 1 Variants Elevate Aβ1–42/1–40 Ratio In Vitro and In Vivo. *Neuron* **17**, 1005-1013 (1996).

105. Kumar-singh, S., Theuns, Ã.J., Broeck, B.V., Pirici, D., Vennekens, K., Corsmit, E., Cruts, M., Dermaut, B., Wang, R. & Broeckhoven, C.V. Mean Age-of-Onset of Familial Alzheimer Disease Caused by Presenilin Mutations Correlates With Both Increased Aβ42 and Decreased Aβ40. *Human Mutation* **27**, 686-695 (2006).

106. Walker, E.S., Martinez, M., Brunkan, A.L. & Goate, A. Presenilin 2 familial Alzheimer's disease mutations result in partial loss of function and dramatic changes in Aβ 42/40 ratios. *Journal of Neurochemistry* **92**, 294-301 (2005).

107. Narayan, P., Orte, A., Clarke, R.W., Bolognesi, B., Hook, S., Ganzinger, K. a, Meehan, S., Wilson, M.R., Dobson, C.M. & Klenerman, D. The extracellular chaperone clusterin sequesters oligomeric forms of the amyloid-β(1-40) peptide. *Nature Structural & Molecular Biology* **19**, 79-83 (2012).

108. Bernstein, S.L., Dupuis, N.F., Lazo, N.D., Wyttenbach, T., Condron, M.M., Bitan, G., Teplow, D.B., Shea, J.-emma, Ruotolo, B.T., Robinson, C.V. & Bowers, M.T. Amyloid-β protein oligomerization and the importance of tetramers and dodecamers in the aetiology of Alzheimer's disease. *Nature Chemistry* **1**, 326-331 (2009).

109. Murray, M., Bernstein, S., Nyugen, V., Condron, M.M., Teplow, D.B. & Bowers, M.T. Amyloid β Protein : Aβ40 Inhibits Aβ42 Oligomerization. *Journal of the American Chemical Society* **313**, 6316-6317 (2009).

110. Kuperstein, I., Broersen, K., Benilova, I., Rozenski, J., Jonckheere, W., Debulpaep, M., Segers-nolten, I., Werf, K.V.D., Subramaniam, V., Braeken, D., Callewaert, G., Bartic, C., D'Hooge, R.D., Martins, I.C., Rousseau, F., Schymkowitz, J. & De Strooper, B. Neurotoxicity of Alzheimer's disease Aβ peptides is induced by small changes in the Aβ42 to Aβ40 ratio. *EMBO Journal* **29**, 3408-3420 (2010).

111. Renner, M., Domanov, Y., Sandrin, F., Izeddin, I., Bassereau, P. & Triller, A. Lateral diffusion on tubular membranes: quantification of measurements bias. *PloS one* **6**, e25731 (2011).

112. Kusumi, A., Nakada, C., Ritchie, K., Murase, K., Suzuki, K., Murakoshi, H., Kasai, R.S., Kondo, J. & Fujiwara, T. Paradigm shift of the plasma membrane concept from the two-dimensional continuum fluid to the partitioned fluid: high-speed single-molecule tracking of membrane molecules. *Annual Review of Biophysics and Biomolecular Structure* **34**, 351-78 (2005).

113. Andrews, N.L., Lidke, K.A., Pfeiffer, J.R., Burns, A.R., Wilson, B.S., Oliver, J.M. & Lidke, D.S. Actin restricts FcepsilonRI diffusion and facilitates antigen-induced receptor immobilization. *Nature Cell Biology* **10**, 955-63 (2008).

114. Frischknecht, R., Heine, M., Perrais, D., Seidenbecher, C.I., Choquet, D. & Gundelfinger, E.D. Brain extracellular matrix affects AMPA receptor lateral mobility and short-term synaptic plasticity. *Nature Neuroscience* **12**, 897-904 (2009).

115. Saxton, M.J. & Jacobson, K. SINGLE-PARTICLE TRACKING: Applications to Membrane Dynamics. *Annual Review of Biophysics and Biomolecular Structure* **26**, 373-399 (1997).

116. Grafstein, B. & Forman, D.S. Intracellular Transport in Neurons. *Physiological Reviews* **60**, (1980).

117. Viancour, T.A. & Kreiter, N.A. Vesicular fast axonal transport rates in young and old rat axons. *Brain Research* **628**, 209-217 (1993).

118. Triller, A. & Choquet, D. New concepts in synaptic biology derived from single-molecule imaging. *Neuron* **59**, 359-74 (2008).

119. Valentine, C.D. & Haggie, P.M. Confinement of 1- and 2-adrenergic receptors in the plasma membrane of cardiomyocyte-like H9c2 cells is mediated by selective

interactions with PDZ domain and A-kinase anchoring proteins but not caveolae. *Molecular Biology of the Cell* **22**, 2970-2982 (2011).

120. Koffie, R.M., Meyer-Luehmann, M., Hashimoto, T., Adams, K.W., Mielke, M.L., Garcia-Alloza, M., Micheva, K.D., Smith, S.J., Kim, M.L., Lee, V.M., Hyman, B.T. & Spires-Jones, T.L. Oligomeric amyloid beta associates with postsynaptic densities and correlates with excitatory synapse loss near senile plaques. *Proceedings of the National Academy of Sciences of the United States of America* **106**, 4012-7 (2009).

121. Mitrano, D.A. & Smith, Y. Comparative Analysis of the Subcellular and Subsynaptic Localization of mGluR1a and mGluR5 Metabotropic Glutamate Receptors in the Shell and Core of the Nucleus Accumbens in Rat. *Comparative and General Pharmacology* **806**, 788-806 (2007).

122. Hardingham, G.E. & Bading, H. Synaptic versus extrasynaptic NMDA receptor signalling: implications for neurodegenerative disorders. *Nature Reviews. Neuroscience* **11**, 682-96 (2010).

123. Smith, D.L., Pozueta, J., Gong, B., Arancio, O. & Shelanski, M. Reversal of long-term dendritic spine alterations in Alzheimer disease models. *Proceedings of the National Academy of Sciences of the United States of America* **106**, 16877-82 (2009).

124. Busche, M.A., Eichhoff, G., Adelsberger, H., Abramowski, D., Wiederhold, K.-H., Haass, C., Staufenbiel, M., Konnerth, A. & Garaschuk, O. Clusters of hyperactive neurons near amyloid plaques in a mouse model of Alzheimer's disease. *Science* **321**, 1686-9 (2008).

125. Kuchibhotla, K., Lattarulo, C. & Hyman, B. Synchronous hyperactivity and intercellular calcium waves in astrocytes in Alzheimer mice. *Science* **868**, 1211-1215 (2009).

126. Riera, J., Hatanaka, R., Uchida, T., Ozaki, T. & Kawashima, R. Quantifying the uncertainty of spontaneous Ca2+ oscillations in astrocytes: particulars of Alzheimer's disease. *Biophysical journal* **101**, 554-64 (2011).

127. Ji, W., Xu, P., Li, Z., Lu, J., Liu, L., Zhan, Y., Chen, Y., Hille, B., Xu, T. & Chen, L. Functional stoichiometry of the unitary calcium-release-activated calcium channel. *PNAS* **105**, 13668-13673 (2008).

128. Lenne, P.-F., Wawrezinieck, L., Conchonaud, F., Wurtz, O., Boned, A., Guo, X.-J., Rigneault, H., He, H.-T. & Marguet, D. Dynamic molecular confinement in the plasma membrane by microdomains and the cytoskeleton meshwork. *EMBO Journal* **25**, 3245-3256 (2006).

129. Groc, L., Heine, M., Cognet, L., Brickley, K., Stephenson, F.A., Lounis, B. & Choquet, D. Differential activity-dependent regulation of the lateral mobilities of AMPA and NMDA receptors. *Nature Neuroscience* **7**, 695-6 (2004).

130. Bürli, T., Baer, K., Ewers, H., Sidler, C., Fuhrer, C. & Fritschy, J.-M. Single particle tracking of α7 nicotinic AChR in hippocampal neurons reveals regulated confinement at glutamatergic and GABAergic perisynaptic sites. *PloS one* **5**, e11507 (2010).

131. Kulikov, A.V., Rzhaninova, A.A., Goldshtein, D.V. & Boldyrev, A.A. Expression of NMDA receptors in multipotent stromal cells of human adipose tissue under conditions of retinoic acid-induced differentiation. *Bulletin of Experimental Biology and Medicine* **144**, 626-9 (2007).

132. Gao, Q., Liu, Y.-J. & Guan, Z.-Z. Oxidative stress might be a mechanism connected with the decreased alpha 7 nicotinic receptor influenced by high-concentration of fluoride in SH-SY5Y neuroblastoma cells. *Toxicology in Vitro* **22**, 837-43 (2008).

133. Poomthavorn, P., Wong, S.H.X., Higgins, S., Werther, G.A. & Russo, V.C. Activation of a prometastatic gene expression program in hypoxic neuroblastoma cells. *Endocrine-Related Cancer* **16**, 991-1004 (2009).

134. Pauwels, K., Williams, T.L., Morris, K.L., Jonckheere, W., Vandersteen, A., Kelly, G., Schymkowitz, J., Rousseau, F., Pastore, A., Serpell, L.C. & Broersen, K. Structural basis for increased toxicity of pathological Aβ42:Aβ40 ratios in Alzheimer disease. *The Journal of Biological Chemistry* **287**, 5650-60 (2012).

135. Jan, A., Gokce, O., Luthi-Carter, R. & Lashuel, H.A. The ratio of monomeric to aggregated forms of Aβ40 and Aβ42 is an important determinant of amyloid-β aggregation, fibrillogenesis, and toxicity. *The Journal of Biological Chemistry* **283**, 28176-89 (2008).